A Heat Kernel Approach to Hawking Radiation

Heijer, Matthijs den

A Heat Kernel Approach to Hawking Radiation

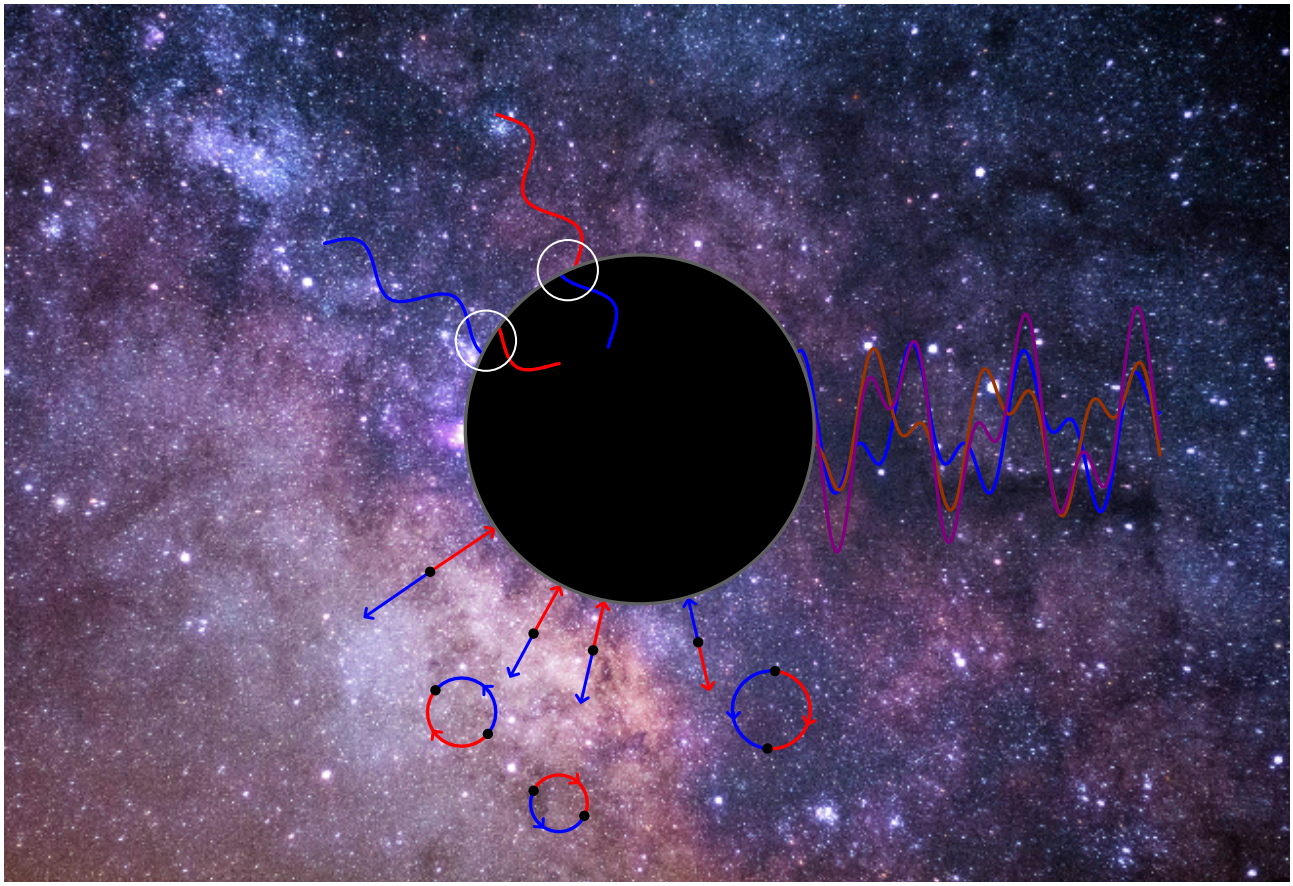

THESIS

submitted in partial fulfillment of the
requirements for the degree of

MASTER OF SCIENCE
in
PHYSICS

Author:	Matthijs Cornelis den Heijer
Student ID:	s3177734
Supervisor:	Dr. Subodh Patil
Second corrector:	Prof.Dr. Koenraad Schalm

Leiden, The Netherlands, January 22, 2025

A Heat Kernel Approach To Hawking Radiation

Matthijs Cornelis den Heijer

Huygens-Kamerlingh Onnes Laboratory, Leiden University
P.O. Box 9500, 2300 RA Leiden, The Netherlands

January 22, 2025

Abstract

This thesis explores the connection between the Schwinger effect and Hawking radiation through a heat kernel approach. Through scattering theory, it can be argued that the inverse square potential given by the field equation in the near horizon limit is directly associated with particle production. Through the eigenvalues of this field equation, where solely the inverse square potential is present, the imaginary part of the Lagrangian can be calculated using the poles of the heat kernel. However, this approach involves discarding order terms that are proportional to the eigenvalues. By including these terms, the new non-trivial eigenvalues can be expressed as a sum over the original eigenvalues plus some perturbation, which is assumed to only contribute to the greybody factor. The result is consistent with other approaches and directly shows that the presence of the event horizon is the working mechanism driving particle production analogous to the electric field in sQED.

Contents

Acknowledgements

Firstly, I am thankful to Dr. Subodh Patil for his guidance and excellent advice throughout my research. I really enjoyed the freedom he gave me during my research. He provided me weekly with various reading materials, which gave me great insight into topics such as EFT, QFT and Hawking radiation. I am also grateful to Prof. Dr. Koenraad Schalm, my second supervisor. He would take time out of his day to hear about my research, which he always sounded enthusiastic about. He gave me important advice and guidance on how research is conducted.

Moreover, this thesis would not have been possible without the support of my friends and family. I would like to thank my friends from office 602 at the Huygens building, Alek, Benjamin, Floris, Hans and Lindsay. The fun environment created by many discussions on random topics, coffee breaks and walks made working on this thesis very enjoyable. I want to thank Floris Fassin for helping me with various complex topics and calculations. I am grateful to my parents, who supported me emotionally and financially. They have always encouraged me to do what I love: physics. Lastly, I would like to thank Lindsay Spoor for always supporting me through tough times.

Notations and Conventions

Many different kinds of conventions and notations are used in the scientific community to describe the same physical concepts, even within the same field of research. Some authors do not explicitly state their notations and conventions, leading to difficulties in reading literature. To avoid this problem for you, the reader, the notations and conventions will be listed before any calculations.

God-given units, also known as *natural units*, are used for simplicity, which is best suited for theoretical research.

Reduced Planck's constant,	$\hbar = 1$
Speed of Light,	$c = 1$
Gravitational constant,	$G = 1$
Bolzmann's constant,	$k_B = 1$

Abbreviation	Definition
CHE	Confluent Heun Equation
GRS	Generalized Riemann Scheme
QNM	Quasi-normal mode
QFT	Quantum Field Theory
sQED	scalar Quantum Electrodynamics
KG	Klein Gordon
BTZ black hole	Bañados-Teitelboim-Zanelli black hole
AdS	Anti-de Sitter

Notation	Definition
μ	Scalar field's mass.
l, m	Orbital and magnetic quantum number, respectively.
M	Black hole's mass.
$\mathrm{M}_\odot$	Solar Mass.
r_s	Event horizon of a Schwarzschild black hole, $r_s = \frac{2GM}{c^2}$.
$\eta_{\mu\nu}$	Minkowski metric, where for all sQED related problems, $\eta_{\mu\nu} = \mathrm{diag}\,(1, -1, -1, -1)$.
$g_{\mu\nu}$	Metric tensor.
g	Determinant of the metric tensor, $g = \det\left(g_{\mu\nu}\right).$
a	Normalized angular momentum.
$F_{\mu\nu}$	Electromagnetic field tensor.
$T_{\mu\nu}$	Energy-stress tensor.
R	Ricci scalar.
$R_{\mu\nu}$	Ricci tensor.
$R_{\mu\nu\rho\sigma}$	Riemann tensor.
$\mathrm{Ei}\,(x)$	Exponential integral function.
$M_{a,b}(x)$	Whittaker M-function.
$W_{a,b}(x)$	Whittaker W-function.
$H(x)$	Heaviside step function.
$D_p(x)$	Parabolic cylinder function.
i^+	Future timelike infinity.
i^-	Past timelike infinity.
i^0	Spatial infinity.
$\mathscr{I}^+$	Future null infinity.
$\mathscr{I}^-$	Past null infinity.

A bold symbol indicates a three-dimensional vector, example; $\boldsymbol{k} = (k_1, k_2, k_3)$.

$\phi_1(x)\overleftrightarrow{\partial_\mu}\phi_2(x) = \phi_1(x)\partial_\mu\phi_2(x) - \phi_2(x)\partial_\mu\phi_1(x)$

$\mathrm{Tr}\,(M) = \int d^4x\sqrt{-g}\,\langle x|\,M\,|x\rangle$

$\mathrm{tr}\,(M) = \langle x|\,M\,|x\rangle$

Introduction

Black holes are among the most fascinating objects in our universe. They produce gravitational waves, emit Hawking radiation and swallow everything in their path. Moreover, it is where quantum mechanics and general relativity meet. Unfortunately, a full theory of quantum gravity still eludes physicists, and approximations have to be made. It was in 1975 that Hawking discovered via the semi-classical approach that black holes radiate particles as a thermal spectrum [1]. At the time, this discovery was very contradictory, as classical particles would never be able to escape the gravitational pull once captured inside the event horizon. Nonetheless, numerous papers were later released confirming Hawking's original result [2–4]. However, the thermal spectrum implies that previously infallen information can not be retrieved. Even if it is assumed that the information is encoded within the radiation spectrum, it still violates either principles of quantum mechanics or general relativity.

Black holes are not the only system capable of producing particles. Particle production plays a central role in cosmological models and also occurs in strong electric fields. The latter is known as the Schwinger effect and describes how quantum fluctuations can create real particles in the presence of strong electric fields [5]. A recent paper by Wondrak et al. [6] attempts to relate the Schwinger effect with Hawking radiation and provides a non-thermal radiation spectrum. This non-thermal radiation spectrum suggests that there are discrepancies in their methodology, which is the motivation behind this thesis.

This master's thesis was conducted as part of the Theoretical Physics track at Leiden University under the supervision of Dr.Subodh P. Patil. The goal is to introduce a novel heat kernel approach to Hawking radiation for scalar particles in Schwarzschild geometry. To achieve this, the well-established Schwinger effect will be analysed using three different approaches: scattering theory, Bogolubov coefficients and the heat kernel. This will serve as a foundation on which the calculations for Schwarzschild black holes will be based. Secondly, the focus will be on particle production of Schwarzschild black holes, where the well-known Hawking radiation results obtained through the Bogolubov and scattering approach will be derived. Lastly, an attempt is made to establish a connection between the Schwinger effect and Hawking radiation through a novel heat kernel approach. This thesis is outlined in the following manner:

• **Chapter 1: Quantum Field Theory** outlines the essential features of Quantum Field Theory in Minkowski spacetime and introduces crucial mathematical formalisms, such as the heat kernel, that will be utilized throughout this thesis. Moreover, particle production in scalar Quantum Electrodynamics will be introduced and studied using the heat kernel.

• **Chapter 2: Quantum Field Theory in Curved Spacetime** extends the concept of field quantization and the heat kernel to curved spacetime. Continuing with sQED, particle production will be derived using the Bogolubov coefficients and scattering theory.

• **Chapter 3: Black Holes** provides insight into the physics of black holes and gives an overview of the different coordinate systems applicable to a Schwarzschild black hole.

• **Chapter 4: Hawking Radiation** studies Hawking radiation through scattering theory and Bogolubov coefficients. Furthermore, the working mechanism driving particle production for black holes will be discussed.

• **Chapter 5: A Heat Kernel Approach to Hawking Radiation** will provide a short derivation on the work of Wondrak et al. [6] and show its discrepancies. Then, through the Bogolubov approach, a heat kernel-type integral will be given, which will provide insight into the supposed eigenvalues of the system. Then, the particle production rate of black holes in the near horizon limit is computed using appropriate boundary conditions.

• **Chapter 6: Conclusion and Future Directions** summarizes and concludes the findings of this thesis and proposes an outlook for future research directions.

Quantum Field Theory

This chapter will outline the essential features of Quantum Field Theory in Minkowski spacetime. The aim is to introduce crucial mathematical formalisms, such as the generating functionals and the heat kernel, which will be used throughout this thesis. The second aim is to provide a toy model, a scalar field, on which all interesting physics will be done. Lastly, using the toy model coupled with an external electromagnetic field, it will be demonstrated through the heat kernel formalism that strong, constant electric fields will destabilize the vacuum, resulting in particle creation.

Classical Field Theory

Firstly, a minimal treatment of classical field theory is required to understand how Quantum Field Theory is formulated. Classical field theory is postulated in terms of Lagrangian formalisms and uses the principle of stationary action to calculate the corresponding field equations. Consider a massive scalar field $\phi(x)$ in Minkowski spacetime. The corresponding Lagrangian density is given by,

$$\mathscr{L}(x) = \frac{1}{2}\left[\eta^{\mu\nu}\partial_\mu\phi(x)\partial_\nu\phi(x) - \mu^2\phi(x)^2\right], \tag{1}$$

where μ is the mass of the field quanta. The action is given by,

$$S = \int d^4x \mathscr{L}(x). \tag{2}$$

Varying the action with respect to the field $\phi(x)$ such that it extremizes the action between configuration states yields the equations of motion for its corresponding field. Then the (Klein-Gordon) field equation for a massive scalar field reads,

$$\left[\Box + \mu^2\right]\phi(x) = 0, \tag{3}$$

where $\Box = \eta^{\mu\nu}\partial_\mu\partial_\nu$. The set of mode solutions that solve the field equation are,

$$u_{\boldsymbol{k}}(t, \boldsymbol{x}) = Ne^{i\boldsymbol{k}\cdot\boldsymbol{x} - i\omega t}, \tag{4}$$

where $\omega \equiv \sqrt{|\boldsymbol{k}|^2 + \mu^2}$ and N is a normalization constant. Normalizing the mode solutions in classical field theory is not a necessary requirement but becomes important when quantizing the field. The *wavenumber* $\boldsymbol{k}$ is free to take the values, $-\infty < k_i < \infty, \quad i = 1, 2, 3$. Since the Minkowski spacetime is orthonormal to the spacelike hypersurface for constant t, it contains a Killing vector $\frac{\partial}{\partial t}$. Therefore, the mode solutions are eigenfunctions of the Killing vector with eigenvalues,

$$\frac{\partial}{\partial t}u_{\boldsymbol{k}}(t, \boldsymbol{x}) = -i\omega u_{\boldsymbol{k}}(t, \boldsymbol{x}), \quad \omega > 0. \tag{5}$$

To ensure that the mode solutions of the field are normalized, define the scalar product,

$$(\phi_1, \phi_2) = -i\int_\Sigma \phi_1(x)\overleftrightarrow{\partial_t}\phi_2^\star(x)d^3x, \tag{6}$$

where Σ is a spacelike Cauchy surface [7]. The mode solutions are then normalized by,

$$(u_{\boldsymbol{k}}, u_{\boldsymbol{k}'}) = \delta^3(\boldsymbol{k} - \boldsymbol{k}'). \tag{7}$$

Thus, the set of orthonormal mode solutions of the field equation is given by,

$$u_{\boldsymbol{k}}(t, \boldsymbol{x}) = \frac{1}{\sqrt{2\omega\,(2\pi)^3}}e^{i\boldsymbol{k}\cdot\boldsymbol{x} - i\omega t}, \tag{8}$$

where these mode solutions and their complex conjugates form a complete orthonormal basis. Therefore, any linear combination yields a solution to the field equation,

$$\phi(x) = \int d^3k \left(a_{\boldsymbol{k}}u_{\boldsymbol{k}}(t, \boldsymbol{x}) + a_{\boldsymbol{k}}^\dagger u_{\boldsymbol{k}}^\star(t, \boldsymbol{x})\right). \tag{9}$$

The coefficients $a_{\boldsymbol{k}}$ and $a_{\boldsymbol{k}}^\star$ are determined by the boundary conditions of the system.

Canonical Quantization

Firstly, to quantize the classical field theory, define

$$\pi(x) = \frac{\partial \mathscr{L}}{\partial(\partial_t \phi(x))}, \tag{10}$$

as the *conjugate momentum* to $\phi(x)$. To transition from classical to quantum field theory, the field $\phi(x)$ and its conjugate momentum $\pi(x)$ are promoted to operators. Moreover, this also involves imposing canonical equal-time commutation relations,

$$\begin{aligned} [\phi(t,\boldsymbol{x}), \phi(t,\boldsymbol{x}')] &= 0, \\ [\pi(t,\boldsymbol{x}), \pi(t,\boldsymbol{x}')] &= 0, \\ [\phi(t,\boldsymbol{x}), \pi(t,\boldsymbol{x}')] &= i\delta^3(\boldsymbol{x}-\boldsymbol{x}'). \end{aligned} \tag{11}$$

Consequently, the coefficients $a_{\boldsymbol{k}}$ and $a^\dagger_{\boldsymbol{k}}$ are also promoted to operators with equal-time commutation relations equivalent to $\pi(x)$ and $\phi(x)$,

$$\begin{aligned} \left[a_{\boldsymbol{k}}, a_{\boldsymbol{k}'}\right] &= 0, \\ \left[a^\dagger_{\boldsymbol{k}}, a^\dagger_{\boldsymbol{k}'}\right] &= 0, \\ \left[a_{\boldsymbol{k}}, a^\dagger_{\boldsymbol{k}'}\right] &= \delta^3(\boldsymbol{k}-\boldsymbol{k}'). \end{aligned} \tag{12}$$

These operators are commonly referred to as the *annihilation operator* $a_{\boldsymbol{k}}$ and *creation operator* $a^\dagger_{\boldsymbol{k}}$. The operators act on a number state $|..., n_{\boldsymbol{k}}, ...\rangle$ in the following manner,

$$a_{\boldsymbol{k}} |..., n_{\boldsymbol{k}}, ...\rangle = \sqrt{n_{\boldsymbol{k}}}\, |..., n_{\boldsymbol{k}} - 1, ...\rangle \tag{13}$$

and

$$a^\dagger_{\boldsymbol{k}} |..., n_{\boldsymbol{k}}, ...\rangle = \sqrt{n_{\boldsymbol{k}} + 1}\, |..., n_{\boldsymbol{k}} + 1, ...\rangle \tag{14}$$

where the number state $|..., n_{\boldsymbol{k}}, ...\rangle$ is the basis vector that spans the Fock space [8]. The creation operator $a^\dagger_{\boldsymbol{k}}$ creates a particle in mode $\boldsymbol{k}$, while the annihilation operator $a_{\boldsymbol{k}}$ removes a particle in mode $\boldsymbol{k}$. A number state containing no particles in every mode $\boldsymbol{k}$ is called the *vacuum state* and is constructed from,

$$a_{\boldsymbol{k}} |0\rangle = 0. \tag{15}$$

The vacuum state in Minkowski spacetime is not unique but is invariant under the Poincaré group [9]. This allows for a natural interpretation of a particle as an excitation in the field.

Generating Functionals

Another approach to quantization is the *path-integral* formalism, which consists of computing all (infinite) possible trajectories that are quantum mechanically allowed. The *generating functional* for a scalar field $\phi(x)$ is defined as,

$$Z[J] = \langle \text{out}, 0 | 0, \text{in} \rangle = \int \mathcal{D}\phi e^{\frac{i}{\hbar}\int d^4x [\mathscr{L}(x) + J(x)\phi(x)]}, \tag{16}$$

where an *external source* $J(x)$ is coupled to the scalar field. The $\langle \text{out}, 0 | 0, \text{in} \rangle$ denotes the vacuum to vacuum transition amplitude, also referred to as the *vacuum persistence*, which indicates how much of the in-vacuum remains unchanged over time. The generating functional gives the transition amplitude between vacua in the presence of an external source and consists of both disconnected and connected Feynman diagrams. Any n-point correlation function can be constructed using [10],

$$\langle T\phi(x_1)\phi(x_2)...\phi(x_n)\rangle = \frac{1}{Z[0]} \prod_{i=1}^{n} \left(-i\frac{\delta}{\delta J(x_i)}\right) Z[J]\bigg|_{J=0}. \tag{17}$$

The two-point correlation function $G(x_1, x_2) = \langle T\phi(x_1)\phi(x_2)\rangle$ is a Green function, also known as the *Feynman propagator*, which provides the amplitude of a particle traversing from x_1 to x_2. In QFT, the vacuum-vacuum interactions correspond to an infinite number of Feynman diagrams with zero external legs. These disconnected diagrams do not contribute to any observable process. Moreover, they can be interpreted as a sum of all possible combinations of the creation and annihilation of virtual particle-antiparticle pairs. A virtual particle is an excitation in the field consisting of many modes in a *wave packet*. Virtual particles differ

from particles in that they are not observable. In a vacuum, all the excitations created by Heisenberg's uncertainty principle must cancel out, as shown in Figure (1). Taking the logarithm of Eq.(16), all the disconnected diagrams are subtracted from the generating functional. Therefore, define the *generating functional of the connected Green functions* $W[J]$ as,

$$W[J] = -i\hbar \ln\left(Z[J]\right) = -i\hbar \ln \langle \text{out}, 0|0, \text{in}\rangle, \tag{18}$$

with

$$\frac{\delta W[J]}{\delta J(x)} \equiv \langle \phi(x) \rangle = \Phi(x) \tag{19}$$

being the source-dependent mean field. The generating functional $W[J]$ is often called the *effective action*. In the presence of an external source, the vacuum may no longer remain unchanged and can transition from its initial in-state to a final out-state. The vacuum persistence may be written in terms of the effective action [11],

$$\langle \text{out}, 0|0, \text{in}\rangle = e^{iW} = e^{i(\Re(W)+i\Im(W))}. \tag{20}$$

If the effective action contains an imaginary part, then the probability of not transitioning between vacua is given by

$$|\langle \text{out}, 0|0, \text{in}\rangle|^2 = e^{-2\Im(W)}, \tag{21}$$

with adiabatic condition [12],

$$\partial\Re(W) >> \left(\partial^2\Re(W)\right)^{\frac{1}{2}}, \left(\partial^3\Re(W)\right)^{\frac{1}{3}}, \dots . \tag{22}$$

The in-and-out vacua exist in different Hilbert spaces due to the non-unitary behaviour of the probability coming from the non-zero imaginary effective action. This non-unitary behaviour corresponds to the decay of one set of particles to another through the *optical theorem* [13]. Thus, the imaginary component, $2\Im(W)$, is the probability that any number of particle pairs are created. The next subsection shows an example of pair particle production in a constant electromagnetic field. Later, this concept will be extended to black holes.

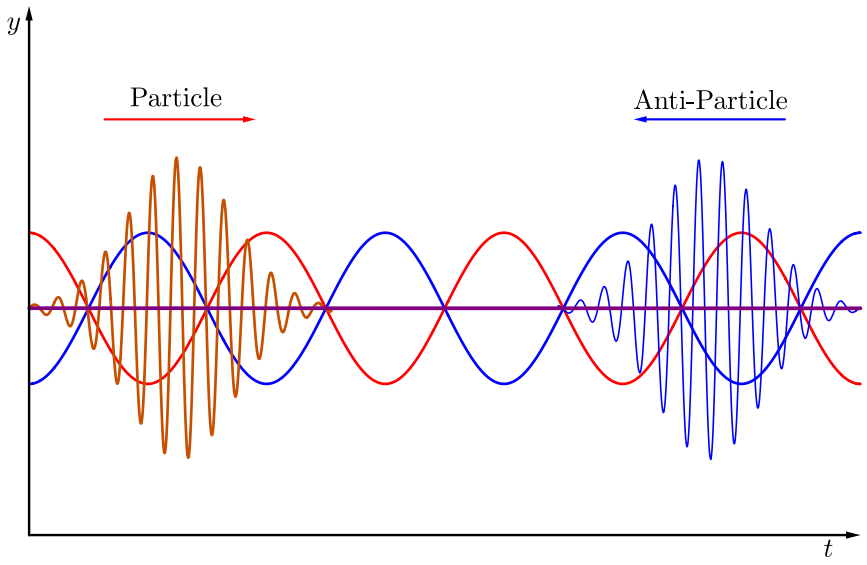

Figure 1: A schematic representation of positive (red) and negative (blue) frequency modes. In a vacuum, these modes cancel each other out (purple), and no real particles exist. Moreover, these modes can fluctuate in energy due to the Heisenberg uncertainty principle, creating excitations in the field. The red wave packet is an excitation in the field representing a particle. The blue wave packet represents an anti-particle.

Furthermore, define the *quantum effective action*,

$$\Gamma[\Phi] \equiv W[J] - \int d^4x \Phi(x) J(x), \tag{23}$$

with condition,

$$\frac{\delta\Gamma[\Phi]}{\delta\Phi(x)} = -J(x). \tag{24}$$

Therefore, using the generating functional yields the functional integral,

$$e^{\frac{i}{\hbar}\Gamma[\Phi]} = \int \mathcal{D}\phi e^{\frac{i}{\hbar}\left(S[\phi]+\int d^4x[\phi(x)J(x)-\Phi(x)J(x)]\right)}. \tag{25}$$

The quantum effective action generates Feynman diagrams that are 1-particle-irreducible and provides perturbative quantum corrections to the classical theory. Consider quantum fluctuations of the field $\phi(x)$ around the mean field of order $\sqrt{\hbar}$, $\phi(x) \to \Phi(x) + \sqrt{\hbar}\phi(x)$,

$$e^{\frac{i}{\hbar}\Gamma[\Phi]} = \int \mathcal{D}\phi e^{\frac{i}{\hbar}\left(S[\Phi+\sqrt{\hbar}\phi] - \sqrt{\hbar}\int d^4x \phi(x)\frac{\delta\Gamma[\Phi]}{\delta\Phi(x)}\right)}. \tag{26}$$

Expanding the action as a power series in $\hbar$,

$$S[\Phi + \sqrt{\hbar}\phi] = S[\Phi] + \sum_{n=1}^{\infty} \frac{\left(\sqrt{\hbar}\right)^n}{n!} S_{,n}(x_n)\phi^n \tag{27}$$

where

$$S_{,n}(x_n)\phi^n = \int d^4x_1 ... d^4x_n \frac{\delta^n S[\phi]}{\delta\phi(x_1)...\delta\phi(x_n)}\phi(x_1)...\phi(x_n). \tag{28}$$

This expansion in powers of $\hbar$ gives the successive quantum corrections to the classical action in terms of loop diagrams. Note that the classical action is the zeroth order in $\hbar$ of the quantum effective action,

$$\Gamma[\Phi] = S[\Phi]. \tag{29}$$

Using Eq.(24), the classical path is described by,

$$\frac{\delta S[\phi]}{\delta\phi(x)} + J(x) = 0. \tag{30}$$

To incorporate the first-order one-loop quantum correction in the effective action, consider the expansion of the power series up to order $\hbar$. This reduces Eq.(26) to,

$$e^{\frac{i}{\hbar}\Gamma[\Phi]} = e^{\frac{i}{\hbar}S[\Phi]} \int \mathcal{D}\phi e^{\frac{i}{2}S_{,2}[\Phi]\phi^2}. \tag{31}$$

The functional integral can be rewritten as a functional determinant [10],

$$\int \mathcal{D}\phi e^{\frac{i}{2}S_{,2}[\Phi]\phi^2} = \det(S_{,2}[\Phi])^{-\frac{1}{2}}. \tag{32}$$

Therefore, the first-order quantum corrections in the quantum effective action are given by the *one-loop quantum effective action* [10],

$$\Gamma[\Phi] = S[\Phi] + \frac{i}{2}\hbar \mathrm{Tr}\ln\left(S_{,2}[\Phi]\right). \tag{33}$$

The generating functional for a real massive scalar field reads,

$$Z[J] = \int \mathcal{D}\phi e^{\frac{i}{\hbar}\int d^4x\left[\frac{1}{2}\left(\eta^{\mu\nu}\partial_\mu\phi(x)\partial_\nu\phi(x) - \mu^2\phi(x)^2\right) + J(x)\phi(x)\right]}. \tag{34}$$

The integral has an infrared divergence, which can be regularized by introducing an infinitesimal term $-\frac{1}{2}\int d^4x \epsilon\phi(x)^2$ to the exponent and taking the limit $\epsilon \to 0^+$ in the final expressions. After integrating by parts and discarding the boundary terms, the generating functional reads,

$$Z[J] = \int \mathcal{D}\phi e^{\frac{i}{\hbar}\int d^4x\left[-\frac{1}{2}\phi(x)(\Box+\mu^2-i\epsilon)\phi(x) + J(x)\phi(x)\right]}. \tag{35}$$

Therefore, the one-loop quantum effective action for a massive scalar field is

$$\Gamma[\Phi] = S[\Phi] + \frac{i}{2}\hbar \mathrm{Tr}\ln\left(\Box + \mu^2\right). \tag{36}$$

Generally, the one-loop effective action for arbitrary background fields is not exactly solvable, and approximations are required. Nonetheless, there are methods to calculate the functional determinant, such as the heat kernel, which may not require perturbative expansions. Typically, the one-loop effective action contains Feynman diagrams that are UV-divergent. These divergencies do not contribute to observable quantities and must be removed by a renormalization prescription. Firstly, using *regularization*, the divergent parts of the diagram are separated from the finite parts. Common regularization prescriptions are cut-off regularization, dimensional regularization and zeta-regularization. Secondly, *counterterms* absorb the infinities and leave any observable quantity finite. These counterterms are not suddenly added to the Lagrangian but follow from rewriting the bare constants in terms of observable constants and infinite contributions. Lastly, the observable constants must be defined through *renormalization conditions*.

The Heat Kernel

In classical mechanics, any physical information is contained in the Hamiltonian of the system. In quantum mechanics, the physical information is extracted from the Schrödinger equation,

$$H\phi_\lambda(x) = \lambda\phi_\lambda(x), \tag{37}$$

using the eigenvalues λ and eigenfunctions ϕ_λ of the system. The *heat kernel* is a spectral function that contains all the system information as it is constructed from the eigenfunctions and eigenvalues,

$$K(s;x,y;H) = \sum_\lambda \phi_\lambda^\dagger(x)\phi_\lambda(y)e^{-s\lambda} = \langle x|\, e^{-sH}\, |y\rangle\,, \tag{38}$$

where $\{\phi_\lambda\}$ is a complete set of orthonormal eigenfunctions with corresponding eigenvalues $\{\lambda\}$ of the operator H. Moreover, the latter expression is written in braket notation. The traced heat kernel only contains the physical information derived from the system's eigenvalues. The variable s is known as the *Schwinger proper time* and is used as a gauge invariant regulator [14]. In Lorentzian signature, $s \to is_M$, there exists an intuitive interpretation: The transition amplitude, $\langle y|\, e^{-iHs_M}\, |x\rangle$, represents a particle propagating from x to y in time s_M. Furthermore, the heat kernel must satisfy the normalization condition,

$$\left(\frac{\partial}{\partial s} + H\right) K(s;x,y;H) = \delta(s)\delta^4(x-y). \tag{39}$$

The Feynman propagator $G(x,y)$ can be defined through the heat kernel,

$$G(x,y) = \frac{1}{H(x,y)} = \int_0^\infty dsK(s;x,y;H). \tag{40}$$

Additionally, the one-loop effective action can be related to the heat kernel in the following manner. Consider the functional determinant in Eq.(33). Using the fact that,

$$\lim_{\epsilon^2\to 0}\int_{\epsilon^2}^\infty \frac{ds}{s}e^{-sx} = \lim_{\epsilon^2\to 0} -\mathrm{Ei}[-x\epsilon^2] \approx \infty + \ln(x), \tag{41}$$

where an appropriate counterterm can absorb the constant infinite term [11]. The functional determinant in terms of the heat kernel reads,

$$W = \frac{i}{2}\mathrm{Tr}\left\{\ln(H)\right\} = \frac{i}{2}\int_0^\infty \frac{ds}{s}\mathrm{Tr}\left(e^{-sH}\right) = \frac{i}{2}\int_0^\infty \frac{ds}{s}K(s;H), \tag{42}$$

where

$$K(s;H) = \mathrm{Tr}\left(e^{-sH}\right) = \mathrm{Tr}K(s;x,y;H)\big|_{x=y}\,. \tag{43}$$

The Euclidean signature ensures the integral is mathematically well-defined. Calculating the effective action reduces to calculating the eigenvalues of the operator H.

Although the heat kernel is a powerful tool, it has its limitations. The heat kernel can not be utilized to calculate beyond the one-loop approximation. Moreover, computing the heat kernel becomes extremely non-trivial for systems with both fermionic and bosonic fields [15].

Particle production in sQED

In 1936, Heisenberg and Euler published a paper, [16], that provided a non-perturbative, non-linear correction to the Maxwell Lagrangian for an electromagnetic background field. This effective Lagrangian is called the *Euler-Heisenberg* Lagrangian. In 1950, Schwinger introduced the proper time formalism, which closely represents the heat kernel approach [5]. Schwinger extracted the (non-perturbative) imaginary part of the Euler-Heisenberg Lagrangian, contributing to a process known as the *Schwinger effect*.

This section aims to provide an example of the Schwinger/heat kernel approach using sQED and to demonstrate the framework for calculating Schwinger pair production. It has been established that a large constant electric field produces particles, in contrast to a constant magnetic field, which does not. Consider a massive complex scalar field coupled to an electromagnetic field through the scalar QED Lagrangian [13, 17],

$$\mathscr{L}_{sQED} = -\frac{1}{4}\left(F^{\mu\nu}\right)^2 + \left|D_\mu\phi\right|^2 - \mu^2\left|\phi\right|^2 \tag{44}$$

where $D_\mu = \partial_\mu + iA_\mu$ and μ is the mass of the scalar quanta. Moreover, the Lagrangian is invariant under gauge transformation. The effective action can be computed using the path-integral approach and by integrating out the scalar field. The effective action reads,

$$\exp\left(i\Gamma[A]\right) = \int \mathcal{D}\phi\mathcal{D}\phi^\star \exp\left[i\int d^4x \left(-\frac{1}{4}\left(F^{\mu\nu}\right)^2 + \left|D_\mu\phi\right|^2 - \mu^2\left|\phi\right|^2\right)\right]. \tag{45}$$

Integrating out the scalar field gives,

$$\Gamma[A] = \int d^4x \left(-\frac{1}{4}\left(F^{\mu\nu}\right)^2\right) - i\int_0^\infty \frac{ds}{s}\mathrm{Tr}\left(e^{-Hs}\right) \tag{46}$$

where the Hamiltonian reads,

$$H[A] = -(i\partial_\mu - A_\mu)(i\partial^\mu - A^\mu) + \mu^2 \tag{47}$$

The vacuum persistence in the presence of an external electromagnetic field is given by,

$$\langle \mathrm{out}, 0|0, \mathrm{in}\rangle = \frac{Z[A]}{Z[0]} \tag{48}$$

which has been normalized to account for the absence of the electromagnetic field. Therefore, the effective action becomes,

$$\tilde{\Gamma}[A] = \Gamma[A] - \Gamma[0] = \int d^4x \mathscr{L}_{eff}[A] \tag{49}$$

with effective Lagrangian,

$$\mathscr{L}_{eff}[A] = -\frac{1}{4}\left(F^{\mu\nu}\right)^2 - i\int_0^\infty \frac{ds}{s}\left\langle x\right|\left(e^{-H[A]s} - e^{-H[0]s}\right)\left|x\right\rangle \tag{50}$$

Rotating to Lorentzian signature $s \to is_M$, the term $\langle x| e^{-iH[A]s_M}|x\rangle = \langle x;0|\, x;s_M\,\rangle$ represents the transition amplitude of a particle traversing from x to x over a closed path within some (Lorentzian) proper time s_M in accordance to the Hamiltonian. Note that, in the absence of the electromagnetic field, the effective action $\Gamma[0]$ corresponds to the vacuum energy of the system,

$$i\int_0^\infty \frac{ds}{s}\left\langle x\right| e^{-iH[0]s_M}\left|x\right\rangle = \frac{1}{16\pi^2}\int_0^\infty \frac{ds_M}{s_M^3} e^{-i\mu^2 s_M} = \frac{1}{s_M}\left(\quad\right) \tag{51}$$

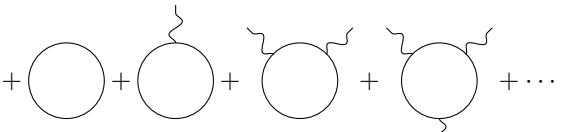

The proper time integral sums over all possible loop configurations with external scalar quanta, and so the effective action is given by,

$$\mathscr{L}_{eff}[A] = -\frac{1}{4}\left(F^{\mu\nu}\right)^2 + \quad + \quad + \quad + \quad + \cdots \tag{52}$$

This includes all possible loop diagrams with any number of external scalar quanta. The effective Langragian captures the non-linear quantum corrections of the electromagnetic fields of the vacuum. Moreover, the effective Lagrangian and the vacuum persistence amplitude are Lorentz and gauge invariant. [13]

The Effective Lagrangian For A Constant Magnetic Field

Having rewritten the effective Lagrangian in terms of the heat kernel in Eq. (50), the remaining calculation reduces to tracing the eigenvalues of the Hamiltonian. Moreover, calculating the effective Lagrangian for a general electromagnetic field becomes increasingly non-trivial. Therefore, for simplicity, the electromagnetic field considered will be either a constant electric or magnetic field. Firstly, consider the scalar field in a constant magnetic background (in the Lorentz gauge) $A_\mu = (0, 0, 0, By)$. The Hamiltonian becomes,

$$H[A] = \partial_0^2 - \partial_x^2 - \partial_y^2 + \left(i\partial_z - By\right)^2 + \mu^2 \tag{53}$$

As tracing over the heat kernel is equivalent to calculating the eigenvalues of the Hamiltonian, the problem reduces to an eigenvalue problem,

$$H[A]\psi_n = \lambda[A]\psi_n. \tag{54}$$

The Hamiltonian has a resemblance to the quantum harmonic oscillator [18], and so the eigenfunctions are given by,

$$\psi_n^{k_z k_0 k_x}(x) = \phi_n\left(y - \frac{k_z}{B}\right) e^{ik_0 t} e^{-ik_x x} e^{-ik_z z} \tag{55}$$

where ϕ_n is the harmonic oscillator wavefunction. The corresponding eigenvalues are given by,

$$\lambda[A] = -k_0^2 + k_x^2 + 2B\left(n + \frac{1}{2}\right) + \mu^2 \tag{56}$$

Evaluating the trace over the eigenvalues yields,

$$\begin{aligned} i\int_0^\infty \frac{ds}{s} \langle x| e^{-H[A]s} |x\rangle &= i\int_0^\infty \frac{ds}{s} \frac{1}{(2\pi)^2} \int_{-\infty}^\infty dk_0 dk_x e^{\left(k_0^2 - k_x^2\right)s} \frac{B}{2\pi} \sum_{n=0}^\infty e^{-2Bs\left(n+\frac{1}{2}\right)} e^{-\mu^2 s} \\ &= \frac{B}{16\pi^2} \int_0^\infty \frac{ds}{s^2} e^{-\mu^2 s} \mathrm{csch}\,(Bs) \end{aligned} \tag{57}$$

where $\frac{B}{2\pi}$ is the degeneracy in each Landau level per unit area, representing the number of quantum states per unit area available within a single level [18]. The effective action reads

$$\mathscr{L}_{eff}[A] = -\frac{1}{2}B^2 - \frac{1}{16\pi^2}\int_0^\infty \frac{ds}{s^3} e^{-\mu^2 s} \left[Bs\ \mathrm{csch}\,(Bs) - 1\right] \tag{58}$$

Lastly, the effective Lagrangian should be renormalized as it diverges at $s = 0$. This can be achieved in numerous ways; the simplest is by expanding the integrand,

$$\left[Bs\ \mathrm{csch}\,(Bs) - 1\right] e^{-\mu^2 s} = \left[-\frac{B^2 s^2}{6} + \frac{7B^4 s^4}{360} + \mathcal{O}(B^6)\right] e^{-\mu^2 s}. \tag{59}$$

The first term of the expansion is UV divergent, whilst higher-order terms are well-behaved. The first term is proportional in magnetic strength to the Maxwell Lagrangian, $-\frac{1}{2}B^2$,

$$\frac{B^2}{96\pi^2}\int_0^\infty \frac{ds}{s} e^{-\mu^2 s}, \tag{60}$$

and so can be removed by (charge) renormalization. Adding[1] the counterterm yields the final renormalized effective action in a constant magnetic field,

$$\mathscr{L}_{eff}^{ren}[A] = -\frac{1}{2}B^2 - \frac{1}{16\pi^2}\int_0^\infty \frac{ds}{s^3} e^{-\mu^2 s} \left[Bs\ \mathrm{csch}\,(Bs) - 1 + \frac{B^2 s^2}{6}\right]. \tag{61}$$

The pole at $s = 0$ is no longer present after renormalization and the effective Lagrangian contains no other poles for $s > 0$.

The Effective Lagrangian For A Constant Electric Field

The calculation for the effective Lagrangian for a constant electric field is very similar but with analytical continuation, $B \to iE$. Consider the scalar field in a constant electric background (in the Lorentz gauge) $A_\mu = (0, Et, 0, 0)$. The Hamiltonian reads,

$$H[A] = \partial_0^2 + (i\partial_x - Et)^2 - \partial_y^2 - \partial_z^2 + \mu^2. \tag{62}$$

In contrast to the constant magnetic field, this Hamiltonian resembles an inverted harmonic oscillator[18], and so the eigenfunctions are,

$$\psi_n^{k_x k_y k_z}(x) = D_n\left(\sqrt{\frac{2}{E}} e^{-\frac{i\pi}{4}} (k_x - Et)\right) e^{-ik_x x} e^{-ik_y y} e^{-ik_z z}, \tag{63}$$

where $D_n\left(\sqrt{\frac{2}{E}} e^{-\frac{i\pi}{4}} (k_x - Et)\right)$ is the parabolic cylinder function [19]. The corresponding eigenvalues are [18],

$$\lambda = k_y^2 + k_z^2 + 2iE\left(n + \frac{1}{2}\right) + \mu^2. \tag{64}$$

[1] A counterterm is not simply added/introduced in the Lagrangian. The counterterms follow from rescaling the field and rewriting in terms of bare constants.

Note that the eigenvalues are complex, indicating that the system has become unstable. Following the same renormalization prescription as the constant magnetic field, the renormalized effective Lagrangian reads,

$$\mathscr{L}_{eff}^{ren}[A] = \frac{1}{2}E^2 - \frac{1}{16\pi^2}\int_0^\infty \frac{ds}{s^3}e^{-\mu^2 s}\left[Es\csc(Es) - 1 - \frac{E^2s^2}{6}\right] \tag{65}$$

where the last term follows from charge renormalization corresponding to the counterterm,

$$-\frac{E^2}{96\pi^2}\int_0^\infty \frac{ds}{s}e^{-\mu^2 s}. \tag{66}$$

The effective action is non-linear in the electric field. While the counterterms have removed the pole at $s = 0$, the poles at $s = \frac{n\pi}{E}$ for $n = 1, 2, ...$ remain.

Particle production

For particle production to occur in an electromagnetic field, the effective action must have a non-zero imaginary part, as shown in Eq.(21). If an imaginary contribution exists for the electric and magnetic fields, it must follow from its poles as the principal part of the integrals are real. The poles are related to the imaginary part by the residue theory [20]. Firstly, for the constant magnetic field, the effective Lagrangian, Eq. (61), has no poles for $s \geq 0$, indicating a stable vacuum. The stability of the vacuum can be directly linked to the magnetic field states $\psi_n^{k_z k_0 k_x}(x)$ of Eq.(55) being time-independent. Hence, there is *no particle production in a constant magnetic field*. In a heuristic view, as shown in Figure (2), the magnetic field creates virtual particles that can never become real as the trajectories of the particles coincide again and are annihilated.

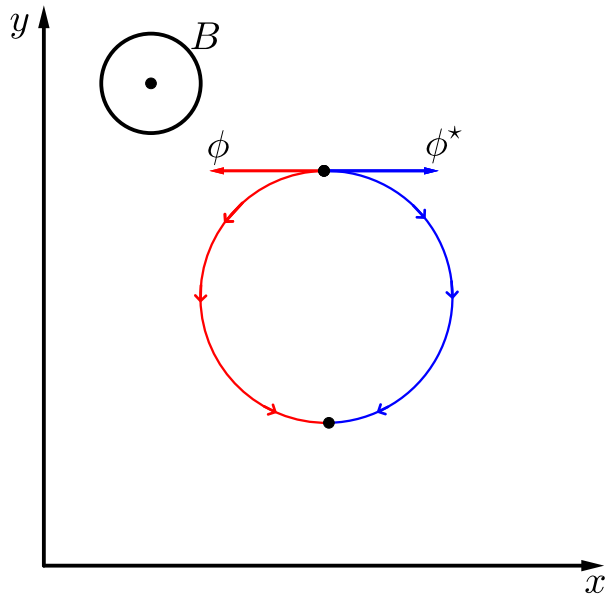

Figure 2: A schematic representation of the vacuum creating a virtual particle pair and annihilating. The top left circle indicates the magnetic field B coming out of the paper. The vacuum creates virtual particle pairs. However, due to the magnetic field, the particle's worldlines coincide again and are annihilated, never having a chance to become real particles.

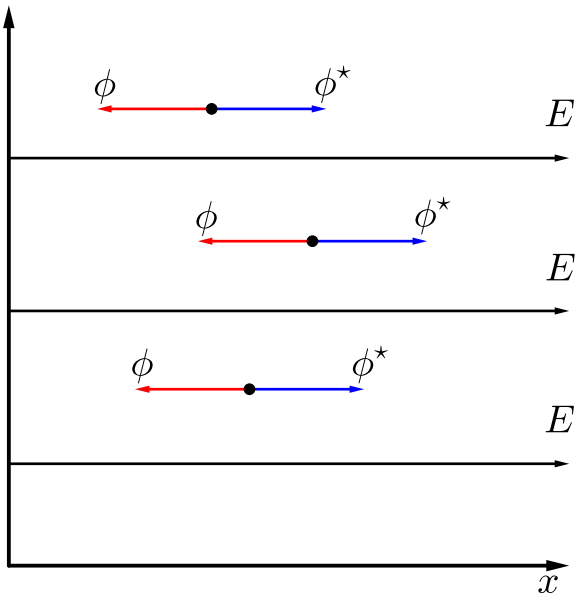

Figure 3: A schematic representation of pair particle creation in an electric field. The negatively charged scalar quanta $\phi^\star$ accelerates away from the source, while the positively charged scalar quanta ϕ goes towards the source of the electric field. Due to energy conservation, the electric field E decays as it creates particle pairs.

The effective Lagrangian of the electric field, Eq.(65), does contain poles for $s > 0$. Evaluating the imaginary part of the effective action using residue theory [20] yields,

$$2\Im(\mathscr{L}_{eff}[A]) = \frac{E^2}{8\pi^3}\sum_{n=1}^{\infty}\frac{(-1)^{n+1}}{n^2}e^{-\frac{\mu^2\pi n}{E}}. \tag{67}$$

The vacuum becomes unstable in a constant electric field given that the electric state $\psi_n^{k_x k_y k_z}(x)$ of Eq. (63) is time-dependent. This vacuum decay shows that *a constant electric field produces particles*.

In the absence of a background field, the vacuum fluctuates, creating virtual particle pairs that annihilate shortly after. However, in the presence of an electric field, the virtual particle pairs may be accelerated apart to some distance d and become real particles, as shown in Figure (3). This occurs under the condition provided that the energy given by the electric field Ed exceeds their rest mass 2μ. This phenomenon can be seen as particles tunnelling through the energy gap 2μ, which will be explored in a later chapter. The Heisenberg uncertainty principle $\Delta x \Delta p \geq \frac{\hbar}{2}$ constraints the separation distance $\Delta x \sim d$ and momentum[2] $\Delta p \sim \mu$, implying that $d \sim \frac{1}{\mu}$. Therefore, under the first condition, the electric field must exceed $E_s = \frac{\mu^2 c^3}{\hbar e}$ (in SI units) for the particle production to become relevant [21, 22].

[2] In case of non-relativistic velocities.

QFT in Curved Spacetime

The goal of this chapter is to extend the quantization procedure in Minkowski spacetime to include curved spacetimes. These spacetimes are assumed to be infinitely differentiable, globally hyperbolic pseudo-Riemannian manifolds. This guarantees the existence of Cauchy hypersurfaces and differential equations [21]. Due to covariance, the vacuum in curved spacetime is generally no longer unique. This allows for more than one way to decompose the field. These different decompositions are connected via Bogolubov transformations. The Bogolubov transformations give an alternative (QFT) approach to calculate the vacuum persistence compared to the Schwinger approach. Additionally, a connection exists between Bogolubov coefficients and scattering theory's reflection and transmission coefficients. This chapter will demonstrate the connections between the three methodologies using the toy model of sQED as an example.

Scalar Field Quantization in Curved Spacetime

The Lagrangian density for a massive scalar field $\phi(x)$ in curved space is given by,

$$\mathscr{L}(x) = \frac{1}{2}\sqrt{-g}\left[g^{\mu\nu}\nabla_\mu\phi(x)\nabla_\nu\phi(x) - \left(\mu^2 + \xi R\right)\phi(x)^2\right], \tag{68}$$

where μ is the mass of the field quanta and ∇_μ is the covariant derivative [7]. The scalar field is coupled to the gravitational field with coupling constant ξ and Ricci scalar R. The scalar field equation reads,

$$\left[\Box + \mu^2 + \xi R\right]\phi(x) = 0, \tag{69}$$

with

$$\Box = \frac{1}{\sqrt{-g}}\partial_\mu\left[\sqrt{-g}g^{\mu\nu}\partial_\nu\right]. \tag{70}$$

Consider a set of mode solutions $u_i(x)$ that solves the field equation. Generally, these solutions are non-trivial in curved spacetime. To quantize the field, define the canonical commutation relations in curved spacetime as [7],

$$\begin{aligned}
&[\phi(t,\boldsymbol{x}),\phi(t,\boldsymbol{x'})] = 0,\\
&[\pi(t,\boldsymbol{x}),\pi(t,\boldsymbol{x'})] = 0,\\
&[\phi(t,\boldsymbol{x}),\pi(t,\boldsymbol{x'})] = \frac{i}{\sqrt{-g}}\delta^3(\boldsymbol{x}-\boldsymbol{x'}).
\end{aligned} \tag{71}$$

where

$$\pi(x) = \frac{\partial\mathcal{L}}{\partial\left(\nabla_0\phi\right)}. \tag{72}$$

To normalize the mode solutions, the scalar product in Minkowski spacetime can be generalized to curved space,

$$(\phi_1,\phi_2) = -i\int_\Sigma \phi_1(x)\overleftrightarrow{\partial_\mu}\phi_2^\star(x)\sqrt{-g_\Sigma}n^\mu d\Sigma, \tag{73}$$

where n^μ is the future-directed orthonormal vector to the spacelike Cauchy surface Σ. The field solutions $u_i(x)$ are then normalized by,

$$(u_i,u_j) = \delta_{ij}, \qquad \left(u_i^\star,u_j^\star\right) = -\delta_{ij}, \qquad \left(u_i,u_j^\star\right) = 0. \tag{74}$$

The general field solution $\phi(x)$ consists of a linear combination of the orthonormal mode solutions,

$$\phi(x) = \sum_i\left[a_iu_i(x) + a_i^\dagger u_i^\star(x)\right], \quad a_i\left|0\right\rangle = 0, \quad \forall i, \tag{75}$$

where the vacuum $|0\rangle$ and operators a_i and $a_i^\dagger$ are constructed analogously to Minkowski spacetime.

Bogolubov Transformation

In Minkowski spacetime, all inertial observers perceive the same vacuum due to the invariance of the vacuum under the Poincaré group. In curved spacetime, the Poincaré group is generally no longer the symmetry

group associated with the spacetime. However, the theory is symmetric under general coordinate transformations, also known as covariance. Consequently, a natural set of coordinates does not exist and the mode decomposition of Eq.(75) is no longer unique. This allows for a second complete set of modes,

$$\phi(x) = \sum_j \left[\overline{a}_j \overline{u}_j(x) + \overline{a}_j^\dagger \overline{u}_j^\star(x)\right], \quad \overline{a}_j \left|\overline{0}\right\rangle = 0, \quad \forall j. \tag{76}$$

Both sets of solutions form a complete orthonormal basis and may be expanded in terms of each other through *Bogolubov Transformation*,

$$\begin{aligned} \overline{u}_j &= \sum_i \left(\alpha_{ji} u_i + \beta_{ji} u_i^\star\right), \\ u_i &= \sum_j \left(\alpha_{ji}^\star \overline{u}_j - \beta_{ji} \overline{u}_j^\star\right). \end{aligned} \tag{77}$$

Similarly, the creation and annihilation operators are related by

$$\begin{aligned} a_i &= \sum_j \left(\alpha_{ji} \overline{a}_j + \beta_{ji}^\star \overline{a}_j^\dagger\right), \\ \overline{a}_j &= \sum_i \left(\alpha_{ji}^\star a_i - \beta_{ji}^\star a_i^\dagger\right). \end{aligned} \tag{78}$$

The coefficients α and β represent the *Bogolubov coefficients* and are evaluated by

$$\alpha_{ij} = \left(\overline{u}_i, u_j\right), \quad \beta_{ij} = \left(\overline{u}_i, u_j^\star\right). \tag{79}$$

As a consequence of orthonormality, the coefficients must satisfy,

$$\begin{aligned} \sum_l \left(\alpha_{il} \alpha_{jl}^\star - \beta_{il} \beta_{jl}^\star\right) &= \delta_{ij}, \\ \sum_l \left(\alpha_{il} \beta_{jl} - \beta_{il} \alpha_{jl}\right) &= 0. \end{aligned} \tag{80}$$

Moreover, the mode solutions of u_i involve a combination of positive and negative frequencies from $\overline{u}_j$. This means that the vacua are distinct from each other, and the vacuum associated with the mode solutions of u_i contains particles from the mode solutions of $\overline{u}_j$. The expectation value of the number operator $\hat{N}_i = a_i a_i^\dagger$ is given by,

$$N = \left\langle \overline{0} \right| \hat{N}_i \left| \overline{0} \right\rangle = \sum_j \left|\beta_{ji}\right|^2 \tag{81}$$

An observer in one frame of reference will detect particles, whilst another does not. The idea of a "particle" becomes an abstract concept, where its existence is observer-dependent. Therefore, particles are not a robust method to probe the physics of a state and a more localized quantity is needed, such as the stress-energy tensor $\langle T^{\mu\nu}(x) \rangle$. [21]

An important concept in particle production is called *spacetime sandwiching*, where the spacetime is stationary till time $t < t_1$ in the remote past and again after time $t > t_2$ in the remote future. The spacetime is asymptotically Minkowskian in the remote past and future but is topologically complex at times $t_1 < t < t_2$. Furthermore, define the in-vacuum corresponding to the Minkowskian vacuum in the remote past and the out-vacuum corresponding to the Minkowskian vacuum in the remote future. Although the regions are Minkowskian in the past and future, the Killing vectors in their respective regions may differ. Therefore, an inertial observer in the out region may detect in-particles. The sudden particle creation is said to be created by an external field. This spacetime sandwiching provides a useful framework for calculating particle production.[23]

The vacua are related by,

$$\left|\overline{0}\right\rangle = S(\xi) \left|0\right\rangle, \tag{82}$$

where

$$S\left(\xi\right) = \exp\left[\frac{1}{2}\left(\xi^\star a_i^2 - \xi a_i^{\dagger 2}\right)\right], \tag{83}$$

is the squeeze operator and $\xi = re^{i\theta}$ [24]. The variables r and θ are related to the Bogolubov coefficients through, $\alpha = \cosh(r)$ and $\beta = e^{i\theta}\sinh(r)$, which are written in matrix notation. Decomposing the vacuum $\left|\overline{0}\right\rangle$ in terms of number states from the vacuum $\left|0\right\rangle$ yields,

$$\left|\overline{0}\right\rangle = \sum_n C_n \left|n\right\rangle, \tag{84}$$

where

$$C_{2n} = (-1)^n \frac{\sqrt{(2n)!}}{2^n n!} \frac{\left(e^{-i\theta}\tanh(r)\right)^n}{\sqrt{\cosh(r)}}. \tag{85}$$

Using the squeeze operator for a single-mode field, the vacuum persistence can be written as

$$\langle 0, \text{out}|0, \text{in}\rangle = \langle 0, \text{out}| S^\dagger(\xi) |0, \text{out}\rangle = \frac{1}{\sqrt{\det(\alpha^\star)}}. \tag{86}$$

Therefore, the Bogolubov coefficients are related to the effective action by, [25]

$$W = \frac{i}{2}\text{Tr}\big\{\ln(\alpha^\star)\big\}, \tag{87}$$

where the trace is a sum of all states. The probability of creating particles is

$$2\Im(W) = \text{Tr}\big\{\ln|\alpha|\big\} = \frac{1}{2}\text{Tr}\big\{\ln(1+N)\big\} \tag{88}$$

The field considered for the Bogolubov transformation only consists of real scalar particles. For a complex scalar field, the mode decomposition becomes,

$$\phi(x) = \sum_i \Big[a_i u_i(x) + b_i^\dagger u_i^\star(x)\Big] \quad a_i|0\rangle = b_i|0\rangle = 0, \quad \forall i \tag{89}$$

where the vacuum is a two-mode vacuum $|0\rangle = |0\rangle_a \otimes |0\rangle_b$. Following the same procedure as the real scalar field [26], the effective action becomes

$$W = \text{Tr}\big\{\ln(\alpha^\star)\big\}. \tag{90}$$

The probability of creating particle pairs is

$$2\Im(W) = 2\text{Tr}\big\{\ln|\alpha|\big\} = \text{Tr}\big\{\ln(1+N)\big\}. \tag{91}$$

This provides an alternative method for calculating the imaginary part of the action. In contrast to the Schwinger approach, which requires the system's eigenvalues, this approach requires the Bogolubov coefficients. Due to the connection between Bogolubov coefficients and transmission and reflection coefficients [17], there also exists a scattering approach for calculating the imaginary part,

$$\prod_\lambda T_{r,\lambda} = \exp\left[-2V\Im(\mathcal{L}_{eff})\right] \quad \text{or} \quad \prod_\lambda R_{l,\lambda} = \exp\left[-2V\Im(\mathcal{L}_{eff})\right]. \tag{92}$$

If either the reflection or transmission coefficient resembles, through interpretation, the probability of no pair creation occurring in state λ, then the vacuum persistence is calculated by its corresponding coefficient in Eq.(92). The product over the coefficients follows from the fact that every state λ is independent,

$$|0\rangle = \bigotimes_\lambda |0_\lambda\rangle \tag{93}$$

Therefore, the total probability of the vacuum changing is the product of all independent states λ. These three approaches lead to different physical interpretations of particle production in sQED.

Particle Production in sQED: Bogolubov coefficients and Tunneling

To show the correspondence between the Bogolubov coefficients and the Schwinger approach, consider (again) the sQED Lagrangian. Firstly, the (KG) field equation in a constant magnetic field (in the Lorentz gauge) reads,

$$\left[\partial_0^2 - \partial_x^2 - \partial_y^2 + (i\partial_z - By)^2 + \mu^2\right]\Phi(x) = 0. \tag{94}$$

The mode solutions that solve the field equation are,

$$\Phi(x) = e^{-ik_0 t} e^{ik_x x + ik_z z}\phi(y') \tag{95}$$

where

$$y' = \sqrt{\frac{2}{B}} i(k_z + By), \quad \lambda = \frac{1}{B}\left(\mu^2 + k_x^2 - k_0^2\right), \quad p = \frac{1}{2}(\lambda - 1) \tag{96}$$

Since the function $\phi(y')$ is time-independent, the mode solutions in the remote future and past remain in the same positive frequency mode $e^{-ik_0 t}$. There is one unique mode decomposition for a constant magnetic background, so the vacuum does not change. Consider the (KG) field equation in a constant electric field (in the Lorentz gauge) [17],

$$\left[\partial_0^2 + (i\partial_x - Et)^2 - \partial_y^2 - \partial_z^2 + \mu^2\right]\Phi(x) = 0 \tag{97}$$

The mode solutions may be expressed as

$$\Phi(x) = \phi(t')e^{i\boldsymbol{k}\cdot\boldsymbol{x}} \tag{98}$$

where

$$t' = \sqrt{\frac{2}{E}}e^{\frac{i\pi}{4}}\left(k_x - Et\right) \quad , \lambda = \frac{1}{E}\left(\mu^2 + k_z^2 + k_y^2\right) \quad , p = -\frac{1}{2}\left(i\lambda + 1\right) \tag{99}$$

The KG field equation reduces to

$$\left[\partial_0^2 + t'^2 + \lambda\right]\phi(t') = 0 \tag{100}$$

Notably, the equation is reduced to a Schrodinger form corresponding to an inverted harmonic oscillator with potential $V(t') = -\frac{1}{2}\omega^2 t'^2$. The potential causes an incoming mode from the remote past $t' \to -\infty$ to scatter into a superposition of transmitted and reflected modes. The outgoing modes in the remote future $t' \to \infty$ contain a mix of positive and negative frequency modes. Furthermore, the set of possible solutions is

$$D_p\left(t'\right), \quad D_{p^\star}\left(t'^\star\right), \quad D_p\left(-t'\right), \quad D_{p^\star}\left(-t'^\star\right) \tag{101}$$

where $D_p(t')$ is the parabolic cylinder function [19]. Due to the time-dependent gauge, the mode solutions are not easily identified as positive or negative frequency modes. This may be done by probing the solutions at $E = 0$ in their corresponding asymptotic limit. The ingoing positive frequency mode solution in the remote past becomes,

$$\phi_{\text{in}}(t') = D_{p^\star}\left(-t'^\star\right), \quad t' \to -\infty \tag{102}$$

Furthermore, as the ingoing positive frequency mode evolves, it will become a superposition of outgoing positive and negative frequency modes [19]

$$D_{p^\star}\left(-t'^\star\right) = \frac{\sqrt{2\pi}}{\Gamma\left(-p^\star\right)}e^{\frac{-i\pi}{2}\left(p^\star+1\right)}D_p\left(t'\right) + e^{i\pi p^\star}D_{p^\star}\left(t'^\star\right), \quad t' \to \infty \tag{103}$$

where $D_p\left(t'\right)$ and $D_{p^\star}\left(t'^\star\right)$ are the positive and negative frequency modes respectively. Therefore, the Bogolubov coefficients are,

$$\alpha_\lambda = \frac{\sqrt{2\pi}}{\Gamma(-p^\star)}e^{-\frac{i\pi}{2}\left(p^\star+1\right)}, \quad \beta_\lambda = e^{\pi i p^\star} \tag{104}$$

The effective Lagrangian reads,

$$\mathscr{L}_{eff} = i\frac{E}{2\pi}\int\frac{dk_z dk_y}{(2\pi)^2}\left[\ln\left(\sqrt{2\pi}\right) - \ln\left(\Gamma\left(-p^\star\right)\right) - \frac{i\pi}{2}\left(p^\star + 1\right)\right] \tag{105}$$

which contains divergencies which may be removed by regularization [27]. The probability of creating particle pairs can be found using Eq.(91). However, it may also be extracted from effective Lagrangian. The gamma function can be written as a heat kernel-type integral [19],

$$\ln\left(\Gamma\left(-p^\star\right)\right) \sim \int_0^\infty \frac{1}{s_M}\frac{e^{p^\star s_M}}{1 - e^{-s_M}}ds_M = \frac{1}{2}\int_0^\infty \frac{1}{s_M}e^{p^\star s_M}e^{\frac{1}{2}s_M}\operatorname{csch}\left(\frac{s_M}{2}\right)ds_M \tag{106}$$

Due to the poles on top of the integration contour R_+, the integral is mathematically ill-defined [28]. By wick rotating to Euclidean Schwinger proper time $s_M \to 2iEs$ and performing the k_z and k_y integrals, the effective Lagrangian reads

$$\mathscr{L}_{eff} = -\frac{1}{16\pi^2}\int_0^\infty \frac{ds}{s^3}e^{-\mu^2 s}\left[Es\csc\left(Es\right) - 1 - \frac{E^2 s^2}{6}\right] \tag{107}$$

The latter two terms follow from the renormalization prescription. The result agrees with Eq.(65) and yields the same probability of creating a particle pair per spacetime volume. Using the Bogolubov prescription, the probability of creating particle pairs using Eq.(91) is,

$$2\Im(\mathscr{L}_{eff}) = \frac{E}{2\pi}\int\frac{dk_z dk_y}{(2\pi)^2}\ln\left(1 + e^{-\frac{\pi}{E}\left(\mu^2 + k_z^2 + k_y^2\right)}\right) = \frac{E^2}{8\pi^3}\sum_{n=1}^{\infty}\frac{(-1)^{n+1}}{n^2}e^{-\frac{\mu^2\pi n}{E}} \tag{108}$$

Therefore, this method recovers the result in Eq.(67) but omits the use of a renormalization prescription. A similar analysis can done using scattering theory, where the ingoing mode scatters into positive and negative

frequency modes. The wave $e^{i\pi p^\star} D_{p^\star}(t'^\star)$ scatters off the potential $V(t') = -\frac{1}{2}\omega^2 t'^2$ into a transmitted wave $\alpha_k D_p(t')$ and a reflected wave $\beta_k D_{p^\star}(t'^\star)$. The reflection and transmission coefficients are, respectively,

$$R_{r,\lambda} = \frac{|\beta_\lambda|^2}{|\alpha_\lambda|^2} = \frac{1}{e^{\pi\lambda}+1} \tag{109}$$

and

$$T_{r,\lambda} = \frac{1}{|\alpha_\lambda|^2} = \frac{1}{e^{-\pi\lambda}+1} \tag{110}$$

The total probability remains conserved as $T + R = 1$. Assuming that the energy of the incident wave is large, $\lambda >> 1$, then the ingoing positive frequency wave is completely transmitted, and so the outgoing wave does not consist of a mix of positive and negative frequency modes. This implies that no particle pairs are created. A strong electric field decreases λ, making the reflection coefficient near unity. The transmission coefficient can be interpreted as the probability that no pair creation occurs in mode (k_z, k_y). Consequently, the reflection coefficient is the probability of pair creation in mode (k_z, k_y). Therefore, the product of the transmission coefficient of all modes indicates the probability that the vacuum remains unchanged. The vacuum persistence is,

$$|\langle \text{out}, 0|0, \text{in}\rangle|^2 = \prod_\lambda T_{r,\lambda} = \exp\left[-\frac{VE}{(2\pi)^3}\int dk_z dk_y \ln\left(1 + e^{-\frac{\pi}{E}\left(\mu^2+k_z^2+k_y^2\right)}\right)\right] \tag{111}$$

This result matches with Eq. (108). Due to the Lorentz gauge, the positive and negative frequency modes are not of the form $e^{\pm i\omega t}$, leading to another criterion to identify the positive and negative frequency modes. This inconvenience is omitted when using the Coulomb gauge, where $A_\mu = (Ex, 0, 0, 0)$. Since the effective Langragian is gauge-invariant, the choice of gauge would not matter. However, the particles and potentials defined in their respective gauges are different [17].

As discussed in the previous chapter, the creation of particle pairs may be interpreted as particles tunnelling through the energy gap 2μ in the Dirac sea picture. In the Dirac sea picture, the vacuum is filled with negative energy solutions whilst the positive energy solutions are empty. An energy gap of 2μ separates the negative and positive bands. In Figure (4), the gap is tilted due to the potential Ex. This allows for a negative energy state to tunnel through the gap. The tunnelling corresponds to creating a particle in the positive energy band. The negative energy band is no longer completely filled, indicating that the absence of the tunnelled particle creates an anti-particle.

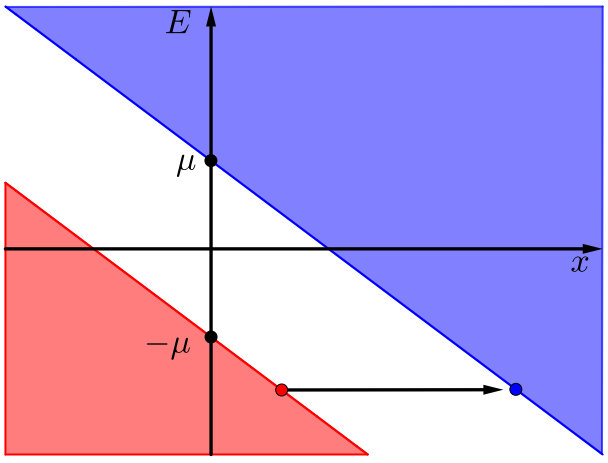

Figure 4: A schematic representation of a negative energy solution E (red dot) in the Dirac sea tunnelling through the tilted gap 2μ to the positive energy solution (blue dot).

Remarkably, the three approaches to calculating the vacuum persistence in sQED for a constant electric and magnetic background yield the same result, even though how these particles are created is physically different. Whilst the scattering approach describes the incoming modes scattering into a mix of outgoing and ingoing modes, the heat kernel approach explains the creation of particles as the separation of virtual particles from the vacuum due to the constant electric field. Furthermore, the Bogolubov approach gives insight into how the vacua are related through different field decompositions in the past and future. The equivalence between these approaches follows from the spectral properties encoded within the operator H, which links the eigenvalues, Bogolubov coefficients and scattering coefficients with particle production.

Semi-classical Gravity

Quantizing gravity is a challenging task, and a full theory of quantum gravity still eludes physicists. However, there are strategies for combining quantum field theory with general relativity. In the *semi-classical* approach, the gravitational field is treated as a classical background, while the matter fields are quantized. This approach is widely applicable to many physical systems where the quantum effects of the matter fields dominate. However, it breaks down in extreme conditions such as singularities where quantum fluctuations in the gravitational field become significant. Quantizing the matter fields in Einstein's field equation yields,

$$R_{\mu\nu} - \frac{1}{2}Rg_{\mu\nu} + \Lambda g_{\mu\nu} = -8\pi G \left\langle T^{\mu\nu} \right\rangle , \tag{112}$$

where the quantized stress-energy tensor is

$$\left\langle T^{\mu\nu} \right\rangle = \frac{\langle 0, \text{out}| \, T_{\mu\nu} \, |0, \text{in}\rangle}{\langle 0, \text{out} \, |0, \text{in}\rangle} = \frac{2}{\sqrt{-g}} \frac{\delta W}{\delta g^{\mu\nu}}. \tag{113}$$

In Minkowski spacetime, particle creation requires an external source $J(x)$, as, for example, shown by the Schwinger effect. In curved spacetime, in the absence of external sources, the gravitational field generally ensures that the in-and out-vacuum differ,

$$\langle 0, \text{out} \, |0, \text{in}\rangle \neq 1. \tag{114}$$

Consequently, the effective action may contain an imaginary part with contributions coming from the topology of the manifold [21].

The power of the heat kernel as a mathematical tool comes from the fact that it can be extended to more complex manifolds. The heat kernel connects the complex geometry of the manifold with the behaviour of the quantized matter fields. In general, exact solutions for the heat kernel are unavailable, and approximation schemes are needed [15]. The two most common approximations are the Schwinger-DeWitt representation and the covariant perturbation theory. The Schwinger-DeWitt expansion follows from the small s expansion of the nonlocal form factors in covariant perturbation theory [29]. The effective action in the Schwinger-DeWitt expansion in curvature terms for a scalar field reads [21],

$$W = \frac{1}{2}\frac{1}{(4\pi)^2}\sum_{j=0}^{\infty}\int d^4x\sqrt{g}a_j(x)\int_0^{\infty}\frac{ds}{s^3}s^j e^{-\mu^2 s} \tag{115}$$

where the coefficients $a_j(x)$ are given by

$$a_0(x) = 1, \tag{116a}$$

$$a_1(x) = \left(\frac{1}{6} - \xi\right)R, \tag{116b}$$

$$a_2(x) = \frac{1}{180}\left(R_{\mu\nu\alpha\beta}R^{\mu\nu\alpha\beta} - R_{\mu\nu}R^{\mu\nu}\right) - \frac{1}{6}\left(\frac{1}{5} - \xi\right)\Box R + \frac{1}{2}\left(\frac{1}{6} - \xi\right)R^2 + \frac{1}{12}\hat{\mathcal{R}}_{\mu\nu}\hat{\mathcal{R}}^{\mu\nu}. \tag{116c}$$

These first three terms in the effective action are UV divergent and purely geometrical and can be absorbed by counterterms in the gravitational part of the Lagrangian, which renormalize the cosmological constant, gravitational constant and higher-order curvature terms[21]. Once these different terms have been removed via renormalization, the remaining renormalized effective action can probe the local structure of the manifold and its quantized matter fields.

The Schwinger-DeWitt expansion is only valid for weak fields and small curvatures, which ensures convergence. Moreover, Since the expansion of Eq. (115) for $j \geq 3$ will always be real, extracting an imaginary part will not yield an exact result, as part of the information contained in the Schwinger-DeWitt effective action is discarded. An exact covariant form is required to extract the imaginary part from the poles of the effective action. Therefore, the perturbative heat kernel may not be reliable for calculating particle production in curved spacetimes.

Black Holes

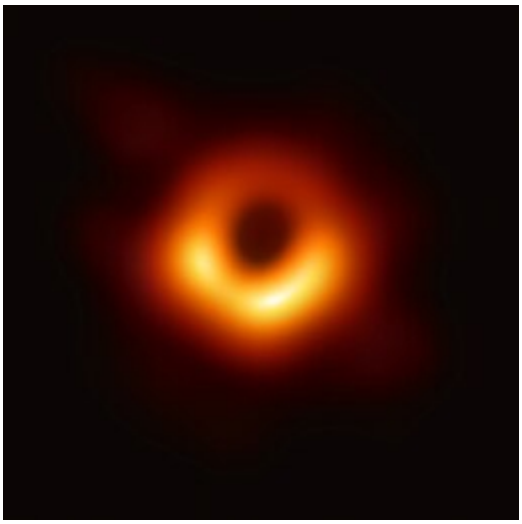

Figure 5: The supermassive black hole at the centre of the galaxy Messier 87. The first image ever taken of a black hole.

Introduction

A sufficient massive spherical (fluid) object will eventually undergo complete gravitational collapse. Not all astrophysical objects will suffer this fate; if the pressure inside the object is great enough, it may live forever. For massive stars, however, the fuel to support the outwards pressure will run out, dooming it to become a black hole. The fate of light stars differs from that of heavy ones as the electron or neutron degeneracy pressure can halt the gravitational collapse, creating white dwarfs or neutron stars, respectively. If a star exceeds the Chandrasekhar limit at a mass of $1.44\mathrm{M}_{\odot}$, the electron degeneracy pressure will not be enough to resist gravitational collapse [7].

The black hole creates a region bounded by a surface in spacetime from which nothing can escape classically. This surface boundary, from which there is no point of return, is called the *event horizon*. Any observer past the event horizon can not escape as all geodesics lead toward the *singularity* of the black hole. This creates an irreversible process in which the system is non-time-symmetric [30].

The initial state of a star potentially consists of an infinite set of parameters to characterize its behaviour precisely. Quantum unitarity formulates that the state's evolution is time-symmetric, so the amount of information captured in the state must be conserved in time. When this well-defined initial state collapses into a black hole, its behaviour can be described by a small number of parameters according to a *no-hair theorem*. However, the question arises: Where did the information go? Classically, the information can be considered hidden behind the event horizon. [7]

However, this answer does not account for quantum mechanics. By introducing quantum mechanics into the dynamics of black holes, it turns out that they are not so black at all. They radiate particles (*Hawking radiation*) and, after a long time, are completely evaporated. Hawking calculated that the radiation spectrum is thermal, which means there is no trace of all the information that made up the black hole [1]. Assuming that the Hawking radiation is entangled with the quanta that fell into the black hole, its information can be retrieved. However, the inconsistency of where the information went remains paradoxical, even if it is assumed to be encoded in the radiation spectrum.

Hawking radiation implies that black holes have an associated temperature characterized by $T = \frac{1}{8\pi M}$.[3] The entropy of a black hole is related to its temperature via the laws of black hole thermodynamics, which are analogous to the laws of classical thermodynamics. The entropy of a black hole is given by,

$$S_{BH} = \frac{A}{4}, \tag{117}$$

[3] The temperature given is for a non-rotating, uncharged black hole in Schwarzschild geometry

where A denotes the area of the black hole. Using statical mechanics, the black hole entropy can be interpreted as a measure of the number of microstates corresponding to the characteristic parameters of the black hole [31]. Therefore, it has been suggested that the information of all pre-infallen quanta is scrambled across the event horizon, as shown in Figure (6) [32]. Before evaporation, the black hole begins in a pure state because of its formation from a gravitational collapse of matter. Moreover, since no particles are emitted, the von Neumann radiation entropy, also known as the entanglement entropy, is zero. [33]

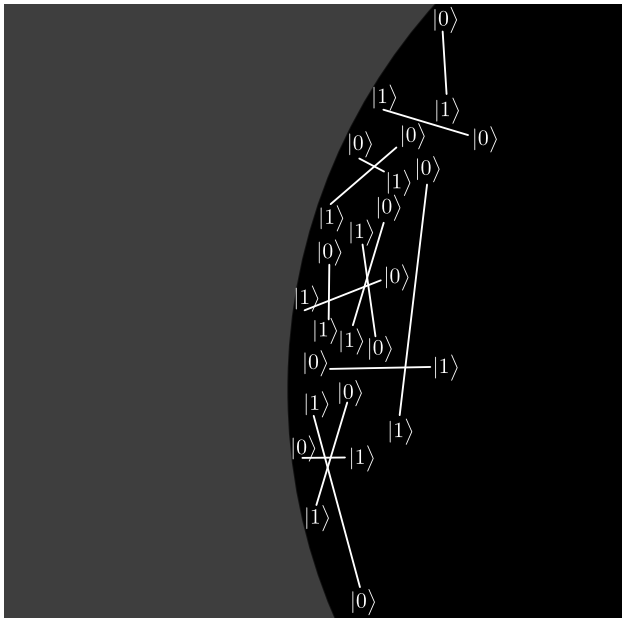

Figure 6: A schematic representation of the scrambled information on a black hole's event horizon at the beginning of its lifetime. The entangled degrees of freedom, represented as links between states, are denoted as qubits and illustrate the scrambled information of all pre-infallen quanta on the event horizon.

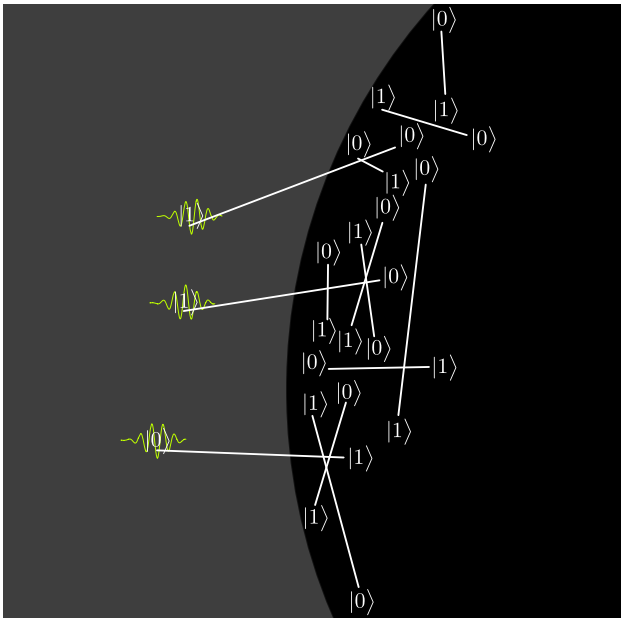

Figure 7: A schematic representation of the encoded information emitted through Hawking radiation. The entangled degrees of freedom, represented as links between states, and Hawking radiation are denoted as qubits.

The entangled degrees of freedom, denoted by qubits, are eventually emitted as Hawking radiation with the encoded information, as shown in Figure (7). The first leakage of Hawking radiation contains little information, as a large part of the information remains at the event horizon. Nonetheless, the von Neumann entropy increases whilst the black hole entropy decreases.

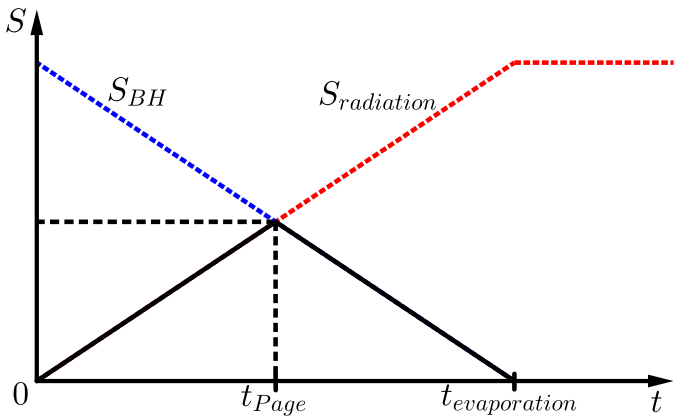

Figure 8: A schematic representation of the Page curve. The dotted red line denotes the calculated Hawking radiation entropy $S_{radiation}$, and the dotted blue line presents the black hole entropy S_{BH}. Up until the Page time, the von Neumann entropy follows the curve of the calculated Hawking radiation entropy. At the Page time, the von Neumann entropy reaches a maximum and decreases proportional to the black hole entropy. During the Page time and evaporation time $t_{evaporation}$, the Hawking radiation becomes increasingly possible to decode.

Eventually, as more Hawking radiation is emitted, the information about the pre-infallen quanta can be reconstructed. Once fully evaporated, the von Neumann entropy is non-zero. This indicates that the initial pure state has evolved into a mixed state, which is forbidden according to unitarity. The black hole entropy and von Neumann entropy will cross during the evaporation. This is contradictory as the number of degrees of freedom of a black hole determines its entropy, which must always be greater than the von Neumann entropy. To preserve unitarity, the von Neumann entropy must decrease to zero after reaching a maximum, as shown in Figure (8). This occurs at the *Page time*, approximately half the total time of full evaporation. Before the Page time, the radiation appears nearly thermal and carries little information.

Information Paradox

When the black hole completely evaporates, the information hidden behind the event horizon will be destroyed. Therefore, the information is somehow encoded in Hawking radiation. However, this is contradictory as it breaks the fundamental principles of general relativity or quantum mechanics. To understand the potential violation of these fundamental principles, consider an inertial observer, Alice, with a single qubit $|\psi\rangle$ of information falling into a black hole. An outside observer, Bob, at fixed radius $r \gg r_s$, witnesses that Alice will never cross the event horizon as Alice redshifts far into the infrared and flattens on the surface of the black hole. However, in Alice's infalling reference frame, she crosses the event horizon and merges with the singularity. Assuming that Bob can capture all the emitted Hawking radiation as the black hole evaporates, he will be able to unscramble the information from the Hawking radiation to fully recover Alice and her qubit $|\psi\rangle$. While Bob recovers the qubit from the radiation, the qubit in Alice's reference frame remains inside the black hole. In Figure (9a), a schematic depiction of this process shows that the infalling and radiated qubits coincide on the Cauchy surfaces from when the qubit is emitted till the full evaporation of the black hole. At emission, the qubit's state is cloned onto the Hawking radiation, indicating a violation of quantum unitarity through the *no-cloning theorem*. When the black hole completely evaporates, only a single worldline of the qubit's state contained in the Hawking radiation remains, and unitarity is again conserved. As shown in Figure (9b), unitarity can also be violated if, instead of being cloned, the qubit's state inside the black hole is deleted during the black hole evaporation, and the Hawking radiation contains no information about the infalling qubit. Alternatively, the qubit never crosses the horizon in both reference frames and is eventually emitted as Hawking radiation, as shown in Figure (9c). Nevertheless, while preserving unitarity, the equivalence principle is violated as Alice and her qubit are no longer an inertial observer. [34]

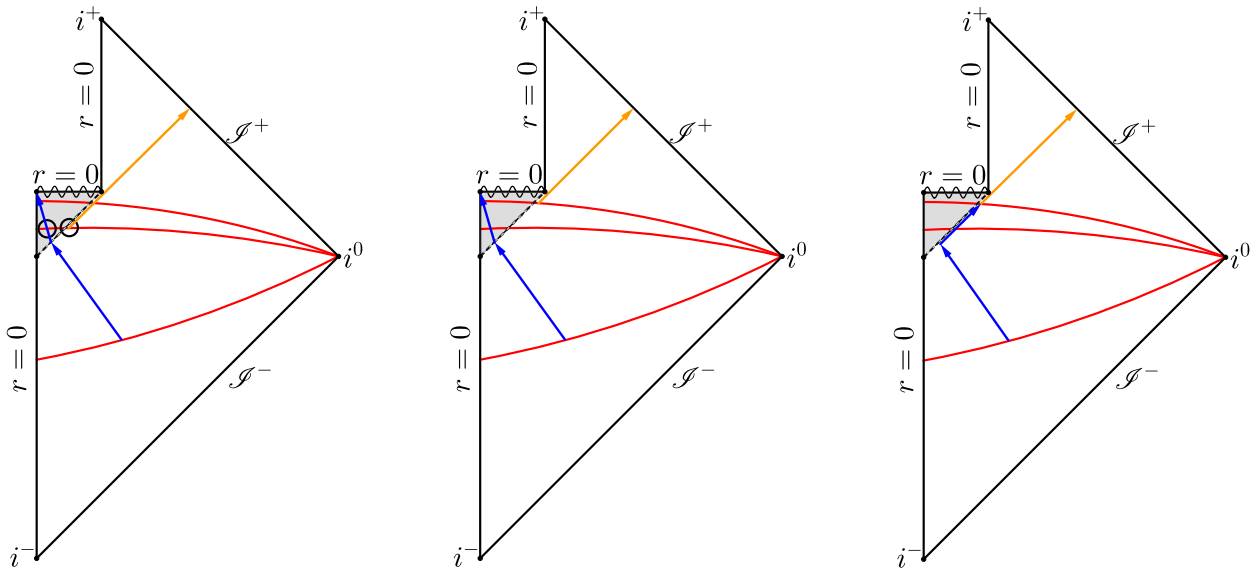

(a) The infalling and radiated qubits coincide on the Cauchy surfaces, indicating that the qubit has been cloned onto the Hawking radiation.

(b) The infalling qubit is deleted, and the Hawking radiation contains no information.

(c) The infalling qubit never crosses the event horizon and eventually is emitted.

Figure 9: Three conformal diagrams for the worldline of a qubit $|\psi\rangle$ (blue arrows) falling into a black hole (grey area). The qubit is emitted through Hawking radiation (orange vector) through the black hole evaporation process. The Cauchy surfaces (red lines) indicate a time slice.

Black Hole Complementarity and Firewalls

Attempts have been made to reconcile the information paradox's inconsistencies while preserving the physics of quantum mechanics and general relativity. One such attempt is *black hole complementarity* [35]. To preserve the qubit's information that fell into the black hole, its state must be encoded into the emitted Hawking radiation. This implies that unitarity is conserved before emission and after the black hole has fully evaporated. However, unitarity is no longer conserved during the intermediate stage as its state is supposedly cloned onto the emitted Hawking radiation and coincides on the same Cauchy surface. Black hole complementarity reconciles the cloning problem by stating that there does not exist an observer to measure both the qubits' states and the Hawking radiation. The infalling qubit will always exist outside the light cone of the emitted Hawking radiation, as shown in Figure (10). Therefore, no observer exists to verify the cloning of the qubit's state onto the Hawking radiation and unitarity is not violated. Moreover, black hole complementarity and wave-particle duality share a similar view of observer-dependent realities. In wave-particle duality, the type of measurement performed determines whether the system reveals its particle-like or wave-like behaviour. Similarly, for black holes, the observer's location, either infalling or stationary outside the black hole, determines where they perceive the state's information. [34]

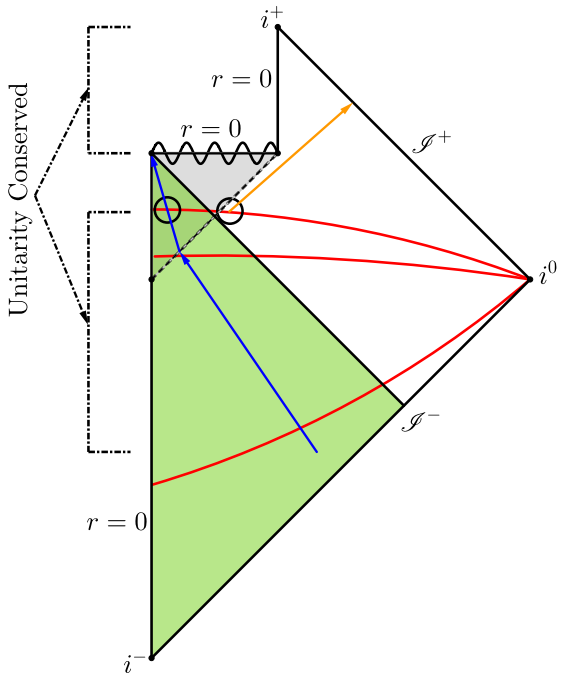

Figure 10: A conformal diagram for the worldline of a qubit $|\psi\rangle$ (blue arrow) falling into a black hole (grey area). The qubit's state is cloned on the emitted Hawking radiation (orange arrow). The green shaded area denotes the qubit's past lightcone at the singularity. Note that the emitted Hawking radiation does not coincide inside the past light cone, indicating that the Hawking radiation and qubit can never be simultaneously observed.

Another such attempt is by considering a screen of extreme energy at the event horizon called a *black hole firewall* [36], which prevents anything from crossing it. Consider a qubit emitted as Hawking radiation and entangled with another qubit that remains on the event horizon as shown in Figure (7). For the remaining qubit to be eventually emitted as Hawking radiation, another entanglement is required, with an adjacent qubit residing in the black hole's interior. The remaining qubit is entangled with both the emitted and the adjacent qubit. Since the emitted qubit and remaining qubit are maximally entangled, monogamy of entanglement does not allow for a third qubit to be entangled with either qubit. To break the entanglement between the remaining qubit and the adjacent qubit, an enormous amount of energy must exist at a Planck-length distance from the event horizon, which is the previously introduced firewall. The firewall completely thermalizes everything falling into it, stopping anyone from observing the black hole's interior. Moreover, the extreme gravitational redshift ensures that this firewall will become faint Hawking radiation and, therefore, almost not observable. However, having preserved unitarity, the equivalence principle is violated as a local observer will not measure an empty vacuum but instead the presence of a firewall. The vacuum is altered by some non-local influence of the black hole [32]. Alternatively, if an infalling observer does not measure a firewall, then it is clear that monogamy of entanglement is violated, and the equivalence principle holds. Therefore, without entering the black hole, an observer can measure which physical law is violated via the absence

or existence of the firewall, as shown in Figure (11). [36]

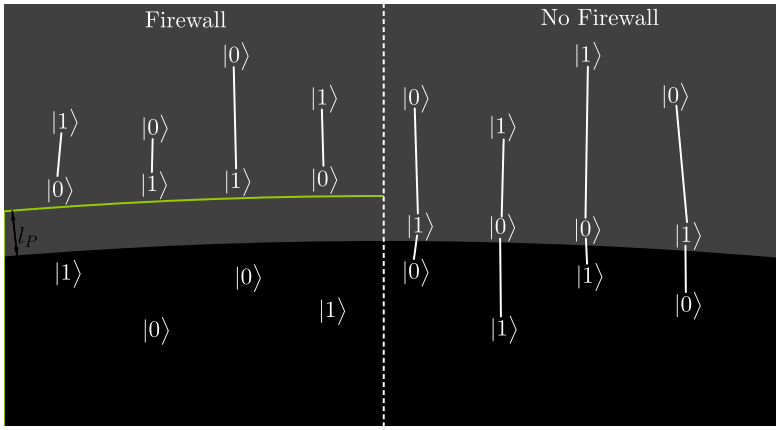

Figure 11: A schematic representation of the existence and absence of a firewall. The firewall is denoted by the yellow line and a Planck-length distance from the event horizon. In the existence of a firewall, the entanglement between the remaining and adjacent qubits is broken. However, this violates the equivalence principle, as an observer will measure an enormous amount of energy close to the event horizon. In the absence of a firewall, the remaining qubit is entangled with its adjacent and emitted qubits. This violates monogamy of entanglement as multiple qubits are maximally entangled.

Although black hole complementarity and firewalls are intriguing attempts to extend and solve the information paradox, each has distinct discrepancies. More attempts have been proposed to resolve the information paradox, but no solution has been generally accepted. To test any of the proposed solutions, black holes must be studied closely. Unfortunately, this will not be possible any time soon as the closest black hole is 1560ly away [37]. As a full theory of quantum gravity still eludes physicists, the information paradox will likely not have an accepted theoretical solution anytime soon.

Quasinormal Modes

Musical instruments, when excited, give instrument-specific notes corresponding to a characteristic vibration mode. For example, pressing a key on a piano will excite a string, creating a musical note that eventually fates. The excited vibrational energy of the string dissipates as sound waves. The sound waves contain information on the piano's properties, such as the length and material of the string.

The event horizon creates a system in which an infalling object undergoes an irreversible process toward the singularity. This non-time-symmetric property makes the boundary-valued problem non-hermitian, so perturbed black holes are intrinsically dissipative [30]. Therefore, black holes also have characteristic oscillations called *quasinormal modes* (QNMs). Much like the sound waves of the piano, the dissipation is through the emission of radiation from the coupled matter and gravitational fields.[4]

The eigenfrequencies and eigenmodes of the QNMs are found by linearizing Einstein's field equations and solving the boundary-valued eigenvalue problem numerically or analytically. The boundary conditions at the event horizon only allow for infalling modes[5] , while at spatial infinity, both ingoing and outgoing modes exist. Given that the mode amplitudes must decay in time, its eigenfrequencies ω_{QNM} contain a real and imaginary part, where the latter is strictly negative. Consequently, the eigenmodes are usually non-normalizable and do not form a complete set as the amplitude blows up at infinity. The QNMs contain information about the characteristic properties of the black hole, such as its mass, spin and charge. The non-normalizability of the eigenmodes arises from the linearization of the field equations. However, in the full quantum theory, these mode solutions must become normalizable.

Although QNMs and Hawking radiation involve dissipative processes, their origin and behaviour are distinct. In contrast to QNMs, Hawking radiation is normalizable, and its eigenfrequencies are real and continuous. While QNMs arise from perturbations in the geometry, Hawking radiation originates from fluctuations in the field that are partially trapped by the event horizon.

[4] The vibrational fluctuations in the gravitational fields are known as gravitational waves.
[5] Classically

Types of Black holes

The Einstein field equations allow for a variety of black hole-type solutions. The most notable of these solutions is the *Schwarzschild metric*, a spherically symmetric vacuum solution. This solution describes (approximately) gravitational fields outside massive bodies like stars or black holes. The Schwarzschild solution will be the primary geometry used throughout this thesis. Other prominent solutions include rotating (Kerr) black holes, charged (Reissner-Nordström) black holes, or a combination of rotation and charge (Kerr-Newman), see Table (1). Other notable spacetime geometries are AdS and dS, which are of great interest in cosmology.

	Non-rotating ($J = 0$)	Rotating ($J \in \mathbb{R}$)
Uncharged ($Q = 0$)	Schwarzschild	Kerr
Charged ($Q \in \mathbb{R}$)	Reissner-Nordström	Kerr-Newman

Table 1: A table consisting of the four most common types of black holes.

Schwarzschild Black Holes

The *Schwarzschild metric* is the unique spherically symmetric vacuum solution [7]. In spherical coordinates $\{t, r, \theta, \varphi\}$, the Schwarzschild metric reads,

$$\mathrm{d}s^2 = -\left(1 - \frac{2GM}{r}\right)\mathrm{d}t^2 + \left(1 - \frac{2GM}{r}\right)^{-1}\mathrm{d}r^2 + r^2\mathrm{d}\Omega^2 \tag{118}$$

where M is the mass of the body and $\mathrm{d}\Omega^2$ is the two-sphere metric,

$$\mathrm{d}\Omega^2 = \mathrm{d}\theta^2 + \sin^2(\theta)\mathrm{d}\varphi^2. \tag{119}$$

As the radial component r increases towards infinity, the spacetime will become indistinguishable from the Minkowski metric (*Asymptotically flat*). The metric will also become Minkowskain when $M \to 0$. There are two coordinate singularities: the Schwarzschild radius $r_s = 2GM$ (event horizon) and $r = 0$. To ensure whether a point is an honest singularity, scalar quantities constructed from curvature terms become infinite; otherwise, the point is a manifestation of the coordinate system used, called a *coordinate singularity*. The contracted Riemann tensor in Schwarzschild coordinates is,

$$R^{\mu\nu\rho\sigma}R_{\mu\nu\rho\sigma} = \frac{12r_s^2}{r^6} \tag{120}$$

shows that the coordinate $r = 0$ is an honest singularity, whilst the event horizon r_s is not.[6]

Moreover, the metric exhibits four Killing vectors, one for time symmetry and three for rotational symmetry. The Killing vector $K^\mu = (\partial_t)^\mu$ corresponding to the invariance of time translation results in energy conservation. Note that the Killing vector in the interior of the black hole becomes spacelike while the exterior becomes timelike. Due to the metric being both stationary and static, the event horizon is a *Killing horizon* with Killing vector ∂_t [7]. The *surface gravity*, $\kappa = \frac{1}{2r_s}$, associated with the Killing horizon, represents the measure of the black hole's gravitational acceleration at the event horizon. The three rotational Killing vectors corresponding to the symmetries of the $SO(3)$ group represent invariance under rotation in the three spatial directions and lead to the conservation of angular momentum.

Suitable coordinate transformations can show that the event horizon is well-behaved and nonsingular. As stated earlier, the event horizon is a point of no return; to see this, consider a fixed observer measuring a massless particle propagating radially towards the singularity. The radial null geodesics are described by,

$$\frac{dt}{dr} = \pm\left(1 - \frac{r_s}{r}\right)^{-1}. \tag{121}$$

The corresponding spacetime diagram in $t - r$ coordinates is given in Figure (12). Infinitely far away from the singularity, the light cone of the particle corresponds to those in Minkowski spacetime, $\frac{dt}{dr} = \pm 1$. As the particle propagates towards the singularity, the light cone gradually closes up, eventually reaching the event horizon, where $\frac{dt}{dr} \to \pm\infty$. From the observer's perspective, the particle will approach the event horizon but never cross it. The light cones inside the event horizon will tilt towards the singularity. Therefore, any geodesics will lead towards the singularity inside the event horizon. The Schwarzschild metric becomes unreliable for the interior of the black hole, introducing *tortoise coordinates*,

$$r_\star = r + r_s \ln\left(\frac{r}{r_s} - 1\right) \tag{122}$$

[6] Verifying honest singularities using scalar quantities is not a hard condition but a test.

such that the metric becomes,

$$\mathrm{d}s^2 = \left(1 - \frac{r_s}{r}\right)\left(-\mathrm{d}t^2 + \mathrm{d}r_\star^2\right) + r^2\mathrm{d}\Omega^2. \tag{123}$$

The coordinate transformation maps $r \in [r_s, \infty)$ onto $r_\star \in (-\infty, \infty)$. As a consequence of the coordinate transformation, the event horizon is now located at minus infinity. The radial null geodesics become,

$$\frac{dt}{dr_\star} = \pm 1 \tag{124}$$

and so,

$$t = \pm r_\star + \text{constant}. \tag{125}$$

The plus corresponds to the outgoing geodesics, and the minus corresponds to the ingoing geodesics.

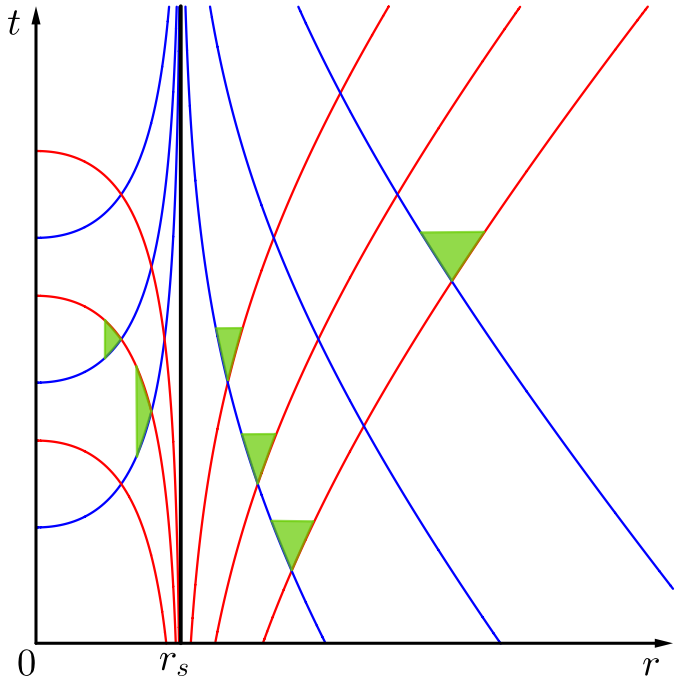

Figure 12: A Schwarzschild spacetime diagram (t, r). The light cones (green) are local projections of the accessible domain in spacetime through timelike trajectories. The blue lines represent ingoing null geodesics, and the red lines represent the outgoing null geodesics.

Additionally, define a set of radial null coordinates,

$$v = t + r_\star \tag{126a}$$

$$u = t - r_\star \tag{126b}$$

From Eq.(125), the ingoing radial null geodesics are described by $v =$ constant, while the outgoing radial null geodesics are described by $u =$ constant. The *ingoing Eddington-Finkelstein metric* is,

$$\mathrm{d}s^2 = -\left(1 - \frac{r_s}{r}\right)\mathrm{d}v^2 + (\mathrm{d}v\mathrm{d}r + \mathrm{d}r\mathrm{d}v) + r^2\mathrm{d}\Omega^2. \tag{127}$$

In these coordinates, the event horizon is no longer a coordinate singularity. The ingoing radial null geodesics are given by,

$$\frac{dv}{dr} = \begin{cases} 0, & \text{(ingoing)} \\ 2\left(1 - \frac{r_s}{r}\right)^{-1}, & \text{(outgoing)} \end{cases} \tag{128}$$

Any trajectory towards the singularity no longer asymptotes at the event horizon, and the light cones no longer close up. Hence, the spacetime is smooth and extended beyond the event horizon. However, the light cones tilt, and all light cones inside the event horizon are future-directed towards the singularity, indicating no possible trajectories to escape the black hole once inside.

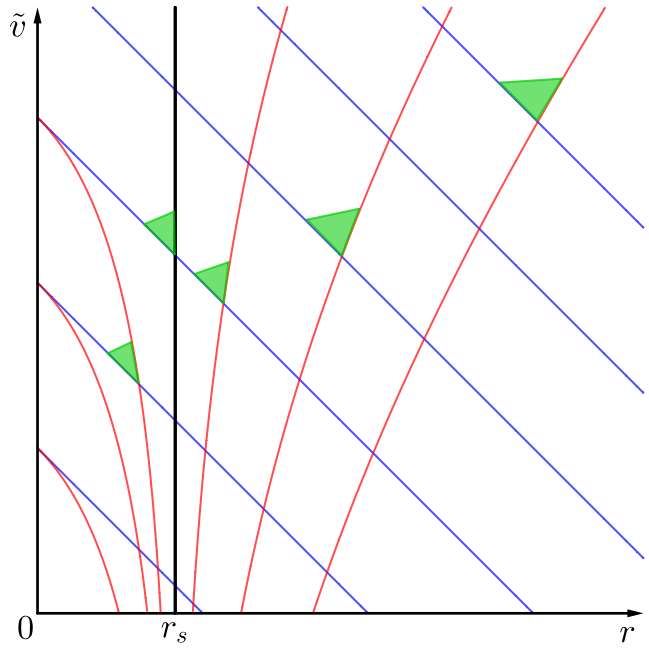

Figure 13: An ingoing Eddington Finkelstein diagram $(\tilde{v}, r)$. The coordinates are adjusted to depict the light cones (green) at 45°, $\tilde{v} = v - r$. Inside the event horizon, the light cones are directed towards the singularity.

Similarly, the *outgoing Eddington-Finkelstein metric* is,

$$\mathrm{d}s^2 = -\left(1 - \frac{r_s}{r}\right)\mathrm{d}u^2 - (\mathrm{d}u\mathrm{d}r + \mathrm{d}r\mathrm{d}u) + r^2\mathrm{d}\Omega^2. \tag{129}$$

which is also smooth across the domain $r \in (0, \infty)$. The outgoing radial null geodesics are given by,

$$\frac{du}{dr} = \begin{cases} -2\left(1 - \frac{r_s}{r}\right)^{-1}, & \text{(ingoing)} \\ 0, & \text{(outgoing)} \end{cases} \tag{130}$$

The light cones are past-directed, so all geodesics inside the event horizon lead away from the singularity. This region of spacetime from which all lightcones are past-directed is called a *white hole*.

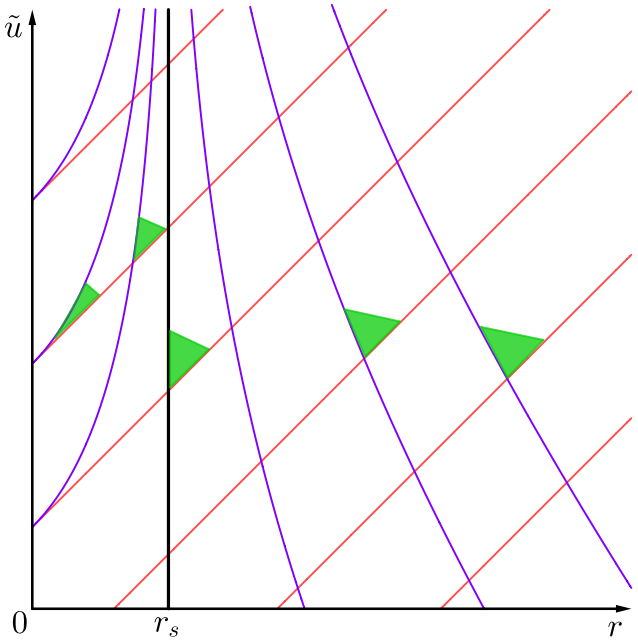

Figure 14: An outgoing Eddington Finkelstein diagram $(\tilde{u}, r)$. The coordinates are adjusted to depict the light cones (green) at 45°, $\tilde{u} = u + r$.

Hawking Radiation

Hawking radiation is a fascinating phenomenon in quantum gravity as it emerges from the combination of General Relativity and Quantum Field Theory. In his original paper, "Particle Creation by Black Holes" [1], Hawking demonstrated that a black hole (immersed in a heat bath) has a thermal radiation spectrum. At the time, this discovery was very contradictory, as classical particles would never be able to escape the gravitational pull once captured inside the event horizon. Nonetheless, numerous papers were later released confirming Hawking's original result and that black holes must evaporate [2–4]. The black hole evaporates through energy transfer between the gravitational background and the emitted radiation. As the black hole evaporates, the spacetime geometry changes. Due to the change in geometry, the radiation spectrum is no longer thermal. This new radiation spectrum may be correlated with the matter substance that fell into the black hole. Hypothetically, this makes it possible to retrieve all previously captured information. However, to this day, it remains a mystery how to incorporate the changing spacetime geometry into the calculation and how to solve the information paradox.

The previous chapters were introductory to the different methodologies that can be used to find the probability of particle production using the sQED model. These different methodologies agreed that particle production occurs in a constant electric field but not in a constant magnetic field,

$$|\langle \text{out}, 0|0, \text{in}\rangle|^2 = \exp\left[-2\Im(W)\right] = \underbrace{\prod_\lambda T_{r,\lambda}}_{\text{Tunnelling}} = \underbrace{\exp\left[-2\text{Tr}\{\ln|\alpha|\}\right]}_{\text{Bogolubov coefficients}} = \underbrace{\exp\left[-\Im\left\{i\int_0^\infty \frac{ds}{s}\text{Tr}\left(e^{-sH}\right)\right\}\right]}_{\text{Heat kernel approach}}. \quad (131)$$

Using the heat kernel approach, it was shown that the electric field made the vacuum unstable, and before annihilation could occur, it would separate the pair. Figure (3) shows that the electric field accelerates the charged quanta away from each other so the virtual particles can become real. Following this same heuristic view, the gravitational background makes the vacuum unstable. As virtual particle pairs are created, the black hole's strong tidal forces allow these virtual particles to become real, as shown in Figure (15).

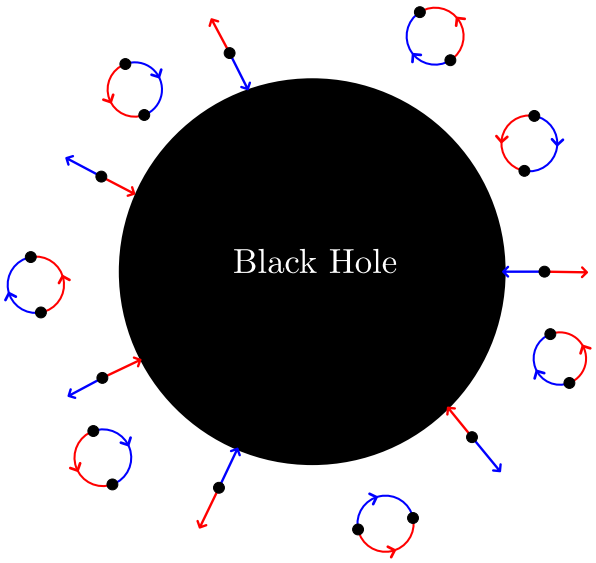

Figure 15: A schematic representation of pair particle production. The vacuum creates virtual pair particles, which may annihilate (red and blue loops) or may become real. Either the negative (red) or positive (blue) frequency modes are captured, and its opposite is emitted as radiation.

Approaching the problem of particle creation in sQED from a scattering theory perspective, i.e. calculating the transmission coefficient of a wave tunnelling through a potential, yielded the same result. Moreover, it was also shown that the result was consistent within a QFT framework through Bogolubov coefficients. Remarkably, this implies that some underlying equivalence exists for these different approaches.

This chapter aims to show that the same equivalence observed in sQED also applies to black hole radiation through the same approaches. First, Hawking's original calculation, which includes Bogolubov coefficients, will be reproduced [1]. Then, Hawking radiation will be analysed using scattering theory and tunnelling with the Damour-Ruffini method [4].

Hawking Radiation via Bogolubov coefficients

Firstly, to calculate the thermal radiation spectrum using the Bogolubov coefficients, the in and out vacua must first be defined, which will be achieved using the framework of spacetime sandwiching. Consider a massive spherical object undergoing complete gravitational collapse, where the exterior region is given by the Schwarzschild spacetime. Before the gravitational collapse, the in-vacuum is assumed to be the standard Minkowski vacuum, as the spacetime is approximately flat far from the object in early times. After the gravitational collapse, spacetime geometry changes from Minkowski to Schwarzschild. Moreover, the Schwarzschild spacetime is stationary at late times, where the out-vacuum is defined. Therefore, the in-vacuum does not correspond to the out-vacuum due to the intermediate stage, where the spacetime is topologically complex. The Bogolubov transformation between in and out vacuum states determines the particle production rate. The spectrum of produced particles is,

$$\langle 0, \text{in}| \, N_\omega \, |0, \text{in}\rangle = \int_0^\infty |\beta_{\omega\omega'}|^2 \, d\omega'. \tag{132}$$

Consider a massless scalar field in Schwarzschild geometry, then the field equation reads,

$$\left[\frac{1}{r^2}\frac{\partial}{\partial r}\left(1-\frac{r_s}{r}\right) r^2 \frac{\partial}{\partial r} - \left(1-\frac{r_s}{r}\right)^{-1}\frac{\partial^2}{\partial t^2} + \Delta\right] \Phi_{\omega lm}(t, r, \theta, \varphi) = 0. \tag{133}$$

where $\Delta = \frac{1}{r^2 \sin(\theta)}\frac{\partial}{\partial\theta}\left(\sin(\theta)\frac{\partial}{\partial\theta}\right) + \frac{1}{r^2\sin^2(\theta)}\frac{\partial^2}{\partial\varphi^2}$. The mode solutions can be decomposed as,

$$\Phi_{\omega lm}(t, r, \theta, \varphi) = \frac{1}{r}\int d\omega \sum_{l=0}^{\infty}\sum_{m=-l}^{l} Y_{lm}(\theta, \varphi) e^{-i\omega t}\phi_{\omega lm}(r), \tag{134}$$

where $Y_{lm}(\theta, \varphi)$ is the spherical harmonic mode satisfying, $\Delta Y_{lm}(\theta, \varphi) = -\frac{l(l+1)}{r^2}Y_{lm}(\theta, \varphi)$ and $\phi_{\omega ml}(r)$ is the radial mode solution. Substituting the decomposition simplifies Eq.(133) to a radial field equation rewritten in tortoise coordinates,

$$\left[\frac{d^2}{dr^{\star 2}} + \left(\omega^2 - \underbrace{\left[\frac{l(l+1)}{r^2} + \frac{r_s}{r^3}\right]\left[1-\frac{r_s}{r}\right]}_{\text{Potential barrier}}\right)\right]\phi_{\omega lm}(r) = 0. \tag{135}$$

The potential barrier partially scatters incoming modes back of the gravitational field, resulting in a superposition of incoming and outgoing modes. Moreover, due to the gravitational backscattering, the total flux at infinity is reduced by a fraction $1-\Gamma_\omega$. Although exact mode solutions exist for the field equation, calculating the Bogolubov coefficients becomes troublesome. The radial mode's exact form is unimportant if observations are done at $r \to \infty$. At $r \to \infty$, the radial equation becomes,

$$\left[\frac{d^2}{dr^{\star 2}} + \omega^2\right]\phi_{\omega lm}(r) = 0. \tag{136}$$

Therefore, the mode solutions at $r \to \infty$ are

$$\phi_{\omega lm}(r) = e^{-i\omega u} \tag{137}$$

and

$$\phi_{\omega lm}(r) = e^{-i\omega v}, \tag{138}$$

in null coordinates $u = t - r^\star$ and $v = t + r^\star$. To calculate the change in vacua, the mode decomposition in the past and future must be defined. The past null infinity $\mathscr{I}^-$ is a Cauchy surface on which a set of positive frequency modes can be defined. Decomposing the scalar field ϕ in terms of f_ω, which form a complete set of positive frequency solutions of the field equation on the $\mathscr{I}^-$,

$$\phi = \int \mathrm{d}\omega \left(f_\omega a_\omega + f_\omega^* a_\omega^\dagger\right), \qquad \forall\omega > 0. \tag{139}$$

The operators a_ω and $a_\omega^\dagger$ are the annihilation and creation operators, respectively, with the vacuum state of the ingoing particles satisfying, $a_\omega \, |0, \text{in}\rangle = 0$. The positive frequency solutions at $\mathscr{I}^-$ are

$$f_\omega = e^{-i\omega v}. \tag{140}$$

Since this wave can either scatter or be absorbed, it can be separated into

$$f_\omega = f^1_\omega + f^2_\omega, \tag{141}$$

where f^1_ω is the part that is backscattered to $\mathscr{I}^+$ and f^2_ω denotes the part that is absorbed by the black hole. In terms of Bogoliubov coefficients, this decomposition reads,

$$\alpha_{\omega\omega'} = \alpha^{(1)}_{\omega\omega'}\delta_{\omega\omega'} + \alpha^{(2)}_{\omega\omega'} \tag{142a}$$

$$\Gamma_\omega = \int d\omega' \left(\left|\alpha^{(2)}_{\omega\omega'}\right|^2 - \left|\beta^{(2)}_{\omega\omega'}\right|^2 \right). \tag{142b}$$

The fraction of the ingoing wave that is absorbed causes the particle production since this part of the wave is no longer transmitted from $\mathscr{I}^-$ to future null infinity $\mathscr{I}^+$ [38]. At late times, to define a complete set of positive frequency modes, solutions of the field equation at the event horizon H^+ and $\mathscr{I}^+$ are required as $\mathscr{I}^+$ does not form a Cauchy surface. Therefore, the scalar field can be expanded as,

$$\phi = \int \mathrm{d}\omega \left(b_\omega p_\omega + b^\dagger_\omega p^*_\omega + c_\omega q_\omega + c^\dagger_\omega q^*_\omega \right), \tag{143}$$

where b_ω and $b^\dagger_\omega$ are the annihilation and creation operators respectively at $\mathscr{I}^+$, while c_ω and $c^\dagger_\omega$ are the annihilation and creation operators respectively at H^+. Additionally, p_ω defines the complete set of purely outgoing solutions, while q_ω is a complete set of solutions containing no outgoing particles. The set p_ω is required only to contain positive frequency modes such that these modes correspond to the Minkowski vacuum. This approximation cannot be made at H^+.

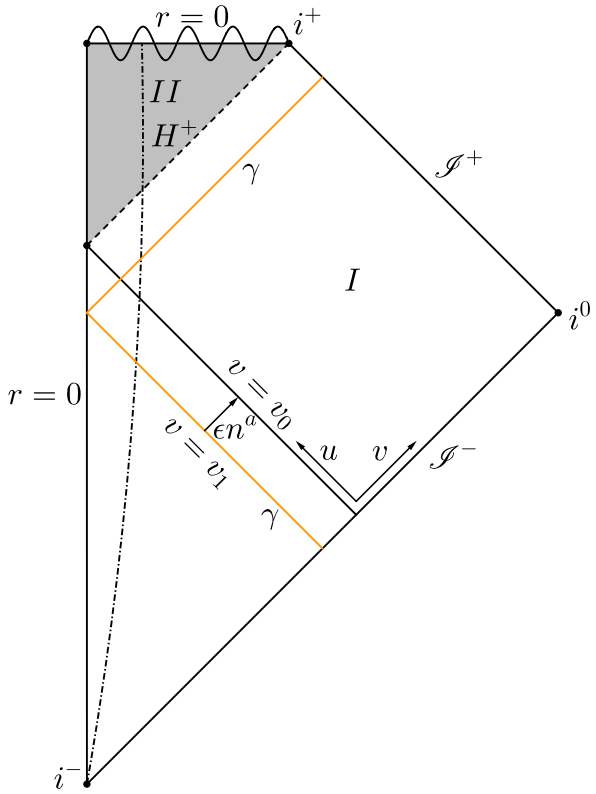

Figure 16: A Penrose diagram of a massive spherical object undergoing complete gravitational collapse (dot-dashed line) and forming a black hole. The interior and exterior of the black hole are denoted by the regions I and II, respectively. A ray γ at $\mathscr{I}^+$ propagating backwards towards the $\mathscr{I}^-$. The ray follows the geodesic $u = u_1$ passing the event horizon H^+ and continues through the collapsing object following the geodesic v_1. The infinite phase shift at $\mathscr{I}^+$ corresponds to a finite shift at $\mathscr{I}^-$ connected through the displacement vector ϵn^a.

Consider a quantum state $|\psi\rangle$ of a system consisting of observably inaccessible and accessible regions, denoted respectively by I and II in Figure (16). The observable states are $|n, I\rangle$, whereas the unobservable states are denoted by $|n, II\rangle$, assuming they are uncorrelated. Then,

$$|\psi\rangle = \sum_n p_n \,|n, I\rangle\,|n, II\rangle\,, \tag{144}$$

with density matrix

$$\hat{\rho} = |\psi\rangle \langle\psi| . \tag{145}$$

Since any observable operator $\hat{O}$ only consists of degrees of freedom in the observable region I, the expectation value is

$$\left\langle \hat{O} \right\rangle = \mathrm{tr}\left(\hat{O}\hat{\rho}^I\right), \tag{146}$$

where

$$\hat{\rho}^I = \sum_n |p_n|^2 |n, I\rangle \langle n, I| . \tag{147}$$

Any dependence on the unobservable states has been coarse-grained out. Therefore, the choice of complete basis of modes on H^+ is irrelevant when computing $\left\langle \hat{O} \right\rangle$. The positive frequency solutions at $\mathscr{I}^+$ are defined as,

$$p_\omega = e^{-i\omega u}. \tag{148}$$

To determine the particle production rate, the outgoing modes are decomposed in terms of the positive and negative frequency components at $\mathscr{I}^-$. Consider a light ray starting at $\mathscr{I}^+$ traversing backwards towards $\mathscr{I}^-$. The ray follows the geodesic u_1 near the event horizon, passes through the collapsing star, and continues along the geodesic v_1 toward $\mathscr{I}^+$, as depicted in Figure (16). The ray tracing along a null geodesic is only valid if it satisfies the geometric optics approximation. Specifically, it requires the effective frequency to be very high near the event horizon relative to the spacetime curvature. As $v_1 \to v_0$, the phase of the wave goes through an infinite number of cycles as the geodesic $u_1 \to u$, justifying the geometric optics approximation [39]. The ray at v_1 is connected to v by a geodesic displacement vector ϵn^a, where $n^a = \frac{\partial}{\partial u}$. At H^+, the vector $p^a = \frac{du}{d\lambda}\frac{\partial}{\partial u}$ is also tangent to an ingoing null geodesic and parallel to n^a, $p^a = Bn^a$. Solving the geodesic equation for p^a gives the affine parameter λ,

$$\lambda = -Be^{-\kappa u}, \tag{149}$$

where B is some constant and $\kappa = \frac{1}{2r_s}$ is the surface gravity [39]. Moreover, in local coordinates, the geodesic equation reads $\frac{dp^\mu}{d\lambda} = 0$, which is solved by,

$$\lambda p^\mu = -\epsilon n^\mu. \tag{150}$$

Substituting Eq.(149) into Eq.(150) gives the relation between geodesics,

$$v_0 - v = \epsilon = Ce^{-\kappa u}, \tag{151}$$

which connects the infinite blueshift of the ray with the deviation ϵ. The parameters v_0 and C can be arbitrarily chosen as they do not contribute to the final answer. The mode solution at $\mathscr{I}^-$ is given by

$$\begin{aligned} &\phi \sim e^{i\frac{\omega}{\kappa}\ln(v_0 - v)}, && v_0 < v, \\ &\phi = 0, && v > v_0. \end{aligned} \tag{152}$$

where $\phi = 0$ for $v > v_0$, since these waves, when ray traced back, would look like they are coming out of the black hole. The Bogolobov coefficients can be computed by substituting the corresponding mode solutions, f_ω and p_ω in v-coordinates into Eq. (79),

$$\alpha^{(2)}_{\omega\omega'} = \frac{1}{2\pi}\int_{-\infty}^{v_0} dv \left(\sqrt{\frac{\omega'}{\omega}} - \sqrt{\frac{\omega}{\omega'}}\frac{1}{\kappa(v - v_0)}\right) e^{i\omega' v} e^{i\frac{\omega}{\kappa}\ln(v_0 - v)} \tag{153a}$$

$$= \frac{1}{i\pi\sqrt{\omega\omega'}} (i\omega')^{-i\frac{\omega}{\kappa}} \Gamma\left(1 + i\frac{\omega}{\kappa}\right), \tag{153b}$$

$$\beta^{(2)}_{\omega\omega'} = -i\alpha^{(2)}_{\omega,-\omega'}, \tag{153c}$$

where $v_0 = 0$ [21]. The Fourier transformation vanishes for $v > v_0$ making the coefficient $\alpha^{(2)}_{\omega\omega'}$ analytic in the lower half complex ω' plane. The spectrum of produced particles, Eq.(132), diverges logarithmically as $\omega' \to 0$. Therefore every mode ω, creates an infinite number of particles at $\mathscr{I}^+$. The coefficient $\alpha^{(2)}_{\omega\omega'}$ contains a logarithmic branch cut at $\omega' = 0$, therefore to obtain $\beta^{(2)}_{\omega\omega'}$ from $\alpha^{(2)}_{\omega\omega'}$ one has to analytically continue $\alpha^{(2)}_{\omega\omega'}$ anticlockwise around the singularity. This leads to,

$$|\alpha_{\omega\omega'}| = e^{\frac{\pi\omega}{\kappa}} |\beta_{\omega\omega'}| . \tag{154}$$

By localizing the modes as wavepackets, the infinite number of particles at $\mathscr{I}^+$ indicate a finite particle flux. This can be done by discretizing the modes confined to a box with periodic boundary conditions [21]. Combining Eq.(142a) and Eq.(154), the number of particles emitted per mode is

$$N_\omega = \frac{\Gamma_\omega}{e^{4\pi\omega r_s} - 1} \tag{155}$$

This spectrum is thermal with temperature $T = \frac{\kappa}{2\pi}$. The black hole is in thermal equilibrium with a surrounding heat bath regardless of the backscattering effect since the rate between emission and absorption per mode is independent of the fraction Γ_ω. The Γ_ω is also known as the *greybody factor*, the classical absorption coefficient for a scattering scalar field. In small and large frequencies, this factor is given by

$$\begin{aligned} \Gamma_\omega &\to 1, & \omega &\gg \frac{1}{M} \\ \Gamma_\omega &\to \frac{A}{4\pi}\omega^2, & \omega &\ll \frac{1}{M}. \end{aligned} \tag{156}$$

The thermal spectrum implies a loss of information as there is no correlation between the emitted quanta and the previously infallen matter. Furthermore, neglecting the backscattering of the potential barrier, the vacuum persistence is given by,

$$2\Im(W) = \mathrm{Tr}\big\{\ln\left(1 + N_\omega\right)\big\} = \int d^4x\sqrt{-g}\frac{1}{4\pi r_s}\sum_{m,l}\int_0^\infty \frac{d\omega}{2\pi}\ln\left(1 + \frac{1}{e^{4\pi\omega r_s} - 1}\right) \tag{157}$$

The factor $\frac{1}{4\pi r_s}$ corresponds to the number of states per mode ω [25]. Thus

$$2\Im(\mathcal{L}_{eff}) = -\frac{1}{4\pi r_s}\sum_{m,l}\int_0^\infty \frac{d\omega}{2\pi}\ln\left(1 - e^{-4\pi\omega r_s}\right) = \sum_{m,l}\frac{1}{192 r_s^2 \pi} \tag{158}$$

is exactly the total flux of emitted radiation [40]. Furthermore, the vacuum persistence becomes near unity for massive black holes, $r_s \to \infty$ and consequently, particle production is suppressed.

In Minkowski spacetime, the quantum fields still vibrate in the absence of particles due to the vacuum fluctuations. These fluctuations are unobservable, as only differences in energy between states are measurable. However, an external field can[7] disrupt the vacuum, and the fluctuating modes may no longer cancel out. For a black hole, the field is disrupted by the event horizon, and fluctuations in the field no longer annihilate each other. These vacuum fluctuations give rise to virtual particle pairs with a broad range of wavelengths. In Figure (17), a schematic representation of the disruption of the field modes is given.

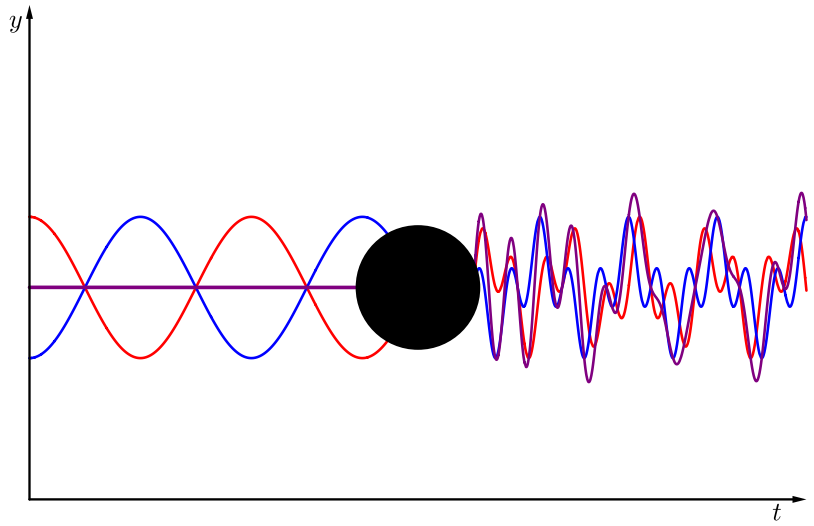

Figure 17: A schematic representation of the disruption a black hole makes in the field. Before the creation of the black hole, the field is in equilibrium; the excitations (red and blue) annihilate each other, and no real particles are created (purple). A black hole disrupts the field, and fluctuations no longer cancel out, creating real particles (purple) that carry away energy from the black hole.

The event horizon entraps some of the modes which can no longer annihilate with their counterparts. The modes with longer wavelengths have a large spatial extent, making them more likely to be partially trapped

[7] Not all external fields disrupt the vacuum.
[8] The interaction is through the partial entrapment of the modes.

inside the event horizon. Shorter wavelengths have a smaller spatial extent and are, therefore, less likely to be partially trapped by the event horizon. Consequently, there are more modes with longer wavelengths trapped than modes with shorter wavelengths. The modes that did not annihilate become real particles and escape the gravitational pull from the black hole. A large black hole predominantly emits longer wavelengths, as those are more likely to interact[8] with the event horizon and not annihilate with their counterpart. This is directly reflected in the radiation spectrum, as smaller frequencies dominate the number of particles emitted per mode for large black holes. These modes carry away energy (proportional to their frequency) from the black hole, causing the black hole to evaporate slowly.

In contrast to the Schwinger effect for a constant electric field, it is the event horizon that causes the creation of particles, not the gravitational field. However, the gravitational background coupled to the scalar field ensures the particle extracts its energy from the mass of the black hole. It is not the gravitational background that accelerates the virtual particles far enough; it is the event horizon that entraps some of the fluctuating modes.

The Damour-Ruffini Method: a Scattering Approach to Hawking Radiation

Similar to particle production in sQED, scattering theory can be used to find the vacuum persistence. This provides a heuristic tunnelling picture, where particles traverse through the event horizon and escape towards infinity. The Bogolubov coefficients are related to the transmission and reflection coefficients by,

$$T_{l,\omega} = \frac{|\beta_{\omega\omega'}|^2}{|\alpha_{\omega\omega'}|^2} = e^{-4\pi\omega r_s}, \tag{159}$$

and

$$R_{l,\omega} = \frac{1}{|\alpha_{\omega\omega'}|^2} = 1 - e^{-4\pi\omega r_s}. \tag{160}$$

The Damour-Ruffini method offers a scattering approach to Hawking radiation by directly computing the reflection and transmission coefficients, eliminating the need to calculate the Bogolubov coefficients [4, 41]. The radial field equation, Eq.(133), in the near horizon limit in tortoise coordinates reduces to,

$$\left(-\frac{\partial^2}{\partial t^2} + \frac{\partial^2}{\partial r_\star^2}\right) R(t,r) = 0, \tag{161}$$

where

$$r_\star = r + r_s \ln|r - r_s| = \begin{cases} r + r_s \ln(r - r_s), & r > r_s, \\ r + r_s \ln(r_s - r), & r < r_s. \end{cases} \tag{162}$$

The ingoing and outgoing mode solutions are, respectively,

$$R^{in}(t,r) = e^{-i\omega v}, \tag{163a}$$

$$R_I^{out}(t,r) = e^{-i\omega u} = (r - r_s)^{2i\omega r_s}\, e^{2i\omega r} e^{-i\omega v}, \quad r > r_s. \tag{163b}$$

The ingoing wave in v coordinates is well-behaved over the entire r- and v-domain. While the outgoing wave is only well-behaved in region I. As the outgoing wave approaches H^+, there are an infinite number of cycles, so it cannot be used inside the black hole. The outgoing wave may be analytically continued such that it is valid beyond H^+ in the region II. Since the radial vector $\frac{\partial}{\partial r}$ is null and past-directed everywhere, the solution is analytically continued through the lower half of the complex r-plane,

$$R_I^{out}(t,r) \to \tilde{R}_{II}^{out}(t,r) = R_{II}^{out*}(t,r) e^{2\pi\omega r_s} \tag{164}$$

where

$$R_{II}^{out*}(t,r) = e^{-i\omega u} = e^{2i\omega r_\star} e^{-i\omega v}, \quad r < r_s. \tag{165}$$

The detailed calculations can be found in Appendix A. The outgoing null geodesics are characterized by $u =$ constant $= v - 2r_\star$, which indicates that the outgoing wave in region II propagates towards the singularity as v increases. Thus, the wave represents an ingoing anti-particle of negative energy $(-\omega)$. A schematic representation of the ingoing and outgoing particles near the event horizon is given in Figure (18). The phase of the outgoing wave makes a discontinuous jump $e^{-2\pi\omega r_s}$ at the event horizon. The general outgoing wave is,

$$\phi_\omega^{out}(t,r) = N_\omega \left(R_I^{out}(t,r) + e^{2\pi\omega r_s} R_{II}^{out*}\right), \tag{166}$$

where N_ω is the normalization factor. The anti-particle traverses back in time to scatter at the event horizon with an outgoing particle. Therefore, from scattering theory as shown in Appendix B, the probability of transmission through the event horizon is,

$$P_\omega = T_\omega = e^{-4\pi\omega r_s}. \tag{167}$$

The transmission coefficient gives the probability that a pair particle is created in mode ω [42]. The Pauli-exclusion principle for bosons allows for any number of particle pair production in each quantum state. The probability of creating any number of pairs must be conserved,

$$\text{probability of creating}\,(0\text{ pairs} + 1\text{ pair} + ... + \text{n pairs}) = C_\omega \sum_{n=0}^{\infty} P_\omega^n = 1. \tag{168}$$

This implies that $C_\omega = 1 - P_\omega$. The probability of creating n particle pairs is [42],

$$P_{n\omega} = (1 - P_\omega)P_\omega^n. \tag{169}$$

Then, the average number of pair particles emitted per mode is given by,

$$\langle N_\omega \rangle = \sum_{n=0}^{\infty} nP_{n\omega} = \frac{1}{e^{4\pi\omega r_s} - 1}, \tag{170}$$

which matches the exact thermal radiation spectrum via the Bogolubov approach. In contrast to the scattering in sQED, the reflection coefficient R_ω can be interpreted as the probability of no pair creation in mode ω. Therefore, the vacuum persistence is given by,

$$|\langle \text{out}, 0|0, \text{in}\rangle|^2 = \prod_{\omega,l,m} R_\omega = \prod_{\omega,l,m} \left(1 - e^{-4\pi\omega r_s}\right) = \exp\left[\frac{V}{4\pi r_s}\sum_{l,m}\int_0^\infty \frac{d\omega}{2\pi}\ln\left(1 - e^{-4\pi\omega r_s}\right)\right], \tag{171}$$

which matches the result found using the Bogolubov coefficients. Unlike Hawking's original method, this approach allows a natural (heuristic) interpretation of vacuum polarization from a gravitational background, where particles tunnel through the event horizon. The pair production occurs at the event horizon, where an outgoing particle propagates towards infinity, and the anti-particle falls towards the singularity, as shown in Figure (18).

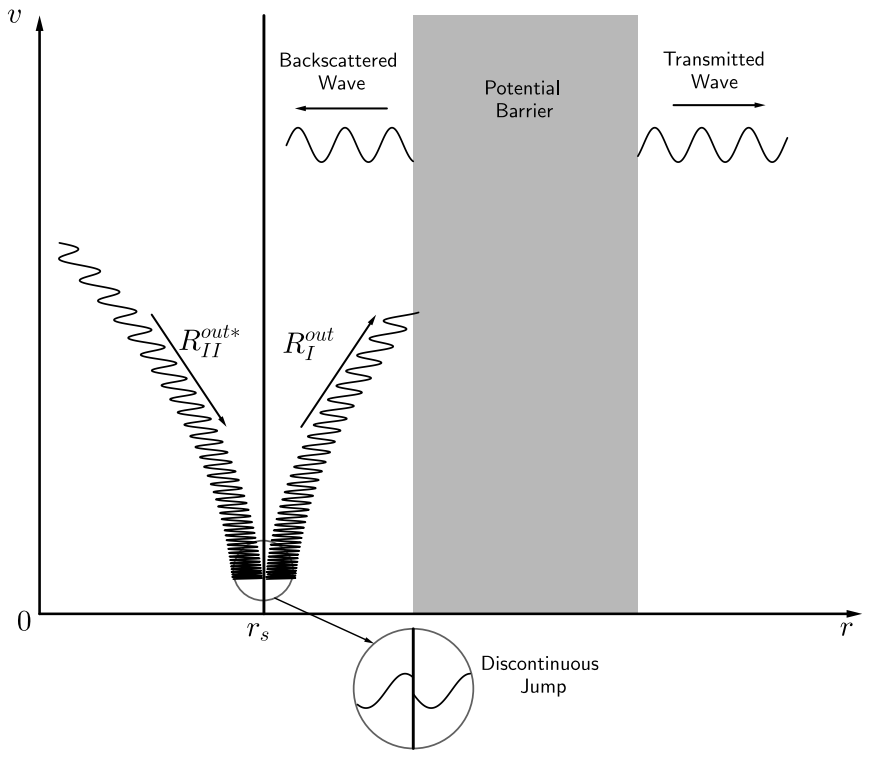

Figure 18: A schematic representation of pair particle production at the event horizon r_s in advanced Eddington-Finkelstein coordinate v. The anti-particle R_{II}^{out*} traverses towards the singularity, whereas the particle traverses the potential barrier and either is backscattered or transmitted to infinity. The anti-particle makes a phase jump at the event horizon.

This suggests that particle production arises directly from the presence of an event horizon, where modes make a discontinuous jump. Moreover, rewriting Eq. (161) in Schrödinger form reduces to,

$$\left[\frac{\partial^2}{\partial x^2} + V_H(x)\right]\phi_{\omega lm}(x) = 0, \tag{172}$$

where

$$V_H(x) = \frac{\omega^2 r_s^2 + \frac{1}{4}}{x^2}. \tag{173}$$

This near horizon field equation is directly related by a coordinate transformation to Eq. (161). It can be argued that the potential V_H is directly associated with the presence of the event horizon and, consequently, particle production, while higher-order terms only contribute to the greybody factor.

Furthermore, the Damour-Ruffini method can also be extended to calculate the Bogolubov coefficients. As opposed to calculating the transmission and reflection coefficients, this methodology gives further insight into the transformation between vacua and observables confined to region I. The field equation in Eq.(161) also allows for the mode solutions to be,

$$\begin{aligned} R^{in}(t,r) &= e^{-i\omega v}, \\ R^{out}_I(t,r) &= e^{-i\omega u}, \quad r > r_s, \\ R^{out}_{II}(t,r) &= e^{i\omega u}, \quad r < r_s. \end{aligned} \tag{174}$$

The ingoing mode solution is analytic over all regions of space-time. Moreover, the outgoing mode solutions are analytic in their respective regions, but neither is at the event horizon. Inside the event horizon, the $r_\star$ coordinate becomes timelike, and t becomes spacelike. These outgoing (Schwarzschild) modes form a second complete orthonormal basis. The field ϕ_ω may be expanded as,

$$\phi^{out}_\omega = \int d\omega \left[b^{(1)}_\omega R^{out}_I + b^{(1)\dagger}_\omega R^{out*}_I + b^{(2)}_\omega R^{out}_{II} + b^{(2)\dagger}_\omega R^{out*}_{II}\right], \tag{175}$$

where $b^{(1)}_\omega$, $b^{(2)}_\omega$,$b^{(1)\dagger}_\omega$ and $b^{(2)\dagger}_\omega$ are the annihilation and creation operators for the modes outside and inside the black hole respectively. The operator $b^{(2)}_\omega$ annihilates an excitation of the Schwarzschild mode outside the black hole in region I. While $b^{(1)}_\omega$ annihilates an excitation inside the black hole in region II. The vacuum state $|0_S\rangle$ is defined as [21],

$$b^{(1)}_\omega |0_S\rangle = b^{(2)}_\omega |0_S\rangle = 0, \quad \forall\omega > 0. \tag{176}$$

The Schwarzschild vacuum is associated with a static observer outside the black hole measuring no particles. An alternative quantization prescription based on the orthonormal mode solutions in Kruskal coordinates provides a different vacuum state $|0_K\rangle$ [41]. Transforming to Kruskal coordinates defined by,

$$\begin{aligned} \bar{u} &= -2r_s e^{-\frac{u}{2r_s}}, \\ \bar{v} &= 2r_s e^{\frac{v}{2r_s}}. \end{aligned} \tag{177}$$

The outgoing mode solutions in Kruskal coordinates are,

$$\begin{aligned} R^{out}_I(t,r) &= e^{2i\omega r_s \ln\left(-\frac{\bar{u}}{2r_s}\right)}, \quad r > r_s, \\ R^{out}_{II}(t,r) &= e^{-2i\omega r_s \ln\left(\frac{\bar{u}}{2r_s}\right)}, \quad r < r_s, \\ \tilde{R}^{out}_{II}(t,r) &= e^{2i\omega r_s \ln\left(-\frac{\bar{u}}{2r_s}\right)}, \quad r < r_s. \end{aligned} \tag{178}$$

When crossing the event horizon $\bar{u} = 0$ (or $\bar{v} = 0$), the modes of Eq.(178) pass smoothly from $\bar{u} < 0$ to $\bar{u} > 0$, and are bounded in the real and lower half of the complex $\bar{u}$-plane [21]. In contrast, the modes of Eq.(174) are non-analytic and do not cross the event horizon smoothly. The non-analytical nature at $\bar{u} = 0$ ensures a mixing of the positive and negative frequency modes. The combinations,

$$\begin{aligned} &R^{out}_I + \tilde{R}^{out}_{II}, \\ &R^{out*}_I + \tilde{R}^{out*}_{II}, \end{aligned} \tag{179}$$

are valid over all regions of space-time. The first combination is the same as Eq.(164). Rewriting the combinations as,

$$\begin{aligned} f_1 &= e^{\pi\omega r_s} R^{out}_I + e^{-\pi\omega r_s} R^{out*}_{II}, \\ f_2 &= e^{-\pi\omega r_s} R^{out*}_I + e^{\pi\omega r_s} R^{out}_{II}, \end{aligned} \tag{180}$$

which are analytic and bounded for all $\bar{u}$ and form a complete orthonormal basis for the outgoing mode solutions. The field may be expanded as,

$$\phi_\omega^{out} = \int d\omega \frac{1}{\sqrt{2\sinh(2\pi\omega r_s)}} \left[d_\omega^{(1)} f_1 + d_\omega^{(1)\dagger} f_1^\star + d_\omega^{(2)} f_2 + d_\omega^{(2)\dagger} f_2^\star \right], \tag{181}$$

where $d_\omega^{(1)}$, $d_\omega^{(2)}$,$d_\omega^{(1)\dagger}$ and $d_\omega^{(2)\dagger}$ are the annihilation and creation operators for the modes outside and inside the black hole respectively. The corresponding vacuum state is,

$$d_\omega^{(1)} |0_K\rangle = d_\omega^{(2)} |0_K\rangle = 0, \quad \forall\omega > 0. \tag{182}$$

The vacuum states $|0_K\rangle$ and $|0_S\rangle$ are not identical due to the non-analytical nature of the Schwarzschild modes at the event horizon. The vacuum $|0_K\rangle$ contains particles associated with the modes of Eq.(174). The operators $b_\omega^{(1,2)}$ and $d_\omega^{(1,2)}$ are related by taking the inner product $(\phi_\omega^{out}, R_I^{out})$ and $(\phi_\omega^{out}, R_{II}^{out})$ for both Eq.(175) and Eq.(181), then,

$$b_\omega^{(1)} = \frac{1}{\sqrt{2\sinh(2\pi\omega r_s)}} \left[e^{\pi\omega r_s} d_\omega^{(1)} + e^{-\pi\omega r_s} d_\omega^{(2)\dagger} \right], \tag{183a}$$

$$b_\omega^{(2)} = \frac{1}{\sqrt{2\sinh(2\pi\omega r_s)}} \left[e^{-\pi\omega r_s} d_\omega^{(1)\dagger} + e^{\pi\omega r_s} d_\omega^{(2)} \right]. \tag{183b}$$

An observer in region I will detect quanta associated with Schwarzschild modes [21]. The vacua are related by Eq. (82),

$$|0_K\rangle = \prod_k e^{\xi_k^\star b_{-k}^{(1)} b_k^{(2)} - \xi_k b_{-k}^{(1)\dagger} b_k^{(2)\dagger}} |0_S\rangle \tag{184}$$

with $\omega = |k|$ and $\xi_k = -\text{arctanh}\left(e^{-2\pi\omega r_s}\right)$. Decomposing the Schwarzschild vacuum in terms of the number states per region, as described in Eq.(144) gives,

$$|0_K\rangle = \prod_k \text{sech}(-\xi_k) \sum_{n_k=0}^{\infty} e^{-\frac{n_k \pi\omega}{\kappa}} |n_k, I\rangle |n_k, II\rangle. \tag{185}$$

The expectation value of an observable operator $\hat{O}$ constrained to region I is given by Eq.(146),

$$\langle 0_K| \hat{O} |0_K\rangle = \sum_{n_k} \prod_k \langle n_k, II| \hat{O} |n_k, II\rangle e^{-\frac{2n_k\pi\omega}{\kappa}} \left(1 - e^{-\frac{2\pi\omega}{\kappa}}\right). \tag{186}$$

Therefore, the reduced density matrix can readily identified as,

$$\hat{\rho}^I = \sum_n \prod_k e^{-\beta\omega n} \left(1 - e^{-\beta\omega}\right) |n_k, I\rangle \langle n_k, I|, \tag{187}$$

where $\beta = \frac{2\pi}{\kappa}$. The unobservable states in the region II are coarse-grained out, and the density matrix has become thermal. Thus the vacuum state $|0_K\rangle$ appears as a mixed state to an observer constrained to region I. [21, 41]

Damour-Ruffini Method: Incorporating The Greybody Factor

In the near horizon limit, the particles are not yet subject to the backscattering of the potential barrier. Including the potential barrier requires computing the greybody factor via numerical methods [43, 44]. In a recent study by Philipp et al. [45], the greybody factor has been computed using semi-analytical methods. This section aims to introduce the greybody factor into the vacuum persistence and provide a semi-analytical method of determining the greybody factor.

Consider the field equation in the outgoing Eddington-Finkelstein coordinates,

$$\left[\frac{1}{r^2}\frac{\partial}{\partial r}\left(r^2\left(1 - \frac{r_s}{r}\right)\frac{\partial}{\partial r}\right) - \frac{1}{r^2}\frac{\partial}{\partial u}\left(r^2\frac{\partial}{\partial r}\right) - \frac{1}{r^2}\frac{\partial}{\partial r}\left(r^2\frac{\partial}{\partial u}\right) + \Delta - \mu^2 \right] \Phi_{\omega lm}(u, r, \theta, \varphi) = 0 \tag{188}$$

The outgoing Eddington-Finkelstein coordinates contain a Killing vector $\frac{\partial}{\partial u}$, which is orthonormal to the null hypersurface $r = r_s$ for constant u. Then, the mode solutions consist of eigenfunctions from the corresponding Killing vector with eigenfrequencies ω,

$$\frac{\partial}{\partial u} u_k(u, r) = -i\omega u_k(u, r), \quad \omega > 0. \tag{189}$$

The mode solutions are decomposed as,

$$\Phi_{\omega lm}(u,r,\theta,\varphi) = \int d\omega \sum_{l=0}^{\infty} \sum_{m=-l}^{l} Y_{lm}(\theta,\varphi) e^{-i\omega u} \phi_{\omega lm}(r). \tag{190}$$

where $\phi_{\omega ml}$ describes the radial part of the mode solutions. Substituting the decomposition of Eq.(190) into Eq.(188), yields the radial field equation,

$$\left[\frac{\partial^2}{\partial r^2} + \left(\frac{2r - r_s + 2i\omega r^2}{r^2 - r r_s}\right)\frac{\partial}{\partial r} + \frac{2i\omega}{r - r_s} - \left[\mu^2 + \frac{l(l+1)}{r^2}\right]\frac{r}{r - r_s}\right]\phi_{\omega lm}(r) = 0. \tag{191}$$

The radial field equation has been written as a Confluent Heun Equation following the theory given in Appendix C. The information on the mode solutions of the CHE is contained within the generalized Riemann scheme. The corresponding outgoing Eddington-Finkelstein GRS is given by [46],

$$\begin{bmatrix} 1 & 1 & 2 & \\ 0 & r_s & \infty & \\ 0 & 0 & 1 + ir_s\omega - ir_s\frac{\mu^2 - 2\omega^2}{2\sqrt{\omega^2 - \mu^2}} & ; \frac{r}{r_s} \\ 0 & -2ir_s\omega & 1 + ir_s\omega + ir_s\frac{\mu^2 - 2\omega^2}{2\sqrt{\omega^2 - \mu^2}} & \\ & & 0 & \\ & & 2ir_s\sqrt{\omega^2 - \mu^2} & \end{bmatrix}, \tag{192}$$

with parameters

$$\begin{aligned} a = -2ir_s\sqrt{\omega^2 - \mu^2}, \quad b = 0, \quad c = 2ir_s\omega, \\ d = -r_s^2\left(\mu^2 - 2\omega^2\right), \quad e = -l(l+1). \end{aligned} \tag{193}$$

Notably, the metric does not diverge at the event horizon in Eddington-Finkelstein coordinates. Therefore, the mode solutions are reliable within the black hole. According to the second column of the GRS, two independent mode solutions exist at the event horizon. The outgoing solution inside the event horizon is given by,

$$\phi^{inner}_{\omega lm}(r) = e^{-i\left(\omega + \sqrt{\omega^2 - \mu^2}\right)r}\left(\frac{r}{r_s} - 1\right)^{-2ir_s\omega} Hc^{(a)}\left(-a, -c, b, -d, d + e; 1 - \frac{r}{r_s}\right), \tag{194}$$

and the outgoing solution outside the event horizon is,

$$\phi^{outer}_{\omega lm}(r) = e^{-i\left(\omega + \sqrt{\omega^2 - \mu^2}\right)r} Hc^{(a)}\left(-a, c, b, -d, d + e; 1 - \frac{r}{r_s}\right). \tag{195}$$

Therefore, the general outgoing solution is,

$$\phi_{\omega lm}(r) = N_\omega\left[H(r_s - r)\phi_{inner}(u,r) + H(r - r_s)\phi_{outer}(u,r)\right], \tag{196}$$

where N_ω is the normalization factor. The general outgoing solution makes a discontinuous jump as it crosses the event horizon. The jump at the event horizon is given by,

$$T_\omega = \lim_{r \to r_s^-}\left|\frac{\phi_{outer}(u,r)}{\phi_{inner}(u,r)}\right|^2 = \lim_{r \to r_s^-}\left|\frac{1}{(r - r_s)^{-2ir_s\omega}}\right|^2 = e^{-4\pi\omega r_s}. \tag{197}$$

The limit is chosen in accordance with the inner outgoing solution traversing through the event horizon from the left, $r \to r_s^-$ [47]. The transmission coefficient matches the result found in the previous chapter, which is no surprise as the radial field equation in the near horizon limit reduces to Eq.(161). To derive the greybody factor from scattering theory, the mode solutions at infinity of the radial field equation must be mapped onto the generic asymptotic form [48],

$$\phi_{\omega ml}(r) \sim \frac{1}{r}\left(A^{in}_{\omega l}e^{-i\omega r_\star} + A^{out}_{\omega l}e^{i\omega r_\star}\right). \tag{198}$$

Here, $A^{in}_{\omega l}$ and $A^{out}_{\omega l}$ are the ingoing and outgoing mode amplitudes, respectively. The third column of the GRS contains the information of the radial mode solutions at infinity, known as the *Thomé* solutions. The Thomé solutions are of the form,

$$\phi_{\omega lm}(r) = Hc^{(r)}(a,b,c,d,e;r) = \frac{1}{r}r^{-2i\omega r_s}\sum_{n=0}^{\infty} a_n^\infty r^{-n} \tag{199}$$

where the coefficients a_n^∞ are given by a recurrence relation given in Appendix C. Although the solution is not generally convergent to Eq.(198), the coefficients a_n^∞ can be fitted onto $A_{\omega l}^{in}$ and $A_{\omega l}^{out}$ over a sufficient large interval of r for fixed ω and l [45]. Through scattering theory, a second transmission coefficient describes the probability of transmitting through the potential barrier, which is given by,

$$\Gamma_\omega = \left| \frac{1}{A_{\omega l}^{in}} \right|^2 . \tag{200}$$

The vacuum persistence must include the greybody factor to adjust for the reduction of particles via the backscattering of the potential barrier. Incorporating the greybody factor into Eq.(158) gives,

$$2\Im(\mathcal{L}_{eff}) = \sum_{m,l} \left(\frac{1}{192 r_s^2 \pi} + \frac{1}{4\pi r_s} \int_0^\infty \frac{d\omega}{2\pi} \ln\left(1 + (\Gamma_\omega - 1)\, e^{-4\pi\omega r_s}\right) \right), \tag{201}$$

where the first term represents the leading contribution and the second term is a correction to the imaginary part of the Lagrangian. The correction term converges to zero in the high-frequency limit as the greybody factor approaches unity indicated by Eq.(156). However, the integral is infrared divergent due to the logarithmic term in the integrand in the low-frequency limit becomes infinite as $\omega \to 0$. It is unclear if this divergence can be removed via a renormalization scheme.

A Heat Kernel Approach to Hawking Radiation

The remaining connection to be established is to calculate the vacuum persistence of the Schwarzschild gravitational field through the heat kernel approach. In this approach, the external constant electric field in sQED is analogous to particle production through a gravitational background, as shown in Figure (15). Extracting Hawking radiation from the heat kernel is a non-trivial task, as black holes can dissipate energy through QNMs and Hawking radiation. A study by Keeler et al. [49] shows a connection between the heat kernel and the quasinormal mode method for a rotating BTZ background. This suggests that the heat kernel encodes the quasinormal modes. Therefore, extracting an imaginary part from the effective action is non-trivial as its contribution may follow from quasinormal modes rather than Hawking radiation. Appropriate boundary conditions must be established to circumvent the quasinormal mode contributions to the heat kernel.

In a recent study by Wondrak et al. [6], pair particle production for a complex scalar field in Schwarzschild spacetime was computed using covariant perturbation theory. They predict that a static observer at fixed $r \approx 1.25 r_s$ measures a temperature that exceeds the standard Hawking temperature by a factor of $\sim (1.9)^{1/4}$. This result is based on two assumptions regarding the radial profile of the escape probability. The difference in their results from the standard Hawking radiation immediately sparks questions about their methodology.

This chapter will outline the computation of the imaginary action through the covariant perturbative approach found by Wondrak et al. [6]. Moreover, the discrepancies in their methodology will be discussed. Lastly, an alternative method of calculating the heat kernel in Schwarzschild geometry will given.

A Covariant Perturbative Approach to Particle Production

Consider a massive scalar field in Schwarzschild spacetime, Eq.(68). The Euclidean effective action reads,

$$W_E = -\frac{1}{2}\int_0^\infty \frac{ds}{s}\mathrm{Tr}\left(e^{-Hs}\right), \tag{202}$$

where $H = -\Box + \mu^2 + \xi R$. Introducing the zeta-regularization prescription to normalize the effective action [15],

$$W_E(z) = -\frac{1}{2}\tilde{\mu}^{2z}\int_0^\infty \frac{ds}{s^{1-z}}\mathrm{Tr}\left(e^{-Hs}\right), \tag{203}$$

where $\tilde{\mu}$ is an arbitrary mass term to ensure proper dimensions, and z is a complex parameter. At the end of the calculation, this regularization prescription requires $z \to 0$. The traced heat kernel may be expressed as the Schwinger-DeWitt expansion. Using, Eq.(115), the Euclidean effective action reads,

$$W_E(z) = -\frac{1}{2}\tilde{\mu}^{2z}\int_0^\infty \frac{ds}{s^{1-z}}e^{-s(\mu^2-i\epsilon)}\frac{1}{(4\pi s)^2}\int d^4x\sqrt{g_E}\sum_{n=0}^{\infty}a_n(x)s^n, \tag{204}$$

where the regulator $i\epsilon$ is reintroduced such that in the massless limit, the imaginary part of the effective action is non-divergent. Furthermore, the coefficients $a_n(x)$ for a scalar field are given by Eq.(116). Performing the integral over s gives,

$$W_E(z) = -\frac{1}{2(4\pi)^2}\tilde{\mu}^{2z}\int d^4x\sqrt{g_E}\sum_{n=0}^{\infty}a_n(x)\frac{\Gamma(n-2+z)}{(\mu^2-i\epsilon)^{n-2+z}}. \tag{205}$$

The imaginary part can be extracted from the branch cut of the logarithms present in the expression,

$$I_{n-2}(z) = \frac{\Gamma(n-2+z)}{(\mu^2-i\epsilon)^{n-2+z}}, \tag{206}$$

for $n + z \leq 2$ [50]. Expanding this expression for the integer values $n = 0, 1, 2$ gives,

$$\begin{aligned}
\lim_{z\to 0} I_{-2}(z) &= \frac{\mu^4}{2z} + \frac{3-2\gamma_E}{4}\mu^4 - \frac{\mu^4}{2}\ln\left(\frac{\mu^2}{\tilde{\mu}^2} - i\epsilon\right) + \mathcal{O}(z),\\
\lim_{z\to 0} I_{-1}(z) &= -\frac{\mu^2}{z} - (1-\gamma_E)\mu^2 + \mu^2\ln\left(\frac{\mu^2}{\tilde{\mu}^2} - i\epsilon\right) + \mathcal{O}(z),\\
\lim_{z\to 0} I_0(z) &= \frac{1}{z} - \gamma_E - \ln\left(\frac{\mu^2}{\tilde{\mu}^2} - i\epsilon\right) + \mathcal{O}(z).
\end{aligned} \tag{207}$$

To extract an imaginary part, the complex logarithm is written as,

$$\ln\left(\frac{\mu^2}{\tilde{\mu}^2}-i\epsilon\right)=\ln\left|\frac{\mu^2}{\tilde{\mu}^2}-i\epsilon\right|+i\,\mathrm{atan2}(-\epsilon,\frac{\mu^2}{\tilde{\mu}^2}). \tag{208}$$

Thus, the imaginary part of the expressions read,

$$\begin{aligned}\Im(I_{-2}(0))&=\frac{\pi\mu^4}{2}H(-\mu^2)\\ \Im(I_{-1}(0))&=-\pi\mu^2H(-\mu^2)\\ \Im(I_{-0}(0))&=\pi H(-\mu^2),\end{aligned} \tag{209}$$

where $H(-\mu^2)$ is a Heaviside step function,

$$H(-\mu^2)=\begin{cases}0, & \mu^2>0\\ \frac{1}{2}, & \mu^2=0\\ 1, & \mu^2<0\end{cases}. \tag{210}$$

Therefore, the imaginary Euclidean action is given by,

$$\Im(W_E(0))=-\frac{1}{32\pi}\int d^4x\sqrt{g_E}\left[\frac{\mu^4}{2}a_0(x)-\mu^2a_1(x)+a_2(x)\right]H(-\mu^2), \tag{211}$$

which can be extended to a complex field by incorporating a factor $N=2$. The form of Eq.(211) indicates that particle production is completely controlled by the mass of the field quanta. For the massless complex scalar field coupled with the Schwarzschild background, the imaginary action only contains contributions from $R_{\mu\nu\alpha\beta}R^{\mu\nu\alpha\beta}=\frac{12r_s^2}{r^6}$.[9] The probability of pair particle creation per unit time is,

$$\frac{dN}{dt}=2\Im\left(L\right)=\frac{r_s^2}{240\pi}\int_{r_s}^{\infty}\int_0^{\pi}\int_0^{2\pi}r^2\sin\left(\theta\right)\frac{1}{r^6}drd\theta d\varphi=\frac{1}{180r_s}. \tag{212}$$

The particle rate must be adjusted by incorporating the radial escape profile of the radiation via a pair-per-event correction and escape probability. A pair-per-event correction factor accounts for the mean number of pairs that can be extracted from the heat kernel's first pole. The escape probability follows from the fact that created particles may fall into the black hole for a static observer at infinity. These adjustments reduce the observed particle rate at infinity to,

$$\frac{dN_{obs}}{dt}=\frac{2059}{85050r_s\pi^2}. \tag{213}$$

Similarly, consider the sQED Lagrangian, where the gauge-field curvature term $\Omega_{\mu\nu}=iF_{\mu\nu}$. Then, according to Eq.(211) the imaginary part of the effective Lagrangian yields,

$$2\Im(\mathcal{L}_{eff,E})=-\frac{E^2}{96\pi}. \tag{214}$$

This result agrees with Eq.(67) for a massless complex scalar particle.

Perturbative Discrepancies

The Schwinger-DeWitt expansion provides a covariant perturbative method of calculating the heat kernel as a series in Schwinger proper time s. The perturbative result found in Eq.(214) matches exactly with the full non-perturbative result in Eq.(67) in the massless limit. However, part of the information captured in the full heat kernel has been discarded by the finite expansion. Subsequently, the imaginary part of the perturbative effective action is insufficient to capture the full features of the theory. To show why this methodology causes the discrepancies, consider a massless complex scalar in a constant magnetic background, described by sQED. In the non-perturbative effective Lagrangian Eq.(61), an imaginary part does not exist due to the lack of poles. Thus, a constant magnetic field cannot produce particles. The perturbative imaginary part of the effective action for a constant magnetic field yields,

$$2\Im(\mathcal{L}_{eff,E})=\frac{B^2}{96\pi}. \tag{215}$$

The non-zero result indicates that in a constant magnetic field, particle production occurs. Wick rotating to Lorentzian signature shows that the vacuum persistence,

$$\left|\langle\mathrm{out},0|0,\mathrm{in}\rangle\right|^2=e^{-2\Im(W)}=e^{\frac{B^2}{96\pi}}>1, \tag{216}$$

[9] This follows from the fact that in Schwarzschild, $R_{\mu\nu}=0$ and $R=0$. Then the Schwinger coefficient $a_2(x)$ (Eq.(116) reduces to $a_2(x)=\frac{12r_s^2}{180r^6}$.

violates unitarity as the probability of not transitioning is greater than unity. The physical implications of this result are unclear. Therefore, the perturbative action is insufficient in capturing all the information of the non-perturbative heat kernel. Moreover, it is unlikely that next-order terms will converge on the established results.

These inconsistencies also extend to pair production in a gravitational field. In a recent study by Zhou et al. [50], a non-perturbative calculation using the heat kernel is performed to find the correct imaginary part of the effective action in (A)dS spacetime. They show that different expansions of the heat kernel predict different imaginary contributions compared to the non-perturbative result.

Furthermore, the study by Wondrak el al. [6] claims that the approach does not require an event horizon as it does not enter into the derivation besides the escape factor. Consequently, any gravitational field can produce particles as long as Eq.(211) gives a nonzero result. However, this is contradictory as not all gravitational fields produce particles, such as in AdS spacetime. Moreover, it has been established that the presence of a global event horizon for a black hole is required for particle production to occur. Since the imaginary contribution of the divergent Schwinger-DeWitt coefficient, $a_2(x)$, only probes the local geometry, it is non-sensitive to global features like an event horizon. However, according to the Bogolubov and scattering approaches, the event horizon is the working mechanism driving particle production.

A Heat Kernel Approach To Hawking Radiation in Schwarzschild Geometry

All methodologies of calculating the vacuum persistence in sQED are in agreement. This consistency suggests that a similar underlying equivalence exists for Hawking radiation. Given that the Bogolubov and scattering approaches for the Schwarzschild gravitational field are in agreement, it is reasonable to assume the Schwinger approach will also predict the same result. Analogous to sQED, the effective action can be mapped into a heat kernel-type integral. Combining Eq.(153) and Eq.(90), the effective Lagrangian reads,

$$\mathcal{L}_{eff} = i\frac{\kappa}{2\pi}\sum_{l,m}\int_{\mu}^{\infty}\frac{d\omega}{2\pi}\left[\ln\left(\Gamma\left(1-i\omega\kappa^{-1}\right)\right)+i\omega\kappa^{-1}\ln\left(-i\omega'\right)-\ln\left(i\pi\sqrt{\omega\omega'}\right)\right]. \tag{217}$$

Similarly to Eq.(105), the divergent terms are discarded, and only the gamma function contributes to the effective Lagrangian. For massless particles, the effective action becomes

$$\mathcal{L}_{eff} = i\frac{\kappa}{2\pi}\sum_{l,m}\int_{0}^{\infty}\frac{d\omega}{2\pi}\left[\ln\left(\Gamma\left(1-i\omega\kappa^{-1}\right)\right)\right] \sim i\frac{\kappa}{2\pi}\sum_{l,m}\int_{0}^{\infty}\frac{d\omega}{2\pi}\int_{0}^{\infty}\frac{ds_M}{s_M}\frac{e^{-s_M(1-i\omega\kappa^{-1})}}{1-e^{-s_M}}, \tag{218}$$

where the former is written as a heat kernel-type integral [19]. Further decomposition into a summation may provide insight into the eigenvalues of the wave equation in Schwarzschild geometry,

$$\frac{e^{-s_M(1-i\omega\kappa^{-1})}}{1-e^{-s_M}} \stackrel{?}{=} \sum_{n=0}^{\infty} e^{-s_M(1+n-i\omega\kappa^{-1})}. \tag{219}$$

Therefore, the supposed system's eigenvalues are $\lambda = 1+n-i\omega\kappa^{-1},\ n\geq 0$. These supposed eigenvalues provide several insights into solving the Klein-Gordon equation for a Schwarzschild black hole with corresponding boundary conditions. The dissipation through Hawking radiation follows from the imaginary part, $-i\omega\kappa^{-1}$, while the real part of the eigenvalues determines the pole structure. Moreover, the form of Eq. (217) does not contain an imaginary contribution from the poles of ω-integral. Instead, the imaginary contribution follows from the gamma function. Therefore,

$$\begin{aligned}
\Im(\mathcal{L}_{eff}) &= \Re\left(\frac{\kappa}{2\pi}\sum_{l,m}\int_{0}^{\infty}\frac{d\omega}{2\pi}\left[\ln\left(\Gamma\left(1-i\omega\kappa^{-1}\right)\right)\right]\right)\\
&= \frac{1}{2}\left(\frac{\kappa}{2\pi}\sum_{l,m}\int_{0}^{\infty}\frac{d\omega}{2\pi}\left[\ln\left(\Gamma\left(1+i\omega\kappa^{-1}\right)\Gamma\left(1-i\omega\kappa^{-1}\right)\right)\right]\right)\\
&= \frac{\kappa}{4\pi}\sum_{l,m}\int_{0}^{\infty}\frac{d\omega}{2\pi}\ln\left(\frac{2\pi\omega\kappa^{-1}e^{-2\pi\omega\kappa^{-1}}}{1-e^{-2\pi\omega\kappa^{-1}}}\right)\\
&= -\frac{\kappa}{4\pi}\sum_{l,m}\int_{0}^{\infty}\frac{d\omega}{2\pi}\ln\left(1-e^{-2\pi\omega\kappa^{-1}}\right),
\end{aligned} \tag{220}$$

where the latter equation has removed the divergencies in the term: $\ln\left(4\pi r_s\omega e^{-\pi\omega\kappa^{-1}}\right)$, via some renormalization prescription [25]. This method of calculating the imaginary part of the effective Lagrangian neglects the use of poles.

The remaining challenge is to formulate the field equation with appropriate boundary conditions so that the vacuum persistence matches the result in Eq.(158). Mirroring the scattering approach, the potential barrier can be neglected by taking the near horizon limit of the field equation. Regardless of the coordinate system used, the near horizon limit in Schwarzschild, Painlevé, and Eddington-Finkelstein coordinates all reduce to the same field equation following Appendix D,

$$\left[\frac{d^2}{dx^2}+\frac{\omega^2 r_s^2+\frac{1}{4}}{x^2}\right]\phi_\omega(x)=0, \tag{221}$$

where $x=r-r_s$. To emulate Hawking radiation, consider purely outgoing waves at the event horizon and infinity. Although the mode solutions are constrained to the near horizon limit, they may be extrapolated to be valid at infinity because the potential barrier only influences the amplitude of the mode solutions. Therefore, the boundary conditions read,

$$\phi_\omega\sim\begin{cases}x^{i\omega r_s} & ,x\to 0,\\ e^{i\omega x}x^{i\omega r_s} & ,x\to\infty.\end{cases} \tag{222}$$

Similar to sQED, the field equation is promoted to an eigenvalue problem: $\Box\phi_\omega(x)=0\to\Box\phi_{\omega k}(x)=k^2\phi_{\omega k}(x)$. Promoting the field equation is a non-trivial operation because the eigenvalues change if done throughout different stages of rewriting the field equation. Therefore, the promotion is done before any approximations or rewritings. The radial eigenvalue equation in x-coordinates reads,

$$\left[\frac{d^2}{dx^2}+\frac{(r_s)^2}{4(x+r_s)^2x^2}+\omega^2\left(\frac{(r_s)^2}{x^2}+\frac{2(r_s)}{x}+1\right)-\left(\frac{r_s}{x}+1\right)\mu^2-\frac{l(l+1)}{x(x+r_s)}\right]\phi_{\omega k}(x)=k^2\left(\frac{x+r_s}{x}\right)\phi_{\omega k}(x). \tag{223}$$

In the near horizon limit, for s-waves ($l=0$) and massless limit $\mu=0$, the field equation up to order $\mathcal{O}\left(x^0\right)$ reads,

$$\left[\frac{d^2}{dx^2}+\frac{4r_s^2\omega^2+1}{4x^2}+\frac{4r_s^2\omega^2-1}{2r_sx}+\frac{3}{4r_s^2}+\omega^2\right]\phi_{\omega k}(x)=k^2\left(\frac{x+r_s}{x}\right)\phi_{\omega k}(x). \tag{224}$$

This approximation is only valid in the near horizon limit, where the inverse square potential dominates. If the eigenvalues satisfy the following conditions,

$$2\omega^2-\frac{1}{2r_s^2}\ll k^2\quad\text{and}\quad\frac{3}{4r_s^2}+\omega^2\ll k^2\quad,\forall\{\omega,r_s\}\geq 0. \tag{225}$$

The radial eigenvalue equation simplifies to,

$$\left[\frac{d^2}{dx^2}+\frac{\omega^2r_s^2+\frac{1}{4}}{x^2}\right]\phi_{\omega k}(x)=k^2\frac{r_s+x}{x}\phi_{\omega k}(x). \tag{226}$$

The general mode solution to the radial eigenvalue equation is given by,

$$\phi_{\omega k}(x)=c_1M_{-\frac{1}{2}kr_s,i\omega r_s}(2kx)+c_2W_{-\frac{1}{2}kr_s,i\omega r_s}(2kx) \tag{227}$$

where $M_{-\frac{1}{2}kr_s,i\omega r_s}(2kx)$ and $W_{-\frac{1}{2}kr_s,i\omega r_s}(2kx)$ are the Whittaker functions [19]. These functions form a linear combination of outgoing and ingoing modes. The behaviour of the Whittaker functions at $x=0$ is given by the expansions,

$$M_{-\frac{1}{2}kr_s,i\omega r_s}(2kx)\overset{x\to 0}{\sim}\sqrt{x}x^{ir_s\omega}, \tag{228a}$$

$$W_{-\frac{1}{2}kr_s,i\omega r_s}(2kx)\overset{x\to 0}{\sim}\frac{\sqrt{x}x^{ir_s\omega}}{\Gamma\left(\frac{1}{2}(kr_s-2i\omega r_s+1)\right)}+\frac{\sqrt{x}x^{-ir_s\omega}}{\Gamma\left(\frac{1}{2}(kr_s+2i\omega r_s+1)\right)}. \tag{228b}$$

To satisfy the boundary condition at the event horizon in Eq.(222), the ingoing mode $x^{-ir_s\omega}$ must vanish. This is achieved through the simple poles at $z=-n$, where $n\in\mathbb{Z}_0^+$ of the Gamma function, $\Gamma(z)$ [18]. Consequently,

$$\frac{1}{\Gamma\left(\frac{1}{2}(kr_s+2ir_s\omega+1)\right)}=0, \tag{229}$$

is satisfied by the eigenvalues,

$$kr_s = -1 - 2n - 2ir_s\omega, \quad \forall n \in \mathbb{Z}_0^+. \tag{230}$$

Moreover, the ingoing modes at infinity must vanish to satisfy the boundary conditions at infinity in Eq.(222). Expanding the Whittaker functions at radial infinity gives,

$$M_{-\frac{1}{2}kr_s, i\omega r_s}(2kx) \overset{x\to\infty}{\sim} \frac{e^{kx}x^{\frac{kr_s}{2}}}{\Gamma\left(\frac{1}{2}(kr_s + 2i\omega r_s + 1)\right)} - \frac{e^{-kx}x^{-\frac{kr_s}{2}}}{\Gamma\left(\frac{1}{2}(-kr_s + 2i\omega r_s + 1)\right)}, \tag{231a}$$

$$W_{-\frac{1}{2}kr_s, i\omega r_s}(2kx) \overset{x\to\infty}{\sim} e^{-kx}x^{-\frac{kr_s}{2}}. \tag{231b}$$

The mode solutions at infinity satisfy the boundary conditions for the eigenvalues given in Eq.(230). The effective action in terms of the eigenvalues k^2 is given by [28],

$$W = \frac{i}{2}\mathrm{Tr}\{\ln\left(k^2\right)\} = i\mathrm{Tr}\{\ln\left(k\right)\} = i\mathrm{Tr}\left\{\int_0^\infty \frac{ds}{s}e^{-sk}\right\}. \tag{232}$$

By rescaling and rotating to Lorentzian Schwinger proper time, $s \to isr_s$, the effective Lagrangian with eigenvalues k given by Eq.(230) reads,

$$\mathcal{L}_{eff} = i\frac{\kappa}{2\pi}\sum_{l,m}\int_0^\infty \frac{ds}{s}\int_0^\infty \frac{d\omega}{2\pi}\sum_{n=0}^\infty e^{is(1+2n+2i\omega r_s)} = -\frac{\kappa^2}{8\pi^2}\sum_{l,m}\int_0^\infty \frac{ds}{s^2}\csc\left(s\right). \tag{233}$$

Which contains poles at $s = \pi j$ for $j = 1, 2, \ldots$. The form of the effective Lagrangian is nearly identical to the sQED effective Lagrangian for a constant electric field given in Eq.(65), with the electric field E replaced by κ. Therefore, the role of the event horizon r_s is analogous to the electric field E, which causes the particle production. This implies that an event horizon is required for particle production to occur for a scalar field in Schwarzschild geometry, not just a gravitational field. Furthermore, a similar analysis as in sQED shows that the renormalized effective Lagrangian is given by,

$$\mathcal{L}_{eff}^{ren} = -\frac{\kappa^2}{8\pi^2}\sum_{l,m}\int_0^\infty \frac{ds}{s^3}\left[s\csc\left(s\right) - 1 - \frac{s^2}{6}\right]. \tag{234}$$

The first renormalized term corresponds to the removal of the divergent vacuum energy of the system. Additionally, the second renormalized term corresponds to the renormalization of the gravitational constant. Extracting the imaginary part of the effective action gives,

$$2\Im(\mathcal{L}_{eff}) = 2\pi\frac{\kappa^2}{8\pi}\sum_{l,m}\sum_{j=1}^\infty \frac{(-1)^{j+1}}{(\pi j)^2} = \sum_{l,m}\frac{\kappa^2}{48\pi}, \tag{235}$$

which follows from the integration poles along the positive s-axis [11]. This result is in agreement with the other approaches to Hawking radiation. The non-zero imaginary effective action indicates that a transition exists between the Schwarzschild vacuum and the Unruh vacuum. The Unruh vacuum is associated with an infalling observer at infinity, measuring particles coming from the black hole but not coming from infinity.

The derivation contains weak statements for which the method is valid. Firstly, at infinity, the Whittaker functions with eigenvalues k become,

$$\phi_{\omega k} = Ne^{2i\omega x}x^{i\omega r_s}e^{\frac{1}{r_s}(1+2n)x}x^{\frac{1}{2}(1+2n)}, \tag{236}$$

where N is a normalization constant. For large x, the term $e^{\frac{1}{r_s}(1+2n)x}x^{\frac{1}{2}(1+2n)}$ blows up. The neglected potential barrier may regulate this term as in the far horizon limit, the field equation yields mode solutions of the form,

$$\phi_\omega(x) \overset{x\to\infty}{\sim} \frac{1}{x}e^{i\omega x}x^{i\omega r_s}. \tag{237}$$

The latter two terms are equivalent to the first two terms in Eq.(236). Secondly, the assumption in Eq.(225) is only satisfied for large n. However, from the scattering approach, it can be argued that the higher-order terms $\mathcal{O}\left(x^{-1}\right)$ in Eq.(224) only contribute to the greybody factor. Therefore, these terms are neglected to isolate particle production originating from the event horizon. Nonetheless, including these higher-order perturbations may provide insight into the greybody factor near the horizon. Rewriting Eq.(224), the eigenvalue equation is given by,

$$\left[\frac{d^2}{dx^2} + \frac{4r_s^2\omega^2 + 1}{4x^2}\right]\phi_{\omega k}(x) = \left(\frac{z^2x + w^2r_s}{x}\right)\phi_{\omega k}(x), \tag{238}$$

where

$$w^2 = k^2 - 2\omega^2 + \frac{1}{2r_s^2} \quad \text{and} \quad z^2 = k^2 - \omega^2 - \frac{3}{4r_s^2}. \tag{239}$$

Following the same procedure as before, the general mode solution is given by,

$$\phi_{\omega k}(x) = c_1 M_{-\frac{w^2}{2z}r_s, i\omega r_s}(2zx) + c_2 W_{-\frac{w^2}{2z}r_s, i\omega r_s}(2zx). \tag{240}$$

Furthermore, expanding the Whittaker functions at $x = 0$ gives,

$$M_{-\frac{w^2}{2z}r_s, i\omega r_s}(2zx) \overset{x\to 0}{\sim} \sqrt{x}x^{ir_s\omega} \tag{241a}$$

$$W_{-\frac{w^2}{2z}r_s, i\omega r_s}(2zx) \overset{x\to 0}{\sim} \frac{\sqrt{x}x^{ir_s\omega}}{\Gamma\left(\frac{1}{2} + \frac{r_s w^2}{2z} - ir_s\omega\right)} + \frac{\sqrt{x}x^{-ir_s\omega}}{\Gamma\left(\frac{1}{2} + \frac{r_s w^2}{2z} + ir_s\omega\right)}. \tag{241b}$$

Then, the boundary conditions are satisfied for,

$$\frac{1}{2} + \frac{r_s w^2}{2z} + ir_s\omega = -n. \tag{242}$$

Substituting w and z into the condition and solving for the eigenvalues k gives,

$$k_{non}r_s = -\sqrt{\sqrt{(2n + 2ir_s\omega + 1)^2\,(n^2 + i(2n+1)r_s\omega + n - 1)} + 2i(2n+1)r_s\omega + 2n(n+1)}, \quad \forall n \in \mathbb{Z}_0^+, \tag{243}$$

which will be called the non-trivial eigenvalues. For large n, the non-trivial eigenvalues converge to Eq.(230), as shown in Figures (19 and 20). How fast the eigenvalues converge depends on ω and r_s. Specifically, when $\frac{1}{r_s} \geq \omega$, the non-trivial eigenvalues converge extremely fast, while for $\omega \gg \frac{1}{r_s}$ they converge slower. As a result, the imaginary part of the effective action becomes Eq.(158).

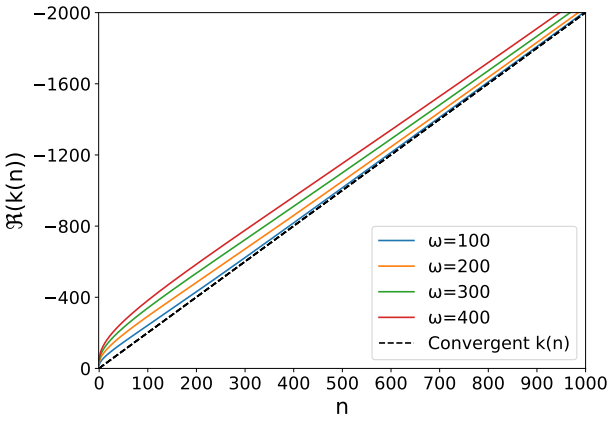

Figure 19: The real part of the non-trivial eigenvalues for different values of ω and $r_s = 1$. The real part of the non-trivial eigenvalues converges slower for values $\omega \gg \frac{1}{r_s}$. Moreover, for $\frac{1}{r_s} \geq \omega$, the non-trivial eigenvalues converge extremely fast.

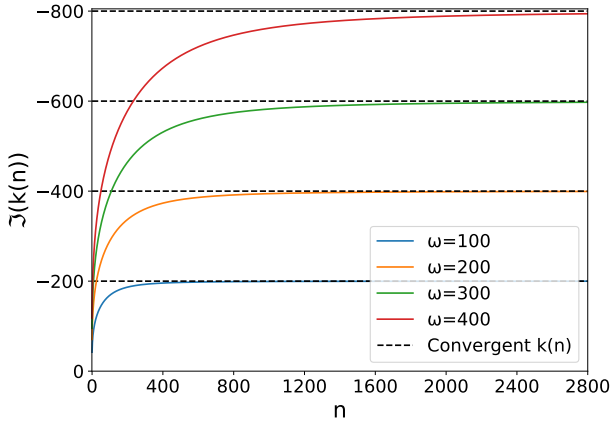

Figure 20: The imaginary part of the eigenvalues for different values of ω and $r_s = 1$. The imaginary part of the non-trivial eigenvalues converges slower for values $\omega \gg \frac{1}{r_s}$. Moreover, for $\frac{1}{r_s} \geq \omega$, the non-trivial eigenvalues converge extremely fast.

Unfortunately, these non-trivial eigenvalues have no analytical solution to the functional determinant in Eq.(232). Rewriting the non-trivial eigenvalues as,

$$k_{non}r_s = -1 - 2n - 2ir_s\omega + f_\omega(n), \quad \forall n \in \mathbb{Z}_0^+, \tag{244}$$

to isolate the contribution of the potential barrier in the near horizon limit. The term $f_\omega(n)$ is the perturbation to the eigenvalues in Eq.(230), which in the large n goes to zero, $f_\omega(n) \to 0$. Although the real part of $f_\omega(n)$ adjusts the pole structure, its contribution can be treated as a perturbation to the original effective Lagrangian given in Eq.(233). Since at $\omega \leq \frac{1}{r_s}$, the perturbation $f_\omega(n)$ is essentially zero which reduces the

effective Lagrangian to,

$$\begin{aligned}\mathcal{L}_{eff} &= i\frac{\kappa}{2\pi}\sum_{l,m}\int_0^\infty \frac{ds}{s}\left(\int_0^{\frac{1}{r_s}}\frac{d\omega}{2\pi}\sum_{n=0}^{\infty}e^{is(1+2n+2i\omega r_s)}+\int_{\frac{1}{r_s}}^{\infty}\frac{d\omega}{2\pi}\sum_{n=0}^{\infty}e^{-isk_{non}}\right)\\ &= \frac{\kappa^2}{8\pi^2}\sum_{l,m}\int_0^\infty\frac{ds}{s^2}\left(\left(e^{-2s}-1\right)\csc\left(s\right)+s\int_{\frac{1}{r_s}}^{\infty}\frac{d\omega}{2\pi}\sum_{n=0}^{\infty}e^{-isk_{non}}\right) \qquad (245)\\ &= -\frac{\kappa^2}{8\pi^2}\sum_{l,m}\int_0^\infty\frac{ds}{s^2}\left(\csc\left(s\right)+\mathcal{L}_{eff}^{perturbation}\right),\end{aligned}$$

where

$$\mathcal{L}_{eff}^{perturbation} = \frac{\kappa^2}{8\pi^2}\sum_{l,m}\int_0^\infty\frac{ds}{s^2}\left(e^{-2s}\csc\left(s\right)+s\int_{\frac{1}{r_s}}^{\infty}\frac{d\omega}{2\pi}\sum_{n=0}^{\infty}e^{-isk_{non}}\right). \qquad (246)$$

The imaginary part of the first term of the perturbation of Eq.(246) yields,

$$2\Im\left(\frac{\kappa^2}{8\pi^2}\sum_{l,m}\int_0^\infty\frac{ds}{s^2}e^{-2s}\csc\left(s\right)\right) = -2\pi\frac{\kappa^2}{8\pi^2}\sum_{l,m}\sum_{j=1}^{\infty}\frac{(-1)^{j+1}}{(\pi j)^2}e^{-2\pi j}\approx -0.0023\sum_{l,m}\frac{\kappa^2}{48\pi}. \qquad (247)$$

Due to the small prefactor, its contribution to the imaginary part is neglectable. This behaviour aligns with the fact that black holes primarily emit Hawking radiation with large wavelengths, as shown in the Bogolubov approach. Furthermore, the perturbation must contain information about the greybody factor, where its imaginary part reduces to the second term of Eq.(201). The perturbation contains only partial information about the greybody factor, as higher-order terms were discarded and only s-waves were considered. Moreover, it is unclear how the function $f_\omega(n)$ is related to the perturbation, and a more thorough analysis is required to show its contribution to the imaginary part.

Conclusion and Future Directions

The imaginary part of the effective Lagrangian in sQED for a constant electric field was calculated using the heat kernel, Bogolubov and scattering approaches. Despite their distinct interpretation of how particle production occurs, the three approaches yielded the same particle production rate. This equivalence may follow from the spectral properties encoded within the operator, which links eigenvalues, Bogolubov coefficients and scattering coefficients with particle production.

Black holes also exhibit particle production through Hawking radiation, which is thoroughly studied through the scattering and Bogolubov approaches. A recent paper by Wondrak et al.[6] attempted to calculate the imaginary part of the effective action for a scalar field in Schwarzschild geometry through a covariant perturbative approach. However, further analysis showed that their results are contradictory as particle production may occur in sQED for a constant magnetic field and AdS spacetime using their approach. These discrepancies motivated this thesis to provide a novel heat kernel approach to Hawking radiation.

Using scattering theory, the inverse square potential was identified as the part that encodes the particle production, while higher orders contributed to the greybody factor. Moreover, reverse engineering the existing effective Lagrangians to a heat kernel-type integral provided an insight into the supposed eigenvalues of the system. Assuming that only the inverse square potential contributes to particle production, the eigenvalues of the radial field equation in the near horizon limit were calculated using boundary conditions that permit only outgoing modes at the event horizon and infinity. Computing the imaginary part of the effective Lagrangian using these eigenvalues showed that all three approaches yielded the same result for a scalar field in Schwarzschild geometry.

Including the higher order terms up to $\mathcal{O}\left(x^0\right)$ into the eigenvalue equation gave non-trivial eigenvalues, which converged for large n to Eq.(230). Analysing the non-trivial eigenvalues showed that its behaviour aligns with the properties of small black holes, where the potential barrier is very weak. Consequently, the non-trivial eigenvalues were rewritten as the original eigenvalues plus a perturbation, Eq.(244), under the assumption that the perturbation only contains information that contributes to the greybody factor. These calculations show that the event horizon is a necessary condition for black holes to produce Hawking radiation, not just the presence of a gravitational field. The analogy with the electric field, shows that Hawking radiation can be described similar to the Schwinger effect. It is the event horizon that exerts a non-local effect on the virtual particles such that they separate and are emitted as Hawking radiation.

Further research could involve a more rigorous mathematical analysis to isolate the particle production and greybody contributions. This includes calculating the perturbative Lagrangian term from the perturbative eigenvalue term. Additionally, since the radial eigenvalue equation was restricted to s-waves, a logical new avenue is to incorporate higher-order orbital moments into the calculation. It is also possible through Heun functions to obtain a polynomial solution to the full radial eigenvalue equation. Moreover, to check the consistency of this novel methodology, it will be intriguing to extend it to other spacetimes. Lastly, an improvement on the covariant perturbative approach given by Wondrak et al. [6] can be done by including non-local terms, which may offer an insight into how the presence of an event horizon causes particle production.

References

[1] S. W. Hawking. Particle Creation by Black Holes. *Commun. Math. Phys.*, 43:199–220, 1975. [Erratum: Commun.Math.Phys. 46, 206 (1976)].

[2] Maulik K. Parikh and Frank Wilczek. Hawking radiation as tunneling. *Physical Review Letters*, 85(24):5042–5045, December 2000.

[3] J. B. Hartle and S. W. Hawking. Path-integral derivation of black-hole radiance. *Phys. Rev. D*, 13:2188–2203, Apr 1976.

[4] T. Damour and R. Ruffini. Black Hole Evaporation in the Klein-Sauter-Heisenberg-Euler Formalism. *Phys. Rev. D*, 14:332–334, 1976.

[5] Julian Schwinger. On gauge invariance and vacuum polarization. *Phys. Rev.*, 82:664–679, Jun 1951.

[6] Michael F. Wondrak, Walter D. van Suijlekom, and Heino Falcke. Gravitational pair production and black hole evaporation. *Physical Review Letters*, 130(22), June 2023.

[7] Sean Carroll. *Spacetime and Geometry: An Introduction to General Relativity*. Benjamin Cummings, 2003.

[8] Yuli V. Nazarov and Jeroen Danon. *Advanced Quantum Mechanics: A Practical Guide*. Cambridge University Press, 2013.

[9] Steven Weinberg. *The Quantum Theory of Fields*. Cambridge University Press, 1995.

[10] Iosif L. Buchbinder and Ilya Shapiro. *Introduction to Quantum Field Theory with Applications to Quantum Gravity*. Oxford Graduate Texts. Oxford University Press, 2 2023.

[11] Subodh Patil. Semi-classical and functional methods, November 2014.

[12] Per Kraus and Frank Wilczek. Self-interaction correction to black hole radiance. *Nuclear Physics B*, 433(2):403–420, January 1995.

[13] Matthew D. Schwartz. *Quantum Field Theory and the Standard Model*. Cambridge University Press, 2013.

[14] GERALD V. DUNNE. The heisenberg–euler effective action: 75 years on. *International Journal of Modern Physics A*, 27(15):1260004, June 2012.

[15] D.V. Vassilevich. Heat kernel expansion: user's manual. *Physics Reports*, 388(5–6):279–360, December 2003.

[16] W. Heisenberg and H. Euler. Consequences of dirac theory of the positron, 2006.

[17] T. Padmanabhan. Quantum theory in external electromagnetic and gravitational fields: A Comparison of some conceptual issues. *Pramana*, 37:179–233, 1991.

[18] Varsha Subramanyan, Suraj S. Hegde, Smitha Vishveshwara, and Barry Bradlyn. Physics of the inverted harmonic oscillator: From the lowest landau level to event horizons. *Annals of Physics*, 435:168470, December 2021.

[19] D. Zwillinger and A. Jeffrey. *Table of Integrals, Series, and Products*. Academic Press, 2007.

[20] D. B. Scott. Complex variables and applications (4th edition), by ruel v. churchill and james ward brown. pp 339. 1983. isbn 0-07-010873-0 (mcgraw-hill). *The Mathematical Gazette*, 69(449):243–244, 1985.

[21] N. D. Birrell and P. C. W. Davies. *Quantum Fields in Curved Space*. Cambridge Monographs on Mathematical Physics. Cambridge Univ. Press, Cambridge, UK, 2 1984.

[22] Yen Chin Ong. Schwinger pair production and the extended uncertainty principle: can heuristic derivations be trusted? *The European Physical Journal C*, 80(8), August 2020.

[23] P. K. Townsend. Black holes, 1997.

[24] Christopher Gerry and Peter Knight. *Introductory Quantum Optics*. Cambridge University Press, 2004.

[25] Sang Pyo Kim and W-Y Hwang. Vacuum polarization and persistence on the black hole horizon. *AIP Conf. Proc.*, 03 2011.

[26] Sang Pyo Kim and Hyun Kyu Lee. Effective Action and Schwinger Pair Production in Scalar QED. *AIP Conf. Proc.*, 1027:24, 2008.

[27] Sunhyung Kim, Jun Hee Sung, Kyung Hyun Ahn, Seung Jong Lee, Albert Co, Gary L. Leal, Ralph H. Colby, and A. Jeffrey Giacomin. The effect of pva adsorption on stress development during drying in pva/silica suspension coating. In *AIP Conference Proceedings*, volume 1027, page 24–26. AIP, 2008.

[28] Qmechanic. Comment on: Euler-Heisenberg Lagrangian and heat kernel: Why do we need to substitute s→is to continue calculating? `https://physics.stackexchange.com/a/828922/401964`, 2024. Accessed: September 24, 2024.

[29] A. O. Barvinsky and G. A. Vilkovisky. Covariant perturbation theory. 2: Second order in the curvature. General algorithms. *Nucl. Phys. B*, 333:471–511, 1990.

[30] Emanuele Berti, Vitor Cardoso, and Andrei O Starinets. Quasinormal modes of black holes and black branes. *Classical and Quantum Gravity*, 26(16):163001, July 2009.

[31] Robert M. Wald. The thermodynamics of black holes. *Living Reviews in Relativity*, 4(1), July 2001.

[32] PBS SpaceTime. Is it impossible to cross the event horizon? — black hole firewall paradox. `https://www.youtube.com/watch?v=4uQF9Egc-fM&t=311s`, 2024. Accessed: December 5, 2024.

[33] Imran Abdul Rahman. On the black hole information paradox and the page curve. Master's dissertation, Imperial College London, Department of Physics, Theoretical Physics Group, 2024. Submitted in partial fulfilment of the requirements for the degree of Master of Science.

[34] PBS SpaceTime. Can black holes unify general relativity and quantum mechanics? `https://www.youtube.com/watch?v=NSqT594RVWQ`, 2024. Accessed: December 5, 2024.

[35] Leonard Susskind, Lárus Thorlacius, and John Uglum. The stretched horizon and black hole complementarity. *Physical Review D*, 48(8):3743–3761, October 1993.

[36] Ahmed Almheiri, Donald Marolf, Joseph Polchinski, and James Sully. Black holes: complementarity or firewalls? *Journal of High Energy Physics*, 2013(2), February 2013.

[37] Wikipedia contributors. List of nearest known black holes, 2024. Accessed December 9, 2024.

[38] Jennie Traschen. An introduction to black hole evaporation, 2000.

[39] Pierre-Henry Lambert. Introduction to black hole evaporation, 2014.

[40] Sean P. Robinson and Frank Wilczek. Relationship between hawking radiation and gravitational anomalies. *Physical Review Letters*, 95(1), June 2005.

[41] Zheng Zhao and Jian-Yang Zhu. Damour-Ruffini and Unruh theories of the Hawking effect. *Int. J. Theor. Phys.*, 33:2147–2155, 1994.

[42] S. Sannan. Heuristic Derivation of the Probability Distributions of Particles Emitted by a Black Hole. *Gen. Rel. Grav.*, 20:239–246, 1988.

[43] Ken-ichiro Kanai and Yasusada Nambu. Viewing black holes by waves. *Classical and Quantum Gravity*, 30(17):175002, July 2013.

[44] Luís C. B. Crispino, Sam R. Dolan, and Ednilton S. Oliveira. Electromagnetic wave scattering by schwarzschild black holes. *Physical Review Letters*, 102(23), June 2009.

[45] Dennis Philipp and Volker Perlick. On analytic solutions of wave equations in regular coordinate systems on schwarzschild background, 2015.

[46] A. Ronveaux and F.M. Arscott. *Heun's Differential Equations*. Oxford science publications. Oxford University Press, 1995.

[47] Wen-Du Li, Yu-Zhu Chen, and Wu-Sheng Dai. Scattering state and bound state of scalar field in schwarzschild spacetime: Exact solution. *Annals of Physics*, 409:167919, October 2019.

[48] N. Andersson. Scattering of massless scalar waves by a Schwarzschild black hole: A Phase integral study. *Phys. Rev. D*, 52:1808–1820, 1995.

[49] Cynthia Keeler, Victoria Martin, and Andrew Svesko. Connecting quasinormal modes and heat kernels in 1-loop determinants. *SciPost Physics*, 8(2), February 2020.

[50] Yu Zhou and Hai-Qing Zhang. Effective action and gravitational pair production in (a)ds spacetime, 2024.

[51] Chiang-Mei Chen, Sang Pyo Kim, I-Chieh Lin, Jia-Rui Sun, and Ming-Fan Wu. Spontaneous pair production in reissner-nordström black holes. *Physical Review D*, 85(12), June 2012.

Appendix A: Damour-Ruffini Method: Analytical Continuation

The outgoing wave solution for the radial field equation in the near horizon limit reads,

$$R_I^{out}(t,r) = e^{-i\omega u} = (r-r_s)^{2i\omega r_s}\, e^{2i\omega r} e^{-i\omega v}, \quad (r > r_s). \tag{A1}$$

where

$$(r-r_s)^{2i\omega r_s} = e^{2i\omega r_s \ln(r-r_s)} \tag{A2}$$

. For $r < r_s$, the argument of logarithm becomes negative. To analytically extend the wave inside the black hole, $r < r_s$, promote $r - r_s \to r - r_s - i\epsilon$, where $\epsilon > 0$. This gives,

$$\ln(r - r_s - i\epsilon) = \ln|r - r_s| + i\text{atan2}(-\epsilon, (r-r_s)) \tag{A3}$$

where

$$\text{atan2}(y,x) = \begin{cases} \arctan\frac{y}{x} + \pi & \text{if} \quad x < 0 \text{ and } y \geq 0, \\ \arctan\frac{y}{x} - \pi & \text{if} \quad x < 0 \text{ and } y < 0, \\ \frac{\pi}{2} & \text{if} \quad x = 0 \text{ and } y > 0, \\ -\frac{\pi}{2} & \text{if} \quad x = 0 \text{ and } y < 0, \\ \text{undefined} & \text{if} \quad x = 0 \text{ and } y = 0. \end{cases} \tag{A4}$$

Therefore, the analytical continuation of the wave such that it is well-defined inside the black hole gives,

$$R_{II}^{out}(t,r) = e^{2i\omega r} e^{-i\omega v} e^{2i\omega r_s(\ln(r_s - r) - i\pi)} = R_{II}^{out*} e^{2\pi\omega r_s}. \tag{A5}$$

Appendix B: Scattering Theory

Scattering and Reflection Coefficients

The Schrödinger equation allows for two different types of solutions, *bound* states and *scattering* states. The former are states localized in some spacetime region within the turning points of a potential $V(x)$. In contrast, scattering states are not bounded by a potential and may *tunnel* through it. Therefore,

$$\begin{cases} E < V(-\infty) & \text{and} \quad V(\infty), & \rightarrow \text{Bound states} \\ E > V(-\infty) & \text{or} \quad\ V(\infty), & \rightarrow \text{Scattering states} \end{cases} \tag{B1}$$

Consider a particle/wave propagating towards a potential $V(x)$ from region I, with wavenumber k, as shown in Figure (B1). The wave may come from the left or right side of the potential.

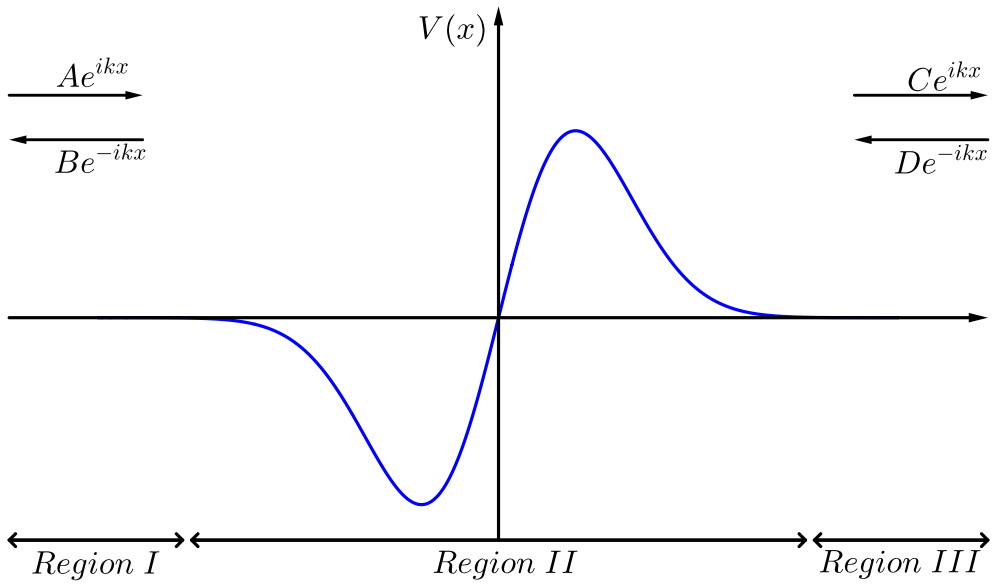

Figure B1: A schematic representation of wave scattering of a potential in region II, where $V(x) \neq 0$. An incoming wave from either region I or III, where $V(x) = 0$, is partially transmitted and reflected by the potential $V(x)$.

Firstly, consider the wave traversing from the left side, $D = 0$. When the wave encounters the potential, it may be transmitted further into region III or reflected back into region I. The *reflection* and *transmission* coefficients are respectively,

$$R_l = \frac{|B|^2}{|A|^2} = \frac{1}{|\alpha|^2} \qquad T_l = \frac{|C|^2}{|A|^2} = \frac{|\beta|^2}{|\alpha|^2} \tag{B2}$$

Due to probability conservation, the transmission and reflection amplitude must be unity, $T + R = 1$. Following [51], these coefficients are also connected to the Bogolubov coefficients α and β by flux conservation. Similarly, a wave scattering from the right has reflection and transmission coefficients,

$$R_r = \frac{|C|^2}{|D|^2} = \frac{|\beta|^2}{|\alpha|^2} \qquad T_r = \frac{|B|^2}{|D|^2} = \frac{1}{|\alpha|^2} \tag{B3}$$

These coefficients are functions of k and are dependent on the type of potential. Classically speaking, a particle with $E < V(x)$ may never tunnel through the potential. However, quantum mechanically, there exists a nonzero probability of finding the particle on the other side of the potential even if $E < V(x)$.

Appendix C: The Confluent Heun Equation

Consider a second-order linear homogeneous equation,

$$\left[\frac{d^2}{dz^2} + p(z)\frac{d}{dz} + q(z)\right] y(z) = 0 \tag{C1}$$

with coefficient functions

$$p(z) = 4p + \frac{\gamma}{z} + \frac{\delta}{z-1} \tag{C2a}$$

$$q(z) = \frac{\sigma}{z} + \frac{4p\alpha - \sigma}{z-1} \tag{C2b}$$

This configuration of $p(z)$ and $q(z)$ represents the non-symmetrical canonical form of the CHE. There are two regular singularities at $z_i = 1, 0$, $i = 1, 2$ and an irregular singularity at $z = \infty$. For each regular singularity, there exist two linearly independent solutions $y_m^i(z)$, $m = 1, 2$ that are only convergent around a circumference at that singular point. The radius of convergence is the distance between regular points. The solutions can be represented as a power series called *Frobenius solutions*,

$$y_m^i(z) = (z - z_i)^{\rho_m(z_i)} \sum_{n=0}^{\infty} a_{mn}^i (z - z_i)^n \tag{C3}$$

where $\rho_m(z_i)$ represents the characteristic exponents at singular point z_i. The characteristic exponents $\rho_m(z_i)$ are the roots of the *indicial equation*,

$$\rho^2 + (A - 1)\,\rho + B = 0 \tag{C4}$$

where,

$$\lim_{z \to z_i} (z - z_i)\, p(z) = A \tag{C5a}$$

$$\lim_{z \to z_i} (z - z_i)^2\, q(z) = B. \tag{C5b}$$

The s-rank of any regular singular point is defined as 1. The irregular singularity at $z = \infty$ can also be expanded as a power series known as Thomé-solutions,

$$y_m^\infty = e^{\kappa_m z^r} z^{-\tau_m} \sum_{n=0}^{\infty} a_{mn}^\infty z^{-rn} \tag{C6}$$

where κ_m,τ_m,$m = 1, 2$ are the characteristic exponents of the second and first order, respectively, at its irregular singular point. The Poincare rank r is given by,

$$r = 1 + \max\left(K_1, \frac{K_2}{2}\right) \tag{C7}$$

where $q(z) = O(z^{K_1})$ and $p(z) = O(z^{K_2})$ as $z \to \infty$. The characteristic exponents are determined by matching them in a way that eliminates the leading order behaviour as $z \to \infty$. The coefficients of Frobenius-and-Thomé solutions are determined by substituting them into Eq.(C1) and solving the recursive relation using appropriate boundary conditions. The singular point $z = \infty$ has s-rank 2 for the non-symmetrical canonical form. When mapping the wave equations to the parameters of the CHE, the length of the equations will become inconvenient. A more convenient convention form of the CHE is,

$$p(z) = a + \frac{b+1}{z} + \frac{c+1}{z-1} \tag{C8a}$$

$$q(z) = \frac{\mu}{z} + \frac{\nu}{z-1} \tag{C8b}$$

with

$$\begin{aligned} \mu &= \frac{1}{2}(a - b - c - 2e + ab - bc) \\ \nu &= \frac{1}{2}(a + b + c + 2d + 2e + ac + bc) \end{aligned} \tag{C9}$$

The parameters p, α, γ, δ, σ are related to the new parameterization by

$$\begin{aligned} a = 4p \quad b = \gamma - 1 \quad c = \delta - 1 \\ d = 4p\alpha - 2p(\gamma + \delta) \quad e = 2p\gamma - \sigma + \frac{1 - \gamma\delta}{2} \end{aligned} \tag{C10}$$

This type of parameterization will be the standard for this thesis. A useful tool to describe the solutions of a differential equation is the *generalized Riemann scheme* (GRS),

$$\begin{array}{r} \text{s-rank} \to \\ \text{Location of singular points} \to \\ \text{First order characteristic exponent} \to \\ \text{First order characteristic exponent} \to \\ \text{Second order characteristic exponent} \to \\ \text{Second order characteristic exponent} \to \end{array} \left[\begin{array}{ccccc} 1 & 1 & & 2 & \\ 0 & 1 & & \infty & \\ 0 & 0 & & \frac{\mu+\nu}{a} & ; z \\ -b & -c & & b+c-\frac{\mu+\nu}{a}+2 & \\ & & & 0 & \\ & & & -a & \end{array}\right] \tag{C11}$$

which contains the necessary information to construct the Frobenius-and-Thomé solutions at corresponding singular points. Another important representation of the CHE is the *normal form*,

$$\left[\frac{d^2}{dz^2} + Q(z)\right] f(z) = 0. \tag{C12}$$

where $Q(z)$ is a potential term. To determine $Q(z)$, consider decomposing the function $y(z) = f(z)g(z)$, such that the differential equation, Eq.(C1), has Schrödinger-form,

$$\left[\frac{d^2}{dz^2} + \frac{1}{f(z)}\frac{\partial^2 f(z)}{\partial z^2} + \frac{p(z)}{f(z)}\frac{\partial f(z)}{\partial z} + q(z)\right] g(z) = 0, \tag{C13}$$

with condition

$$2\frac{\partial f(z)}{\partial z} + p(z)f(z) = 0. \tag{C14}$$

The general solution is then

$$f(z) = e^{-\frac{1}{2}\int p(z)dz}. \tag{C15}$$

The normal form of the CHE in terms of $p(z)$ and $q(z)$ reads,

$$\left[\frac{d^2}{dz^2} - \left(\frac{1}{2}\frac{\partial p(z)}{\partial z} + \frac{1}{4}p(z)^2\right) + q(z)\right] g(z) = 0. \tag{C16}$$

Transformations

In seeking all potential solutions to the CHE, it is imperative to ascertain transformations that conserve the original form. These transformations are instrumental in uncovering all viable solutions. Firstly, consider an *s-homotopic transformation* $y(z) \to w(z)$:

$$y(z) = w(z)e^{\mu_0 z}\prod_i^2 (z - z_i)^{\mu_i} \tag{C17}$$

then the coefficients of Eq.(C1) read,

$$p(z) = a + 2\mu_0 + \frac{1 + b + 2\mu_2}{z} + \frac{1 + c + 2\mu_1}{z - 1} \tag{C18a}$$

$$q(z) = \mu_0(\mu_0 + a) + \frac{\mu_1\left(a + b + 2\mu_2 + 1\right) + \mu_0\left(c + 2\mu_1 + 1\right) + (c+1)\mu_2 + \nu}{x - 1} \tag{C18b}$$

$$+ \frac{\mu_2(a - c - 1) + \mu_0\left(b + 2\mu_2 + 1\right) - \mu_1\left(b + 2\mu_2 + 1\right) + \mu}{x} + \frac{b\mu_2 + \mu_2^2}{x^2} + \frac{c\mu_1 + \mu_1^2}{(x-1)^2} \tag{C18c}$$

Any combination of the following variables conserves the original form of the coefficient $q(z)$,

$$\begin{array}{lll} \mu_0 = -a & \mu_1 = -c & \mu_2 = -b \\ \mu_0 = 0 & \mu_1 = 0 & \mu_2 = 0 \end{array} \tag{C19}$$

Another important transformation is the linear transformation interchanging the singular points: $z \to 1 - z$. Any combination of the transformations provides a solution to the CHE, yielding 16 solutions, which are given in Table C1.

Table C1: All possible combinations of transformations that conserve the form of the CHE.

μ_0	μ_1	μ_2	a	b	c	d	e
0	0	0	a	b	c	d	e
$-a$	0	0	$-a$	b	c	d	e
$-a$	0	$-b$	$-a$	$-b$	c	d	e
$-a$	$-c$	0	$-a$	b	$-c$	d	e
$-a$	$-c$	$-b$	$-a$	$-b$	$-c$	d	e
0	$-c$	0	a	b	$-c$	d	e
0	$-c$	$-b$	a	$-b$	$-c$	d	e
0	0	$-b$	a	$-b$	c	d	e

(a) All combinations of s-homotropic transformations.

μ_0	μ_1	μ_2	a	b	c	d	e
0	0	0	$-a$	c	b	$-d$	$e+d$
$-a$	0	0	a	c	b	$-d$	$e+d$
$-a$	0	$-b$	a	c	$-b$	$-d$	$e+d$
$-a$	$-c$	0	a	$-c$	b	$-d$	$e+d$
$-a$	$-c$	$-b$	a	$-c$	$-b$	$-d$	$e+d$
0	$-c$	0	$-a$	$-c$	b	$-d$	$e+d$
0	$-c$	$-b$	$-a$	$-c$	$-b$	$-d$	$e+d$
0	0	$-b$	$-a$	c	$-b$	$-d$	$e+d$

(b) All combinations of s-homotropic transformations with the interchanging of $z \to 1-z$.

Heun functions

Define two basis solutions to the CHE, $Hc^{(a)}\left(a,b,c,d,e;z\right)$ and $Hc^{(r)}\left(a,b,c,d,e;z\right)$. The former solution is the *angular* solution defined as the Frobenius solution at regular singular point $z=0$:

$$Hc^{(a)}\left(a,b,c,d,e;z\right)=\sum_{n=0}^{\infty}a_n z^n \tag{C20}$$

constrained to the domain $|z|<1$ with condition,

$$Hc^{(a)}\left(a,b,c,d,e;0\right)=1 \tag{C21}$$

Substituting the solution into the CHE gives a three-term recurrence relation for a_n,

$$\begin{aligned} &f_n^{(a)}a_{n+1}+g_n^{(a)}a_n+h_n^{(a)}a_{n-1}\\ &\quad a_0=1, \qquad a_n=0\ \forall n<0 \end{aligned} \tag{C22}$$

where

$$f_n^{(a)}=n(n-a+b+c+1)-\mu \tag{C23a}$$

$$g_n^{(a)}=-(n+1)(n+b+1) \tag{C23b}$$

$$h_n^{(a)}=a\left(n+\frac{\mu+\nu}{a}-1\right) \tag{C23c}$$

The solution is convergent and well-defined for $|z|<1$ as

$$\frac{a_n}{a_{n+1}}=1 \tag{C24}$$

The latter solution is the *radial* solution defined as the Thomé solution at the irregular singular point $z=\infty$:

$$Hc^{(r)}\left(a,b,c,d,e;z\right)=z^{-\frac{\mu+\nu}{a}}\sum_{n=0}^{\infty}a_n^{\infty}z^{-n} \tag{C25}$$

at $z=\infty$ with the condition,

$$\lim_{|z|\to\infty} z^{\frac{\mu+\nu}{a}}Hc^{(r)}\left(a,b,c,d,e;z\right)=1 \tag{C26}$$

$$\begin{aligned} &f_n^{(r)}a_{n+1}^{\infty}+g_n^{(r)}a_n^{\infty}+h_n^{(r)}a_{n-1}^{\infty}=0\\ &a_{-1}^{\infty}=0, \quad a_0^{\infty}=1 \end{aligned} \tag{C27}$$

$$\begin{aligned} g_n^{(r)}&=\left(\frac{\mu+\nu}{a}+n\right)\left(\frac{\mu+\nu}{a}+n+a-b-c-1\right)-\mu\\ f_n^{(r)}&=-a(n+1)\\ h_n^{(r)}&=-\left(n+\frac{\mu+\nu}{a}-1\right)\left(\frac{\mu+\nu}{a}+n-b-1\right). \end{aligned} \tag{C28}$$

Combining all possible transformations, a total of 32 solutions exist for the CHE.

Appendix D:

This appendix will outline the massive scalar field equations of different coordinate systems for a Schwarzschild background. In the near horizon limit, the field equations in Painlevé, Eddington-Finkelstein and Schwarzschild coordinates coincide. Moreover, these field equations must be promoted to an eigenvalue problem such that the effective action can be computed using the heat kernel. Promoting the scalar field equation in a gravitational background, Eq. (69), to an eigenvalue equation,

$$\left[\Box - \mu^2 - \xi R\right]\phi_k(x) = k^2\phi_k(x) \tag{D1}$$

where $\phi_k(x)$ represents the eigenmodes of the field equation with corresponding eigenvalues k^2.

Schwarzschild Field Equation

In Schwarzschild coordinates, Eq.(118), the eigenvalue equation reads,

$$\left[\frac{1}{r^2}\frac{\partial}{\partial r}\left(r^2\left(1-\frac{r_s}{r}\right)\frac{\partial}{\partial r}\right) - \left(1-\frac{r_s}{r}\right)^{-1}\frac{\partial^2}{\partial t^2} + \Delta - \mu^2\right]\phi_{\omega lmk}(t,r,\theta,\varphi) = k^2\phi_{\omega lmk}(t,r,\theta,\varphi) \tag{D2}$$

with

$$\Delta = \frac{1}{r^2\sin(\theta)}\left[\frac{\partial}{\partial\theta}\left(\sin(\theta)\frac{\partial}{\partial\theta}\right) + \frac{1}{\sin(\theta)}\frac{\partial^2}{\partial\varphi^2}\right]. \tag{D3}$$

The mode solutions can be decomposed into,

$$\phi_{\omega lmk}(t,r,\theta,\varphi) = \int d\omega \sum_{l=0}^{\infty}\sum_{m=-l}^{l} Y_{lm}(\theta,\varphi)e^{-i\omega t}\psi_{\omega lmk}(r) \tag{D4}$$

Dividing both sides by $\left(1-\frac{r_s}{r}\right)^{-1}$, then the radial eigenvalue equation reads,

$$\left[\frac{\partial^2}{\partial r^2} + \left(\frac{2r-r_s}{r^2-rr_s}\right)\frac{\partial}{\partial r} + \frac{r^2\omega^2}{(r-r_s)^2} - \left[\mu^2 + \frac{l(l+1)}{r^2}\right]\frac{r}{r-r_s}\right]\psi_{\omega lmk}(r) = \frac{r}{r-r_s}k^2\psi_{\omega lmk}(r) \tag{D5}$$

Using Eq.(C16) Rewriting in Schrödinger-form using Eq.(C16) and decomposing the radial part into $\psi_{\omega lmk}(r) = f(r)\Phi_{\omega lmk}(r)$ gives

$$\left[\frac{\partial^2}{\partial r^2} + \frac{r_s^2}{4r^2(r-r_s)^2} + \frac{r^2\omega^2}{(r-r_s)^2} - \left[\mu^2 + \frac{l(l+1)}{r^2}\right]\frac{r}{r-r_s}\right]\Phi_{\omega lmk}(r) = \frac{r}{r-r_s}k^2\Phi_{\omega lmk}(r) \tag{D6}$$

where $f(r) = \left(r^2-rr_s\right)^{-\frac{1}{2}}$. Substitute $r = x + r_s$ to take the near horizon and expand near $x = 0$ up to order $\mathcal{O}\left(x^0\right)$ gives,

$$\left[\frac{\partial^2}{\partial x^2} + \frac{\frac{1}{4}+\omega^2r_s^2}{x^2} - \frac{l(l+1)+\mu^2r_s^2-2\omega^2r_s^2+\frac{1}{2}}{xr_s} + \omega^2 - \mu^2 + \frac{3}{4r_s^2} + \frac{l(l+1)}{r_s^2}\right]\Phi_{\omega lmk}(x) = \frac{x+r_s}{x}k^2\Phi_{\omega lmk}(x) \tag{D7}$$

Eddington-Finkelstein Field Equation

In outgoing Eddington-Finkelstein coordinates, Eq.(129), the eigenvalues equation reads,

$$\left[\frac{1}{r^2}\frac{\partial}{\partial r}\left(r^2\left(1-\frac{r_s}{r}\right)\frac{\partial}{\partial r}\right) - \frac{1}{r^2}\frac{\partial}{\partial u}\left(r^2\frac{\partial}{\partial r}\right) - \frac{1}{r^2}\frac{\partial}{\partial r}\left(r^2\frac{\partial}{\partial u}\right) + \Delta - \mu^2\right]\phi_{\omega lmk}(u,r,\theta,\varphi) = k^2\phi_{\omega lmk}(u,r,\theta,\varphi) \tag{D8}$$

where Δ is given in Eq.(D3). The mode solutions can be decomposed into,

$$\phi_{\omega lmk}(u,r,\theta,\varphi) = \int d\omega \sum_{l=0}^{\infty}\sum_{m=-l}^{l} Y_{lm}(\theta,\varphi)e^{-i\omega u}\psi_{\omega lmk}(r) \tag{D9}$$

Dividing both sides by $\left(1-\frac{r_s}{r}\right)^{-1}$, then the radial eigenvalue equation reads,

$$\left[\frac{\partial^2}{\partial r^2} + \left(\frac{2r-r_s+2i\omega r^2}{r^2-rr_s}\right)\frac{\partial}{\partial r} + \frac{2i\omega}{r-r_s} - \left[\mu^2 + \frac{l(l+1)}{r^2}\right]\frac{r}{r-r_s}\right]\psi_{\omega lmk}(r) = \frac{r}{r-r_s}k^2\psi_{\omega lmk}(r). \tag{D10}$$

Moreover, rewriting in Schrodinger-form reduces to Eq.(D6) with $f(r) = \left(r^2-rr_s\right)^{-\frac{1}{2}}e^{-ir\omega}\left(r-r_s\right)^{-i\omega r_s}$.